INVESTIGATION ON IMPROVED TAPPING LIFE IN AUTOMOTIVE DIE CAST ALUMINUM-SILICON ALLOY APPLICATIONS

INVESTIGATION ON IMPROVED TAPPING LIFE IN AUTOMOTIVE DIE

CAST ALUMINUM-SILICON ALLOY APPLICATIONS.

By

ROHAN KUMAR BAROOAH, B.ENG

A Thesis

Submitted to the School of Graduate Studies

in Partial Fulfilment of the Requirements

for the Degree

Master of Applied Science,

McMaster University, Hamilton, Ontario

MASTER OF APPLIED SCIENCE (2018)   McMaster University

(Mechanical Engineering)   Hamilton, Ontario

TITLE: INVESTIGATION ON IMPROVED TAPPING LIFE IN

                    AUTOMOTIVE DIE CAST ALUMINUM-SILICON ALLOY

                    APPLICATIONS

AUTHOR: Rohan Kumar Barooah

                    B. ENG (Mechanical Engineering)

                    McMaster University, Hamilton, Ontario

SUPERVISOR: Dr. Stephen C. Veldhuis

                    Department of Mechanical Engineering

                    McMaster University

NUMBER OF PAGES: xvi, 156

Abstract

In the automotive industry, Al-Si alloy is widely used for manufacturing of various engine parts. Machinability of die-cast Al-12Si alloy is challenging due to severe abrasion and adhesion wear of the tools. Form tapping is a common method for generating internal threads in engine blocks. It is usually a finishing process on a production line. An unexpected tap failure may lead to significant scrap and high rework costs.

The objective of this research was to investigate the wear mechanisms of high-speed steel form taps when machining Al-12Si alloy. This research involved replicating the same process conditions as the industry partner to determine a feasible solution without changing the tap geometry or process parameters.

A critical region of wear on the crest was identified where the aluminum adhesion was acute. Intense abrasion wear occurred on the crest and flanks due to hard silicon precipitates. In this study, two methods were proposed for measuring linear and volumetric wear on the chamfered threads. The second and third chamfered threads experienced the most significant wear on the tap.

To improve wear-resistance of the form tap, PVD surface coatings were deposited on it. The preliminary tests of 12 surface coatings showed coating-delamination mostly on the critical region. A progressive wear study of the TiAlN coating showed an improvement in tap performance over the ZrN coating currently used. By the 4320th hole, the volumetric wear of the TiAlN coated tap was reduced by nearly 200% and 50% when compared against the uncoated and ZrN coated taps, respectively.

Acknowledgements

Contents

List of Figures

List of Tables

List of all Abbreviations and Symbols

HSS — High-speed steel

BUE — Built up edge

PVD — Physical vapor deposition

CVD — Chemical vapor deposition

DCD — Dynamic compound deposition

SEM — Scanning electron microscopy

EDS — Energy dispersive spectroscopy

D — Basic major diameter of internal thread or nominal diameter

D_2 — Basic pitch diameter of internal thread

D_1 — Basic minor diameter of internal thread

H — Height of fundamental triangle

P — Pitch

d — Basic major diameter of external thread

d_2 — Basic pitch diameter of external thread

d_1 — Basic minor diameter of external thread

D_M — Major diameter of the tap

D_H — Diameter of drilled hole

Declaration of Academic Achievement

I, Rohan Kumar Barooah, do hereby declare that the thesis entitled "**Investigation on improved tapping life in automotive die cast aluminum-silicon alloy applications**" to be my own work and that I am the sole author of this thesis.

A part of this thesis, as mentioned in Appendix B, is a collaborative work with another graduate student in the MMRI. The results of this study have been provided in Appendix B with the approval of Yousef Shokoohi to prevent any plagiarism issues.

I certify that, to the best of my knowledge, the content of this thesis does not infringe on anyone's copyright.

This thesis has been completed under the supervision of Dr Stephen C. Veldhuis. The technical staff of the MMRI have provided valuable support in all stages of this research work.

Chapter 1. Introduction

1.1 Background

The Aluminum-Silicon (Al-Si) alloy is a eutectic alloy system which is widely used for the casting of complex shapes when wear resistance is needed. The eutectic composition for this binary alloy is 12.5 % Si and the commercial grades of this alloy have several alloying elements to improve mechanical, thermal and chemical properties. Due to its castability, Al-Si alloys are commonly used in automotive, aerospace and consumer products. The D357 alloy is typically used in aerospace applications such as frame brackets, winglet substructures, tail rotor gearboxes, etc. A336.0 alloy is typically used for engine pistons, A355.0 for pump bodies and cylinder heads. SAE alloys 780 and 781 are popular for engine bearing. Hyper-eutectic alloys such as the A390.0 alloy are designed for cylinder blocks without liners, transmission pumps, air compressor housings, etc. The silicon phase is primarily responsible for providing excellent wear resistance of both hypo-eutectic and hyper-eutectic Al-Si alloys. This is possible due to a softer α-Al matrix surrounding the hard silicon particles which facilitates plastic behavior in the alloy [1], [2].

In an effort to reduce the weight of vehicles, the die cast Aluminum-Silicon (Al-Si) alloys have been commercially used to produce engine blocks since the 1950s due to their high strength to weight ratio, good thermal conductivity, higher wear resistance, excellent castability, and lower coefficient of expansion. The machining of Al-Si alloys with silicon content greater than 10 % is difficult due to rapid tool wear caused by the abrasive, hard silicon particles which are present in the form of primary-phase and

eutectic silicon. A390.0 has a greater amount of primary-phase silicon which is desirable for wear resistance but decreases tool life in machining. The hardness of silicon crystals typically ranges from 1000-1200 HV compared to 120-140 HV for pure aluminum casting. Both primary silicon and eutectic silicon particles are coarse and detrimental to tool life. An increase in size and amount of silicon particles may increase the tool wear rate. Refinement of silicon crystal structure with alloying elements is needed, since unrefined primary silicon is almost eight to ten times larger than refined crystals. In order to improve the machinability of Al-Si alloys, a lower content of silicon, close to the eutectic composition of nickel and manganese, has been a favorable substitute [3].

Generation of internal threads is achievable by several processes such as thread turning, thread milling, thread grinding, thread rolling, cut and form tapping. Tapping is one of the most intensively used machining processes for obtaining threads in both ferrous and non-ferrous metals and their alloys. In fact, tapping is one of the final finishing processes widely used in engine block manufacturing. The cost of rework or scrapping an engine at this stage due to the poor quality of internal threads must be avoided in large scale production such as in the automotive industry [4].

Form tapping on high silicon content aluminum alloy engine blocks has replaced cut tapping since the formed threads are superior in quality to cut threads. Stronger internal threads are formed due to uninterrupted grain flow and cold work hardening at the flanks and roots of the thread. Thread strength under tensile load is found to be 27 % greater for formed versus cut threads. Also, the fatigue strength is observed to be

higher for formed threads than for cut threads due to the strain hardening effect on the thread surface. The geometrical precision of formed threads is better than that of cut threads due to minimal flank straightness error and thread pitch error [5].

Moreover, the form tapping process is more advantageous than cut tapping since it produces no chips, which is the chief reason for its popularity in automotive and other manufacturing industries. Roll form taps are stronger than cut taps due to an absence of flutes, since there is no need for chip evacuation while machining blind holes. The flutes are replaced with small channels of grooves for lubrication supply. The tool life of a form tap is thus three to ten times greater than a cutting tap, providing better reliability at a lower overall tooling cost per part [6].

The characteristic feature of a formed thread is the split crest observed at the top of the internal thread. The split crest tends to weaken the overall strength of the thread and the tips of the ridge may chip off during assembly or operation [7]. The split crest is directly dependent on the drilled hole diameter [8]. Form tapping is not used in food or medical industries due to the chance of breakage of the split crest which can lead to contamination issues. In addition, it has been observed that the wear on the chamfered threads can be another cause for the poor quality of internal threads.

Wear of the tap may result in poor forming of the internal threads. As per the ISO standard 1502:1996, the limits of pitch diameter and major diameter are checked by gauging the internal threads with a screw plug gauge to ensure the quality of internal threads. The threaded holes are checked periodically, but there exists no industrially accepted standard practice for checking wear of a form tap. Hence, the formed thread's

quality is fully dependent on the wear of form tap's thread. In mass-scale manufacturing industries, a system of tool wear monitoring can be useful in preventing any bad parts from being produced. A wear measurement methodology is desirable which needs to be easy, accurate and effective at detecting worn taps under production conditions. Furthermore, the development of such a wear measuring method will require greater understanding of the detectable wear pattern. Once the wear pattern is identified, surface modification, tooling design, process parameter and lubrication conditions can be improved to achieve higher tool performance and life.

1.2 Motivation

This academic project was performed in collaboration with an automotive Original Equipment Manufacturer (OEM) that produces high-end quality parts at a mass-scale. One of the critical challenges faced by the OEM was machining correct internal threads with roll form taps in automotive engine components. The root cause of the quality problem was the frequent failure of the roll form taps in the machining of aluminum-silicon (Al-Si) alloy parts. Inspection of every tapped hole in the mass-scale production of parts is difficult and cycle time becomes higher due to frequent quality checks. Furthermore, the reworking time and cost may increase with non-conformity. In an attempt to improve the performance of the form tapping process, extensive research was conducted at the MMRI with the support of the industrial partner.

To investigate the cause of the form tap's failure, this study sets out to establish the major wear mechanisms of the form taps in machining this particular Al-Si alloy grade. Since, there is no ISO standard for the wear measurement of form taps, a suitable

method for quantifying the wear was necessary. Analysis of tool wear progression is now understood by using the proposed wear measurement methods. Since the process parameters and tool geometry were constant, the application of hard and lubricious PVD coatings was tested to impede major wear mechanisms detected in this process. The primary aim of this research was to improve the tool life and provide a reliable solution for producing high-quality internally formed threads.

1.3 Research Objectives

The main research objective for this thesis work are presented below.

1. Investigate the failure modes and establish the dominant wear mechanisms of uncoated HSS roll form taps used for machining die-cast Al-12Si alloy.

2. Propose and develop a wear measurement methodology specifically for form taps.

3. Develop a performance criterion to use during short machining test to perform comparative wear study of form taps.

4. Compare the performance of selected PVD coatings by performing short machining tests.

5. Investigate the performance of the best performing tool coating identified in objective 4 via extensive tests.

6. Investigate the feasibility of accelerated performance tests for assessing form taps.

1.4 Methodology

```
┌──────────────────────┐      ┌─────────────────┐
│ Process parameters   │      │   Literature    │
│    (Industry)        │      │     Review      │
└──────────────────────┘      └─────────────────┘
                                       │
┌──────────────────────┐      ┌─────────────────┐      ┌──────────────────────────┐
│ Workpiece & Tools    │─────▶│    Design of    │      │    Benchmark tool:       │
│    (Industry)        │      │   Experiment    │      │                          │
└──────────────────────┘      └─────────────────┘      │  Identify Major wear     │
                                       │               │     mechanisms.          │
┌──────────────────────┐              │               │                          │
│      Fixture         │─────────────▶│               │  Quantify wear-          │
│   Development        │              │               │  linear & Volume.        │
└──────────────────────┘              ▼               │                          │
                              ┌─────────────────┐      │  Monitor Torque,         │
                              │  Machinability  │─────▶│  & Hole diameter.        │
                              │   Tests on      │      │                          │
                              │  Uncoated HSS   │      │  Perform SEM, EDS,       │
                              │   form taps     │      │  Optical Microscopy.     │
                              │  (4000 holes)   │      │                          │
                              └─────────────────┘      │  Identify metric for     │
                                       │               │  performance evaluation. │
                                       ▼               └──────────────────────────┘
┌──────────────────┐          ┌─────────────────┐      ┌──────────────────────────┐
│  12 Surface      │─────────▶│ Preliminary     │─────▶│   Identify better        │
│  Coatings        │          │ tests for       │      │  performing coatings     │
└──────────────────┘          │ potential       │      └──────────────────────────┘
                              │ coatings        │
                              │ (360 holes)     │
                              └─────────────────┘
                                       │
                                       ▼
                              ┌─────────────────┐      ┌──────────────────────────┐
                              │ Performance     │─────▶│ Identify effective coating│
                              │ tests of the    │      │ w.r.t benchmark and      │
                              │ identified      │      │ industry preference.     │
                              │ coatings        │      └──────────────────────────┘
                              │ (2000 holes)    │
                              └─────────────────┘
                                       │
                                       ▼
                              ┌─────────────────┐      ┌──────────────────────────┐
                              │ Machinability   │─────▶│   Evaluate coating       │
                              │ tests of the    │      │   performance            │
                              │ effective       │      └──────────────────────────┘
                              │ coating         │
                              │ (4000 holes)    │
                              └─────────────────┘
```

Fig.1: Research methodology

1.5 Thesis Outline

A short summary of each chapter of this thesis is as follows:

CHAPTER 1: Introduction — This chapter presents a short background and discusses the motivation for this thesis. The experimental methodology is presented along with the main research objectives.

CHAPTER 2: Literature review — This chapter presents a detailed overview of different threading techniques, mechanics of form tapping, the effect of process parameters in this process and characteristics of the internal formed thread. A critical review on the machinability of die-cast Al-Si, major wear mechanisms and measurement methods is provided. The tribological behaviour of PVD coatings and MWF in form tapping is described as well.

CHAPTER 3: Experimental procedure—A detailed description of the experimental setup for the machining tests is provided along with necessary information about process parameters, workpiece, cutting and forming tools.

CHAPTER 4: Study on the wear mechanism and measurement methods—This chapter discusses the major wear mechanisms identified in the uncoated HSS form tap. An approach has been made to develop a wear measurement methodology for form taps.

CHAPTER 5: Effect of PVD coatings on tool life improvement—This chapter provides results and detailed discussion of the selected PVD coatings' performance in form tapping. A comparative study of an effective coating with the benchmark coating was provided to evaluate common wear mechanisms for this process.

CHAPTER 6: Assessment of form taps with end of tool life condition—This chapter provides a brief overview of the form tap's end of life condition.

CHAPTER 7: Conclusions—A summary of all the findings of this research was provided in this chapter. This chapter also recommends future research work to extend tool life of form taps in Al-Si alloy machining.

Appendix A: Inspection of drilled and tapped hole—This chapter includes the diameters of drilled holes and threaded hole conditions at various stages of all the studies.

Appendix B: Effect of metalworking fluids on drilling and tapping—In this chapter, the performance of select MWFs in drilling and form tapping processes is studied.

Chapter 2. Literature Review

2.1 Threading techniques

During the assembly of various part in a manufacturing setup, screw and bolt joint fastening is the most common method for non-permanent joints. Easy repair and maintenance, cost-effective inspection and interchangeability of certain components in an assembled part requires the use of threaded fasteners [5],[9],[10]. Screw threads provide a clamping force, restrict motions, and transmit power in the mechanical system [11],[12]. These threads can be generated either internally, on nuts and tapped holes, or externally- on studs, bolts and screws. Both internal and external threads can be produced by different machining processes such as thread turning, thread milling, thread grinding, cut tapping, thread rolling and forming. A brief description of each of these processes will be summarized in this section.

Thread turning is one of the most widely used methods of generating threads on cylindrical bars with indexable inserts. A wide range of thread profiles with different sizes of cutting inserts are available commercially. Although thread turning is common, it poses several challenging issues [12]. One of the drawbacks of this process is the requirement of multiple passes to get the full depth of thread. Smaller depths of cut may need a greater number of passes, which result in excessive tool wear and build of heat due to friction. Reducing the number of passes by making deeper cuts may create higher cutting forces and result in premature tool breakage. Under these conditions, rigidly clamping the insert to the tool holder is a critical factor for a stable process. In the case of threading on stainless steels parts, burr formation at the start of the thread must be

avoided by employing a deburring insert. Correct positioning of a deburring insert can be challenging with respect to the thread pitch. Also, multi-start threads are time consuming since a greater number of passes are required for every thread groove. Selecting an optimum infeed strategy is essential for proper chip evacuation, good surface quality and lower cutting forces [13].

Thread milling is mostly used for producing threads in non-rotational large parts by helical ramping of either an indexable inserts or solid cutter. Thread milling is a more versatile process than thread turning and cut tapping in the case of internal threads. It has several advantages, such as one cutter for multiple diameter holes, left and right-handed threads with the same cutter, different pitch with the same tool, and better chip evacuation [14]. In comparison to cut-tap breakage and consequently hole jamming, thread mill cutters can be easily removed from the hole upon breakage [12]. Although thread milling is more favourable for producing threads, high tool costs reduce its appeal in mass production where only a certain hole size may be repetitively machined.

High tolerance parts, such as worm gears, thread gauges and taps, are manufactured by the thread grinding process due to its high accuracy and consistency of the grinding wheel. The grinding wheel can be redressed as required to produce a different geometry and size of thread on a production floor. Single or multi-rib are the two techniques for thread grinding. In single-rib grinding, only one thread pitch is dressed, and a complete thread is generated by continuous material removal in multiple passes. It is mostly used for short batches and hard work piece materials. Multi-rib grinding consists of a few grooves with multiple pitches which gradually remove material. It is popular for large

batch production. In order to maintain high precision threads, certain researchers made an effort to reduce thread error caused by repeated clamping in grinding. For example, Wang et.al [15] developed an automatic tool setting method for grinding accurate internal threads by locating the initial point of the screw helix.

Tapping is a very popular method for producing internal threads in both ferrous and non-ferrous alloys. This process is applied in high volume production found in automotive and heavy machinery industries, food, medical and furniture industries [16]. The wide application of this process is due to its advantages such as high process reliability, greater flexibility in machining, reduced machining stoppage for setup change, longer tool life, reduced machining time (often single pass), and lower tooling costs. Thread tapping is broadly classified either as cut tapping or form tapping.

In the cut tapping process, multiple cutting edges, on the chamfered periphery of the tap, engages with the internal surface of the drilled hole simultaneously to generate the screw threads [17]. The major problem of cut tapping is with chip control in deep blind holes and long, continuous chips. This is a particular problem when tapping steels with low tensile strength and non-ferrous alloys like Al alloys where chips are generally long and stringy. The result of poor chip control can be random torque spikes, thread damage in workpiece, chip snarling, premature tool wear and tap breakage [4],[18]. Since it mostly occurs at the end of the production work flow, tap breakage must be prevented to avoid any rework or stoppage of the process [17],[19]. Torsional fracture of the tap occurs due to excessive tapping torque caused by chip clogging. Optimized tap design with effective chip evacuation strategy could reduce tap breakage [20].

Form tapping is a chipless process which involves plastically deforming material in the workpiece to produce internal threads by a forming tool with the required thread profile. This process is favourable for softer steel grades and ductile materials. It is very popular for generating internal threads in deep blind holes, since there are no chip removal issues. Grooves in the tap are provided for supplying lubrication. Since, grooves are much smaller than the gullets along the flutes of a cutting tap, the form tap is a much stronger tool than a cut tap [6]. Compared to the cut threads, internal formed threads have better geometrical quality, higher tensile strength, shear strength and greater fatigue resistance due to uninterrupted grain flow and cold work hardening [5]. Past literature mentions several limitations of this process. It is limited to both ferrous and non-ferrous alloys having hardness and tensile strength lower than 200 BHN and 800 MPa, respectively [21]. Some researchers reported that the torque would tend to be higher if coolants were not used in this process [21],[22]. The split crest on formed threads also restricts the use of taps in the aerospace and the food industry. Despite these limitations, certain superior qualities such as higher tool life, better geometrical precision, reduced machining time, stronger tool and complete elimination of chip related problems make the form tapping tool very popular in the automotive industry [23],[5],[6].

2.2 Mechanics of form tapping

Internal threads on drilled holes are formed by the penetration of a series of threads at the tapered entry region of the tap. These threads are designed to successively penetrate deeper into the workpiece as the tap is fed into the drilled hole. Each thread's

surface deforms the workpiece to create a deeper groove. Finally, the split crest is formed producing an internal thread on the workpiece. In Fig.2 (a) and (b), the initial threads of the entry taper region are called chamfered threads, since a chamfer angle of 10° is maintained for uniform contribution of individual chamfered thread in the forming [8].The remaining threads on the tap, as shown in Fig.2(a), are just for guiding the tap forward into the hole. These threads are called trailing threads or guiding threads which may have a back taper to reduce the contact area between the surface of the already formed thread and the tap's trailing threads. The length of the tap depends on its application. The sharpest corner of each crest is called the lobe and tangents the nominal diameter circle of the tap. Although, there is no cutting edge in this chip-less process, the thread crest can be divided into two sections- rake edge and relief edge as shown in Fig.3(a). The rake edge is the section of the crest's lobe that has initial contact with the work material. The relief edge is the section of crest from the lobe to the rear end of the crest that provides clearance between the thread and the groove already formed on the workpiece. A higher thread relief or a lower thread length has similar effect on lowering torque during form tapping [8].
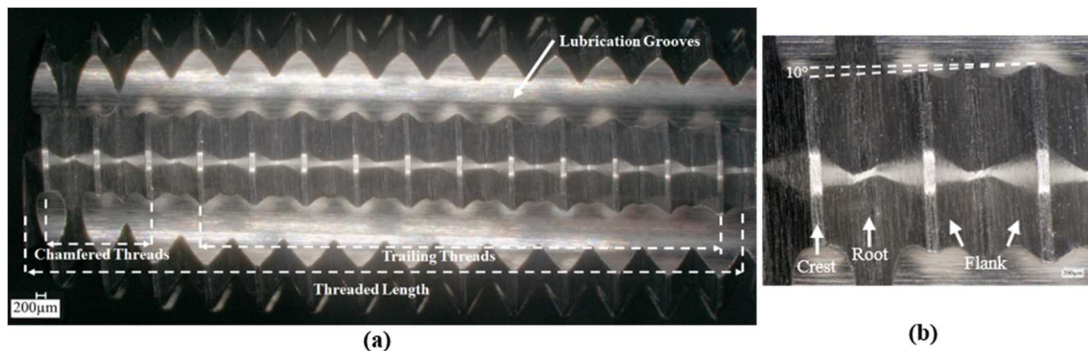
Fig.2: (a)General design of the roll form tap, (b) chamfered threads at entry region

| (a) | (b) | (c) |
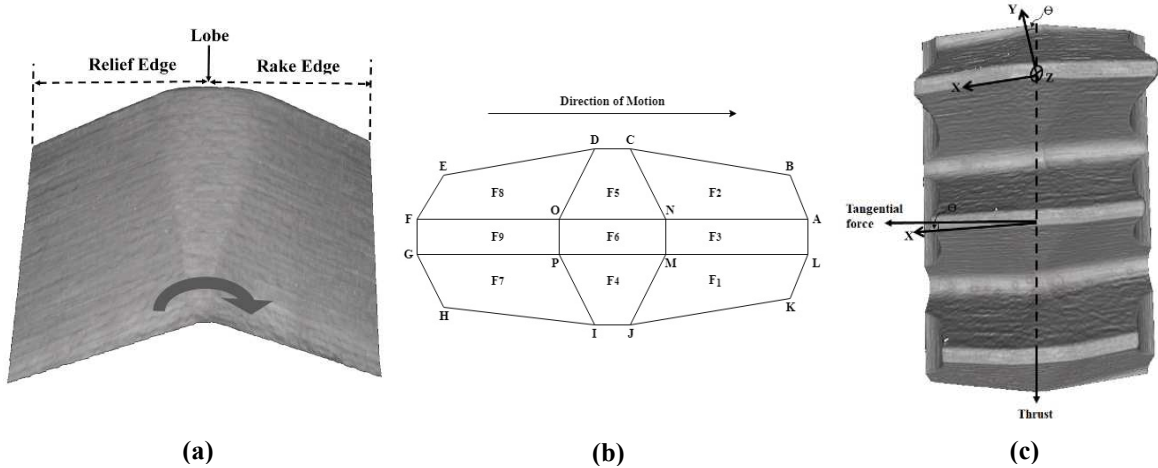
Fig.3: (a)Front view of a thread(based on [5]),(b)top view,(c)thrust and tangential force (based on [8])

Chowdhary et al. [24],[25] developed a prediction model for estimating thrust and torque generated by the form tap in the internal thread forming process. It was concluded that elastic recovery of the workpiece during form threading is needed to accurately predict forces. The mechanics of form tapping is best detailed in these extensive research works. The chamfered threads experience forces primarily due to the plastic deformation and subsequently contact pressure due to restricting elastic recovery. The trailing threads experience forces due to friction between elastic recovered workpiece and trailing threads. Usually, the frictional force is minimal due to a very small back taper angle. If an individual thread on the chamfered surface is considered, the two flanks and the crest can be divided into 9 faces as shown in Fig.3(b). F1, F2, F3 are the leading faces of the crest and the flank. These faces are responsible for plastic deformation normal to each face. The direction of material displacement is from the crest to the roots on both sides of the thread flanks. Each face of an individual thread experiences both normal and frictional forces. The centroid of each face of the thread is the point of application of forces. F4, F5, F6 are the faces neighboring the lobe

14

of the crest. These central faces are responsible for restricting any elastic recovery of the groove formed by faces F1, F2 and F3 previously. The amount of elastic recovery is based on previous plastic deformation caused by the leading faces. Hence, the contact pressure on faces F4, F5, F6 is proportional to the amount of elastic recovery. The normal force on these central faces is dependent on the contact pressure. The trailing faces are F7, F8, F9 are provided with relief and therefore, no contact occurs with the grooves formed in the workpiece. As a result, no forces are experienced by the trailing faces. The frictional forces and normal forces can be resolved into forces in the X, Y and Z directions. As shown in Fig.3(c), the tangential force and thrust force can be calculated from the forces in the X, Y and Z directions. The torque for the forming process is the product of the tangential force and the radial distance between the centroid of the thread and the tap axis. The author also concluded that elastic recovery of work material led to a greater contact area between the threads on the back taper with the already formed grooves. Hence, frictional forces are the major forces affecting the torque and the thrust force remains almost constant [24],[25].

Fig.4 shows the typical time-based torque response of a form tapping process. This process consists of a forward motion and a retracting motion. The plastic deformation of internal threads occurs in the forward motion only. Therefore, the performance of this process is limited to the forward motion.
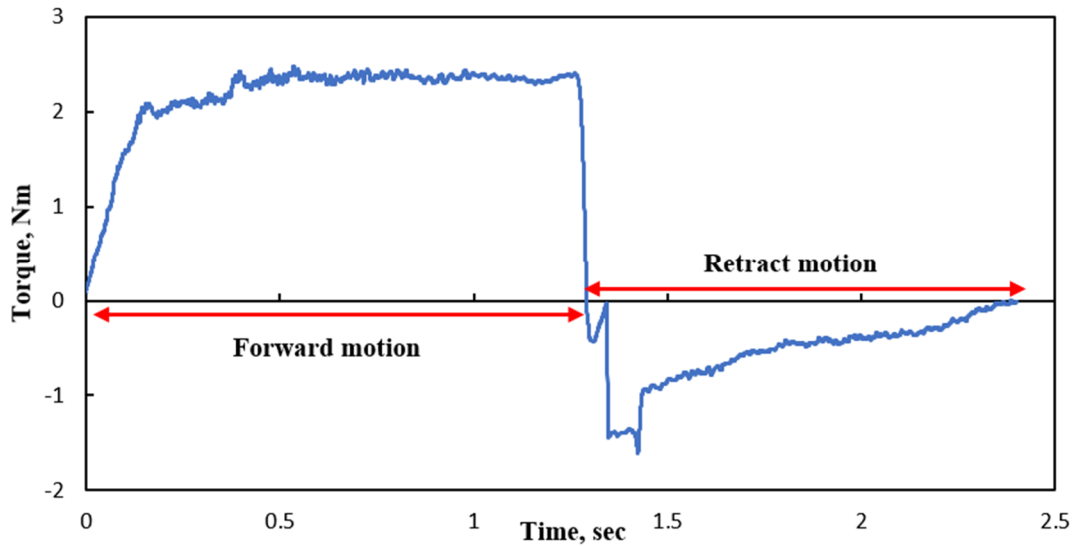
Fig.4: Full torque response of a form tapping process

Fig. 5 shows the torque response for the forward tapping motion. At 0.14 seconds, the first chamfered thread engages with the workpiece. From 0.14 seconds to 0.35 seconds the first three chamfered threads are engaged fully. The elastic recovery of formed threads occurs after forming starts. The tapping torque can be determined by the sum of formation torque and friction torque [22]. The formation torque is the torque value generated by the forming of internal threads. The friction torque is the torque value generated by the elastic recovery of the formed threads, and frictional forces between the formed threads (workpiece) with guiding threads of the tap. The mean torque is calculated over the steady region of the torque response. Here, the steady region is considered from the engagement of the first four threads of the tap. After 0.35 seconds, the guiding thread of the tap engages with the formed threads. In this steady region, the combined effect of both friction and formation torque is considered to

evaluate the performance of the tap. This method of analyzing the torque response has been considered for further analysis in this research study.
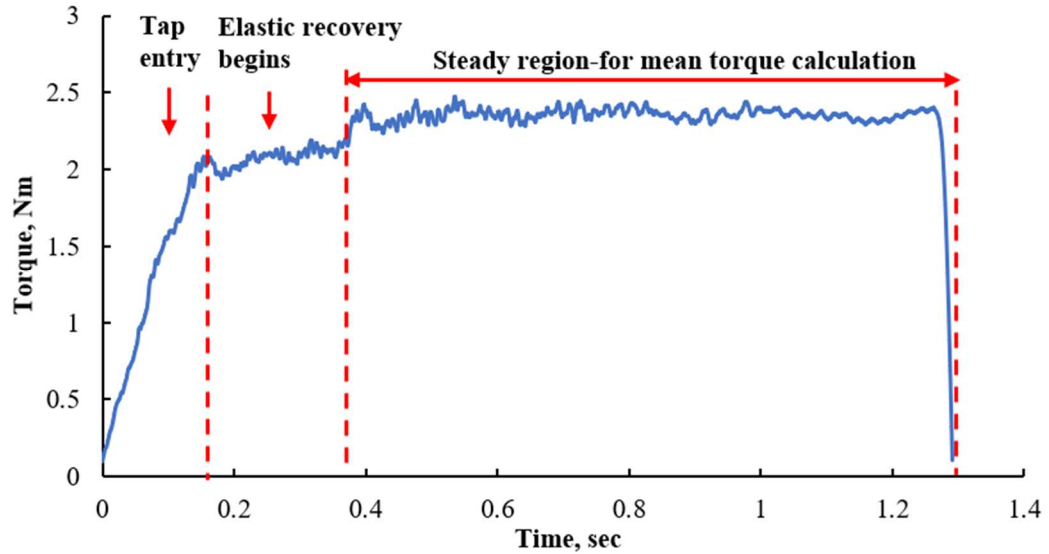
Fig.5: Torque response of the forward motion in form tapping

2.3 Effect of process parameters in form tapping

Literature review suggests that torque is an important metric for assessing the performance of the tap [8]. Fundamentally, the torque required for forming internal threads should depend on the work material, tap geometry, percentage of thread height, spindle speed, metal working fluids and drilled hole diameter. Monitoring of mean and peak torque is necessary, since an excessive torque requirement may lead to tap breakage or failure. Typically, thrust force remains fairly constant within ±5 % of the mean value when using the same tool geometry and process parameters for form taps under lubrication conditions. Landeta et al. [6] reported similar behaviour of thrust forces in tapping.

In form tapping, the drilled hole diameter is bigger than the thread minor diameter unlike in cut tapping, where the hole diameter is equal to the minor diameter of internal threads [8]. Equation 1 is widely used in industry to determine standard hole diameter [7]. Selection of the correct drill diameter is mandatory to maintain proper thread height percentage. The best practice for this selection is based on 65-75 % of thread height for non-ferrous alloys. The thread height percentage increases as the diameter decreases, but the chances of tap failure are higher due to a greater torque. On the contrary, the split crest can be kept small by using a smaller hole diameter [8],[26],[27]. Agapiou reported that both mean and peak torque increased along with the hole diameter. Thrust forces did not vary with thread percentage. The standard deviation for every torque dataset was surprisingly large, which indicated that the torque signal variation is higher with higher thread percentage [8]. It was also reported that thread shear strength increased with higher thread percentage or lower hole diameter due to greater work hardening [8].

$$D_H = D_M - \frac{\%Thread * P}{147.06} \ (mm) \hspace{2cm} \text{Equation 1}$$

The variation of mean torque and peak torque during form tapping was also studied in an effort to decrease tapping cycle time in high speed tapping. The mean torque does not tend to vary at higher speeds unlike the peak torque which increases with speed. The rotational speed in form tapping is limited due to the use of a floating tap holder. Excessive rotational speeds can lead to chatter [8]. Axial compensation with floating tap holders is recommended for tapping to account for spindle speed and axis feed mismatch. The use of a rigid tap holder can lead to frequent tap breakage due to pitch

error [8],[5]. Also, tapping speed does not have a significant effect on the formed thread's shear strength [8]. Carvalho et al. [27] showed that a forming speed greater than 80 m/min lowered thrust forces due to friction decreasing with increase in temperature.

The effect of metal working fluids on the mean torque is very significant, since heat generated in forming is higher than in cut tapping because of greater contact surfaces [8]. Landeta et.al [6] concluded that MWF reduced interfacial friction which resulted in lower torque but did not affect the thrust force. Since, an efficient MWF lowers both the friction and formation torque, the reduction in the friction torque component is much greater than that of the formation torque in the tapping cycle [22]. In a study, the performance of 9 oils were better than 2 water-based emulsions in terms of mean torque. It was confirmed that the viscosity of MWF had no influence on the torque and the presence of additives was responsible for reducing friction [22]. A continuous cyclic process is responsible for lowering the torque. Initially, torque generates heat which triggers the chemical reaction of additives and the MWF consequently reduces the torque [22].

In summary, the mean torque is affected by several process parameters. It is a critical parameter that needs to be monitored to evaluate the performance of form taps.

2.4 Characteristics of an internal formed thread

Plastic flow of work material in form tapping is both radial and tangential to the thread former [26]. As the thread of the form tap penetrates the work material, plastic deformation of the work material occurs radially at the crest of the tap's thread and

subsequently, plastic flow of material is along the flank, from the crest to the root of the tap's thread [7]. Thus, the thread formed on the work piece will create a split crest between the flanks of the tap's thread near its root (see Fig.6(a)).
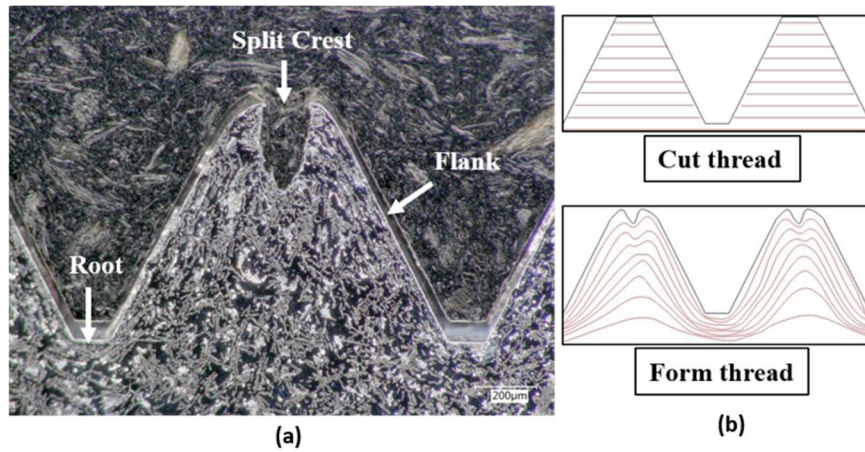
Fig.6: (a) Internal form thread (b) grain structure of cut and form threads

The geometrical precision of formed threads is superior than that of cut threads in terms of pitch error and flank straightness. The use of a floating tap holder for form tapping produced lower pitch error than cut tapping due to minimum synchronous error [5]. A floating tool holder has a spring component which absorbs any synchronous error between the linear and rotational motion of the tap. Flank straightness is improved since there are no cutting edges in form taps [5]. Cutting edges on cut taps usually damage the flanks during the back travel of the tap in the hole.

The overall thread strength is greater in form threads than cut threads due to the former's uninterrupted grain structure and strain hardening(see Fig.6 (b)) [28],[29]. Strain hardening is caused by cold working of the thread formers. In past studies, micro-hardness has been extensively used to evaluate the effect of strain hardening on formed threads. Carvalho observed that micro-hardness was higher on the flanks than on the

roots [27]. Landeta et al. [6] concluded that the strain hardening effect raised micro-hardness values along the entire thread profile from its original micro-hardness. Fromentin stated that the thread root is the most deformed zone in an internal thread. The hardness of this zone increased by 90 % from its initial value due to maximum strain hardening [5],[26]. The hardness at the split crest was observed to be much lower than at the root, since there was no contact between the tool and the split crest [26]. Past research demonstrated that strain hardening is highly dependent on friction between the thread former and work material [5]. Fatigue life improvement of formed threads is caused by compressive residual stress on the flanks of a formed thread [5],[7].

The split crest is a characteristic feature of an internal formed thread. Several researchers showed that a smaller split crest was formed with a smaller hole diameter [8],[26]. This could be explained by the area measured between the split crest of the formed thread, also known as the fill rate. A higher fill rate indicates a smaller split crest. Carvalho et al. [27] reported that the fill rate of the split crest reduced with an increase in hole diameter. It was also concluded that a low fill rate indicated lower forces in form tapping since less effort was needed to deform material in the larger diameter hole. Landeta et al. [6] proposed another method to determine correct hole diameter based on theoretical calculation of the split crest area.

The ridges of the split crests may chip-off during the formed thread's use in assembly [7]. Thus, the split crest must be reduced since it weakens the internal thread. Warrington et al. [7] performed a single-tooth level scratch experiment to understand thread formation. The authors concluded that attack angle (degree of crest relief at the

lobe) and cross-sectional lobe width are the most crucial parameters for determining the shape of the crest. The scratching speed had no effect on the crest's shape. The split crest region was stated to be a potential source of nucleation points for fatigue cracks. Smaller attack angle led to a smaller split crest area which can be beneficial for improving thread strength and reducing fatigue wear.

Formation of the split crest also depends on the lubrication in form tapping. It was found that the split crest was worse in emulsion than in oil. Strain hardening of the threads produced with the application of emulsion was much greater than with the oil [22]. Difficulty in successive plastic deformation of the already hardened surface led to a larger split crest in the case of emulsion. Also, lack of sufficient lubrication can increase frictional forces. With higher frictional forces, the fold-over of the side ridges increases, and the split crest tends to get worse [30].

In recent simulation studies of thread formation, the effect of temperature rise in split crest geometry was insignificant[30]. Usually, a temperature rise in forming can lead to thermal softening as well as reduced flow stress and forces. The influence of the entry taper angle was found to be significant in the split crest size. Bottoming taps with a larger entry taper, i.e. lower number of chamfered threads, produce a smaller split crest than plug taps [30]. This is due to the smaller ridge fold-over with few passes.

The conclusion drawn from the above discussion is that, formed threads are much better than cut threads, provided all efforts are made to reduce split crest formation.

2.5 Machining of Die-cast Al-Si alloys

In the 1950s, the die cast Aluminum-Silicon alloys were commercially used to produce engine blocks due to their high strength over weight ratio, good thermal conductivity, higher wear resistance and excellent castability, and lower coefficient of expansion. Engine blocks with cast iron cylinder liners were expensive to produce. As a result, hyper-eutectic and nearly eutectic aluminum- silicon alloy cylinder blocks were developed without liners. These alloys have greater wear resistance as well as scuffing resistance since the surface preparation of these alloys allow the exposure of hard Si particle on the surface. This arrangement provides better load bearing capacity by preventing adhesion to the Al matrix [31].

In the past, research focused on explaining the wear mechanism common in Al-Si binary alloys. Generally, transfer of material between interacting surfaces is observed in the sliding wear system of this alloy due to the heat developed during friction causing adhesion at welded joints [32]. It was found that this layer of transferred material is observed at certain combinations of speeds and normal loads, especially at a high load and low speed [33].

Su [2] found that a harder matrix can withstand greater loads before plastic deformation occurs. As such, heat treatment of the Al matrix is necessary to harden the matrix and to form spherodized Si particles [32]. Also, plastic deformation in the α-Al matrix may cause fragmentation of brittle Si particle due to its low fracture toughness. This layer of Si debris is highly abrasive and gets embedded into the Al matrix, resulting in increasing shear stress. The author experimentally found that higher sphericity, i.e

rounder Si particle, could have a lower influence on wear volume than irregular, acicular Si particles. This is due to the greater plastic stress of spherical Si particles than plate shaped ones. As such, greater sphericity and a harder Al matrix is preferable for better wear resistance [2]. Moore [34] concluded that sharp edge primary Si particles contribute to the higher wear volume of mating surfaces compared to plate type eutectic Si precipitates in the matrix (see Fig.7(b) and 7(c)).
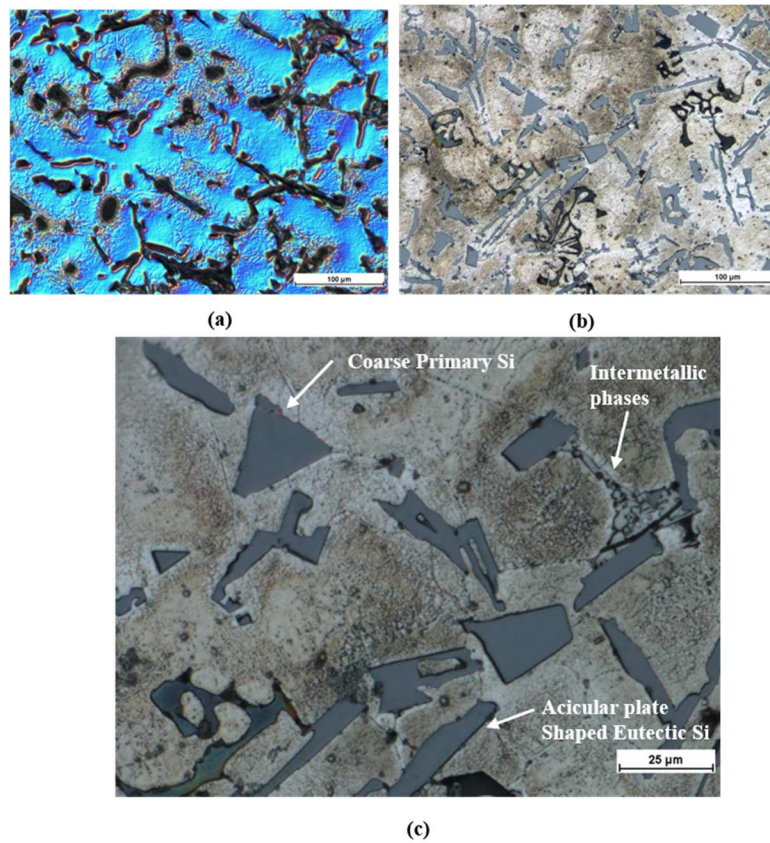
Fig.7: (a) Micro-structure of Al-6Si alloy, (b) Al-12Si alloy, (c) different constituents of Al-12Si alloy

In order to improve the mechanical properties of the Al-Si alloy, common alloying elements such as copper, manganese, magnesium, iron, zinc, nickel, phosphorous etc. are added during the casting process. These alloying elements form intermetallic

precipitates which have a much higher hardness than the Al-matrix. Coarse, brittle intermetallic phases can easily break and produce micro-cracks [35]. Such intermetallic phases could also lead to the abrasion wear of sliding surfaces [36]. The most common non-metallic inclusions are oxides and silicates in the die-cast Al-Si alloy. Microcracks can propagate at these sites under external load since the inclusions have a weak interface with the matrix or with each other. Wear debris generation is greatly accelerated due to such inclusions. These debris particles produce classic three body wear under lubricated contacts [37],[38].

Braga et al. [39] reported that even the diamond coated carbide drill with both MQL and flooded lubrication conditions suffered a large amount of build up formation on the tool nose due to the very high adhesion tendency of Al alloys (SAE 323). This led to an increase in feed forces with the machining length. Dry drilling of B319 Al alloys with five different carbon coatings on HSS drills showed very high temperatures and extreme Al adhesion on the flutes, which resulted in poor tool life [40]. DLC coatings in drilling of B319 alloys under MQL conditions performed better than diamond coatings due to low COF, Al adhesion and residual stresses [41]. Flaking of coating at the tip and chipping on the cutting edge in the diamond coatings were caused by high residual stresses. Intensive adhesion of Al could result in plastic deformation of the contact layers. A harder coating could reduce such deformation and result in lower wear rate due to seizure.

Ng et al. [42] showed that the size of secondary dendrite arm spacing (SDAS) had an effect on tool wear of the uncoated carbide tool during the milling of W319 Al alloy.

With higher SDAS, the average silicon particle size increases in the Al matrix (see Fig.7(a) and (b)). If the perimeter length is greater than the cutting-edge radius, the chances of cutting-edge exposure to larger silicon particles are higher during the shearing process. Flank wear due to abrasion was higher with larger SDAS, i.e., coarse and bigger Si particles. The author concluded that PCD tools had lower wear rate than the uncoated carbide tools due to their superior hardness.

Kishawy et al. [36] showed that high speed face milling of A356 alloy with diamond coated carbide tools had reduced Al adhesion at 5000 m/min than at 2000m/min. The authors observed abrasive wear at the tool tip and adhesion wear mostly localized along the rake and clearance faces of the uncoated carbide tool. Abrasion wear was caused by hard Si particles scoring away the Al build-up from the tool tip. Lower abrasion wear at a distance from the tool tip was attributed to the lower normal stresses in this region than at the tool tip.

There have been a few machinability studies of the Al-Si alloy for the tapping process. Srivastava et al. [43] showed that carbide taps performed better than HSS taps in form tapping AA-A356 Al alloys. TiN coated HSS taps generated the lowest tapping torque compared to both uncoated HSS and uncoated carbide taps. Bhowmick et al. [4] concluded that uncoated HSS cut taps suffered severe Al adhesion under a dry cutting condition of 319 Al alloy. This situation led to very high torque and tool failure. DLC coating performed well as it prevented built-up edge formation due to its low COF. Zedan et al. [44] concluded that TiN-coated HSS cut taps performed poorly as the silicon content increased from hypo-eutectic to eutectic Al-Si alloys. The increase in

tapping force and tool wear was attributed to higher iron-rich intermetallic phases for Al-12 % Si alloys.

Based on past literature review, it can be clearly stated that there is a lack of research dealing with form tapping of Al-12% Si alloys. The machinability of Al-12 % Si alloys clearly poses greater difficulty in machining due to both adhesion and abrasion wear. Therefore, the current study must focus on understanding the wear mechanisms and the machinability behaviour of HSS form taps for internal thread generation in Al-12 % Si alloys.

2.6 Major Wear Mechanisms of Al-Si alloys

As stated in the earlier section, adhesion and abrasion wear are the major wear mechanisms encountered by cutting tools when machining Al-Si alloys. This section is dedicated to understanding both these mechanisms and critically reviewing the factors that limit these wear regimes.

When two surfaces under sliding contact suffer a loss of material from the softer surface due to the cutting action of harder particles (or harder surface) in the mating surface, this is known called abrasion wear. Tylczak [45] stated that plowing, micro-fatigue, wedge, micro-cracking and cutting are the five forms of abrasion wear. In the case of a single abrasive tip sliding against a surface, under lower loads, penetration depth and sliding velocity, ploughing can be defined as the lateral plastic deformation of material along the groove's sides. Micro-fatigue occurs as the cold-work hardened surface is scratched by the abrasive tip upon sliding on the work surface. Wedge formation at the front of the abrasive tip occurs when the shear strength of the contact

interface tends to be greater than half of the shear strength of the bulk material. The wedge causes greater material displacement along the direction of translation than on the sides of the groove. In the case of cutting, the abrasive tip removes material from the surface in the form of chips. The transition of ploughing to cutting action of abrasive particles is dependent on the penetration depth, sliding velocity and grit rake angle. In order to facilitate grooving by shearing, the penetration depth must decrease with higher sliding velocity (cutting velocity) of the abrasive particles. Typically, the rake angle for abrasive particles is negative but ploughing can be prevented if it is greater than the critical angle [46]. In the case of brittle materials, micro-fracture is a common mode of abrasion if the abrasive particles exert forces greater than the fracture toughness of the material.

Wear volume due to abrasion is dependent upon several factors, such as hardness of abrasives and sliding surface, abrasive grit size and shape, sliding distance and speed, as well as normal load. If hardness of the abrasive is comparable to its counter-surface, volume wear tends to be reduced [34]. Higher hardness of abrasives enables the particle to withstand its cutting edges against breaking or rounding for a longer sliding distance [45]. Shaw [47] stated that sliding surfaces could reduce abrasive wear at higher hardness values. This was in accordance with Archard's equation of volume wear for sliding surfaces [48]. The wear volume tends to increase with a larger grit sized abrasive due to formation of larger chips [45]. Moore [34] reported that an increase in wear volume tends to slow down after the abrasives reach a critical size. He also reported that sharper, angular abrasives produce higher wear volume than round, plate like

abrasives. Most research agreed that wear volume is directly dependent on the normal load [47],[48]. At a greater load, the contact points and cutting edges increase proportionally. Severe load may fracture abrasives and create either sharp or round particles which also affects the wear volume. Trezona et al. [49] concluded that abrasion wear may undergo transition from two body to three body depending on the load. The authors observed that two body abrasion occurs at high loads and three body at low loads.

Based on contact of the sliding surfaces, abrasive wear can be either two-body or three body abrasion. Two body abrasion occurs when a hard surface slides against a relatively soft surface and three body abrasion occurs due to the entrapment of harder particles between the two sliding surfaces [45]. Since the third body consists of loose abrasives that are free to roll unlike the fixed abrasives in second body, the wear rate in the two-body is much higher than in three-body wear. Gates [50] classified abrasive wear based on three severity regimes. In the first one, the mild abrasive wear is due to unconstrained, small, rounded abrasives under a low contact stress, which causes micro-ploughing. In the second one, the severe abrasive wear is caused by moderately sized, sharp abrasives partially constrained by a counter-face under moderate contact stress, which results in cutting. In the third regime, extreme abrasive wear is caused by large, strongly constrained, sharp abrasives under very high contact stresses that may lead to macroscopic deformation or fracture of the wearing surface material. However, this classification is not exhaustive, as the combined effect of both fixed particles and

loose abrasive particles, either generated during sliding or entrapped between the two surfaces, is not taken into full consideration in the study of abrasion wear.

Cozza et al. [51] performed ball-cratering wear tests to study the simultaneous action of grooving and rolling abrasive wear modes in the wear craters of the sample. The author kept the normal force constant during the wear test, but the pressure reduced gradually as the projected area of crater increased as the test progressed. Grooving abrasion occurred in the beginning of the test as the normal force of each abrasive was higher. Rolling abrasion was witnessed at a later stage, when the pressure reduced and loose abrasives between the two sliding surfaces had enough space to facilitate the rolling motion. Grooving and rolling abrasion wear occurred at different areas. Cozza and Schon [52] performed a micro-abrasive wear test to analyse the crater wear, which revealed the superposition of rolling abrasion along the grooves. The author had termed this phenomenon "micro-rolling abrasion". It was observed that lower normal force facilitated micro-rolling abrasion because smaller abrasives tend to roll along the grooves made by the larger fixed abrasives under lower normal forces. Thus, micro-rolling will occur when the larger fixed abrasive, under a greater normal force, generate grooves on the softer sliding surface and the smaller free abrasive particles roll and translate along the grooves under a lower normal force. This abrasion wear mode might be useful in understanding the wear mechanism of high-speed steel in Al-Si alloy machining, since the generation of de-bonded silicon particles might have an influence on the overall wear.

Adhesion wear is another wear mechanism commonly encountered in the machining of Al-Si alloys. Shaw [47] defined adhesive wear as loss of material from either of the two sliding surfaces under load. Welded bonds may develop between the surfaces at localized contact area. This welded material breaks away since the weld strength is typically greater than strength of either material. Attrition wear is related to smaller particles and galling to larger wear particles. Wear volume is directly proportional to the real area of contact. Rapid rise in the real area of contact may occur due to bulk subsurface flow of material. In order to have a subsurface flow, the applied load per unit area must become equal to uniaxial flow stress of the material. In order to continue plastic deformation at a certain plastic strain, the stress required is known as the flow stress. Typically, it is within the range of yield and ultimate strength.

Friction force between two sliding surfaces is generally created by surface adhesion and shearing of welded joints at real contact areas, and plastic deformation (ploughing) of the softer surface during sliding, by a harder surface or abrasives. In fact, the shearing friction force is nearly twice that of friction due to deformation in lubrication condition [53]. Since the ploughing component is mostly negligible under dry condition, the friction coefficient depends on shear strength of the junction and yield strength of the material. In the case of Aluminum sliding over high-speed steel, higher normal loads may cause more adhesion, which leads to greater frictional forces between the sliding surfaces, since the real area of contact tends to increase. The coefficient of friction is independent of silicon content, as well as its morphology, contact pressure and sliding velocity [54]. Dwivedi [32] provided an explanation for the generation of

loose wear debris in adhesion. The transfer layer at welded junctions grows and reaches a critical thickness beyond which some of the adhered material breaks away along with other material from either of the sliding surfaces. Mahdavian et al. [38] concluded that transfer of aluminum to steel and steel to aluminum was observed in the wear debris generated by the steel slider on the aluminum sample. Wear debris was flushed out of the interface by the lubricant film. Shaw [47] stated that a steady, continuous layer of lubricant between the sliding surfaces could reduce direct metallic contact and minimize wear due to adhesion.

The wear rate of the Al-Si alloy is dependent on contact load and sliding speed. As the contact load increases, the wear rate tends to increase under dry lubrication due to an increase in metallic intimacy [55],[32]. Subramaniam [56] conducted a pin-on-ring test with an Al-12.3 Si alloy as a pin on a steel counter face under dry condition. The author concluded that wear rate decreases with an increase in sliding speed until it reaches a critical speed beyond which the wear rate starts to rise. Wear particles were found to be finely equiaxed at lower speeds. At the critical speed, the wear particles became compacted and wear was minimal. The author attributed this phenomenon to an increase in strain rate with sliding speed. This will correspondingly increase the material's hardness and thus, flow strength as well, which will reduce the real area of contact and lower the wear rate until critical speed is reached. Once the speed exceeds a critical value, heavy material transfer takes place onto the steel counter face due to heat generated by the high temperature at contact points, which increases the overall bulk temperature and leads to higher asperity contact due to thermal softening.

In summary, the rate of adhesion and abrasion wear have strong dependence on the contact loads, sliding speed and the nature of contact between the mating surfaces. An interesting concept of micro-rolling abrasion was identified in this critical review. This wear mechanism considers the combined effect of both abrasion and adhesion wear. It could be applicable in this current research work, where Al-12 Si alloys will be machined under high forming loads.

2.7 Wear measurement methodologies for form taps

Machining of Al-12Si alloy engine block material with form taps mostly results in adhesion wear caused by aluminum build-up, and abrasive wear due to presence of the high silicon percentage in the alloy (see Fig.8 (a),(b),(c) and (d)). In addition, die-casting Al alloys have inclusions and higher hardness intermetallic phases which can be extremely abrasive to the tool's surface.
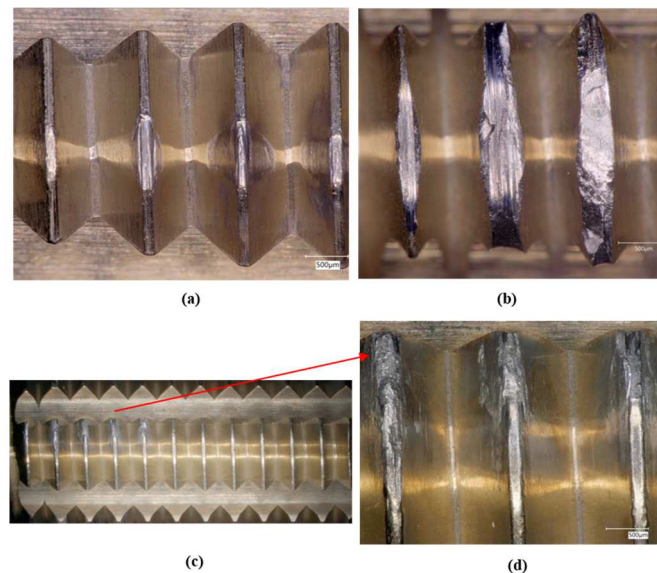
Fig.8: (a)Normal abrasion wear, (b) Unusual abrasion wear, (c) and (d)Adhesion wear

The literature review suggests that optical microscopy is the most popular process for wear measurement in the case of form taps [6],[57],[58]. This is followed by profilometers and electron microscopy which is generally used to investigate wear and identify the failure modes [58]. The existing wear measurement methodologies based on past research are discussed in detail below.

Landeta et al. [6] measured total linear wear on the crest of each lobe in the chamfered region and the successive threads of the form tap. Once the chamfered threads were worn and unable to form threads upto the nominal diameter, the successive threads would begin to perform the extra plastic work. It was also stated that every lobe in the chamfered region induced strain hardening during forming. Hence, plastic deformation by the trailing lobes in the chamfered region must consequently deform a greater amount of hardened work material. The measurement system consisted of measuring the wear on both the rake and flank edges of each crest of every thread of the tap. The total wear was the sum of wear on both the rake and relief edges measured from the central lobe point. The measurement was conducted on an optical microscope and a fixture was developed to reduce positional error. The wear on the relief side grew more than on the rake side of the crest. The rake side suffered abrasion wear. Progressive wear on the relief side was due to both abrasion and adhesion wear. Also, it was concluded that the tap wear increased along with the number of formed threads. This was confirmed by the increasing trendline of wear in the forming of 1000 to 4000 threads. It was commonly observed that the wear was higher in the chamfered threads

for the three types of TiN coated HSS taps. The guiding threads have minimal to zero wear.

Tallai et al. [57] performed tool wear analysis of five different coatings on HSSE form taps in machining commercial grade tool steel. Form tap wear was measured on the crest and the maximum wear required for tool failure was restricted to 1.5 mm. Maximum torque was monitored and an upper limit to the torque was set, beyond which the quality of the formed threads would be inferior. Although the torque had a positive correlation with wear, the wear behaviour was not explained. Furthermore, there are some discontinuities in this study such as lack of wear measurement methodology on the crest, major wear mechanism, and the wear arch measuring region. The maximum value of wear and torque, for setting the failure criterion, did not state the basis or the parameters which were considered critical for either the formed threads or taps.

In 2004, Fromentin [58] conducted an extensive study of form tapping, thread formation, thread characterization, and tool wear analysis. The author used Walter Tool-check, a four-axis digital travel profile projector, to measure the axial gap between two crests, ΔZ, and the radial increment of successive lobes, ΔR. It was concluded that all the lobes on the same thread row in the chamfered region had the same ΔR. The axial gap between the consecutive threads was kept constant. When the crest was worn, the radial change at the lobe was recorded. The length of the worn region on the crest for each lobe of the thread was measured with SEM. The wear on each lobe had increased the radial engagement of the next lobe and required extra plastic work to be executed by the successive lobes. The wear measured after tapping 100 holes was 710

µm and progressed to 1410 µm after tapping 500 holes. A rotary assembly driven by a stepper-motor was used to rotate the tap inside the SEM. The difficulty in controlling the rotational movement led to uncertainty in locating the maximum diameter point on the crest. Also, the SEM setup is impractical for industrial applications since it does not provide an on-line application. The measurement of all the lobes of the form tap consumed a lot of time, which was not effective as reported by the author. In order to compare the different stages of wear with the above difficulties, the author used different tools for wear analysis after threading a certain number of holes. The standard approach uses the same tool to understand wear progression. Hence, the suggested wear measuring methodology might not reflect a complete wear analysis.

Angular movement of the tap around the axis adds to the uncertainty in radial and tangential profile measurement. The linear measurement along the crest is performed along an arc, which is strongly dependent on the angular position of each lobe around the tap axis. This positional error of every lobe was highlighted as the leading cause of uncertainty in measurements.

In the aforementioned research works, the linear measurement of crest wear is very exhaustive, time consuming, and impractical to follow in the industry. Landeta et al. [6] provided very good wear trendlines which suggest that wear on the crest of the chamfered threads is the most important to monitor. Instead, a set of lobes can be monitored to analyze the wear progression. The wear on the other lobes will be similar and the measurement time can be significantly reduced. The fixture design has been very crucial to this linear wear measurement under am optical microscope [6][58].

There is a high chance that positioning the maximum diameter point (i.e. central point of lobe) might not be consistent and possibly cause positional errors. Since, this is the reference position for measuring crest wear, it is imperative that an effective tool fixture design is implemented to ensure the same location of reference point in every measurement during the experimentation. Repeatability of the measurements will be guaranteed if the setup and method are consistent.

Failure of internal threads, due to undesirable forming by the form tap, can be avoided if the chamfered threads are exclusively monitored. Accurate quantification of wear on the form taps will be useful in determining the maximum tap wear to prevent poor thread quality. In this regard, a standard and easy wear measurement method for form taps will ensure effective tool condition monitoring in mass-scale production in the automotive industry.

2.8 Tribological behaviour of PVD coatings in the tapping process

In the 1960s, the introduction of surface coatings for machining tools was a major advancement in the development of tool materials [47]. In tribology, a coating is designed to reduce friction, control heat generation and flow, create thermal barriers, improve wear resistance, increase mechanical load-bearing capacity, prolong tool life, and maintain part accuracy and surface integrity [59],[60].

Physical Vapour Deposition (PVD) and Chemical Vapour Deposition (CVD) are the two most common techniques for depositing coatings on machining tools. The working principle of the PVD process is to remove source material by vaporizing it in the form of atoms or molecules. These vapours are then transported to the substrate

through a vacuum. Condensation of the vapours on the substrate occurs layer by layer resulting in thin surface film formation on the tool. Vapour generation is conducted either by evaporation or by a sputtering process. In the case of CVD, it is a heat activated deposition method where typical temperatures are maintained from 800 to 1200°C during deposition [60]. In this method, the substrate must be suitably heated to react with gaseous chemical compounds. The heat energy from the substrate is used to break apart metal compounds at nearly atmospheric pressures. Since the PVD process occurs at low temperature (~ 500°C), thermal softening and geometrical distortions can be avoided in the tools [61]. Low temperatures enable use of the PVD process to deposit coatings on HSS tools [60]. PVD coated tools are designed for semi-finish and finishing processes and thus, the coating thickness is usually lower than that of CVD coatings. Also, the edge sharpness is higher in PVD coated tools due to better control of coating thickness in deposition [60].

Generally, the coating system consists of the coating, interface and the substrate. Holmberg et al. [62] stated that the behaviour of a coating system depends on the hardness of coating and substrate, coating thickness, roughness of sliding surface and interaction of abrasive particles during sliding. Soft coating on a hard substrate behaves in a different manner than hard coating on a soft substrate. A soft coating is usually preferred for reducing friction and tensile stresses. Cracks due to surface tensile stresses can be prevented with softer coatings. Typically, soft coatings have low shear strength to reduce friction. Ploughing and plastic deformations of the tool surface are reduced in the case of a hard coating on a soft substrate. With the increase in hardness, load

bearing capacity of the surface is improved. Thus, friction and wear of the tool is lower in hard coatings. It is important to note that substrate hardness should be sufficient to prevent any plastic deformation of the substrate. Thin hard coatings often fail due to brittle fracture caused by substrate deformation.

Karlsson [61] broadly classified hard coatings into monolayer and complex coatings. Complex coatings can be subdivided into multi-layer coatings, multi-component coatings, multi-phase coatings, composite coatings and gradient coatings. Multi-layered hard coatings can withstand much greater mechanical loads than mono-layered coatings. This is attributed to the resistance of crack propagation of multi-layered coatings. Cracks that develop on the surface layers are prevented from growing by the next layer underneath. As such, the multi-layered coatings are more durable than monolayer coatings. Chowdhury [63] also classified hard coatings as above. In addition, the author reported that self lubricating coatings such as TiN-MoS_2, $TiAlN$-MoS_2 have lubricious layers embedded over hard coatings. However, since MoS_2 lubricious layers reduce friction and prevent seizure in stamping tools, this coating is thermally unstable. Self-adaptive coatings such as TiB_2 can overcome this limitation by generating certain beneficial tribo-films at certain specific operating temperatures. Therefore, the design of PVD coatings is highly dependent on the tribological conditions between the tool and workpiece of a process.

The selection of a coating is mainly dependent on its desired function in the process. If wear-resistance of the tool needs to be improved, then the primary wear mechanisms in the specific machining process must be identified.

In the automotive industry, usage of internal threads is very significant considering mass scale production of parts. As such, process stability is based on the reliability and productivity of the taps in the manufacturing line. From here on, the performance of several PVD coatings for tapping applications will be summarized based on existing research.

Cut tapping of blind holes deals with process instability due to inferior chip evacuation, cold welding tendency and BUE formation on cutting edges [16]. Low wear rate of coating is desirable for protecting the cutting edge and higher stability of torque in threading. A research study was conducted on several hard and lubricious coatings on HSS cut taps for machining austenitic stainless steel [16]. TiCN demonstrated the best abrasive wear resistant performance compared to CrC, CrN and TiAlN. Also, the TiCN coating exhibited minimum cold welding at the flank and rake face. The DLC coating was found to be better than WC/C for adhesive wear resistance. The authors reported that TiCN, with top layers of DLC, generated very low torque which was attributed to lower build-up formation and lesser BUE wear. AlCrN with 70 at. % Al and 30 at. % Cr had the lowest abrasive wear rate in comparison to the lower Al content. It was also concluded that the Al content had no influence on the anti-adhesive properties of the coating.

In internal threading of 42CrMo4V, the specific forming energy and roughness of the formed threads were significantly lower when machining with TiN/DLC coated HSSE form taps than with both the uncoated and TiN coated taps [64]. The torque results for TiN/DLC coatings exhibited an interesting trend. Initially, the torque

gradually decreased down to 365 holes and then increased up to 1093 holes. This phenomenon was not explained, and tool life was reported to be 1093 threaded holes for the form tap with this coating [64].

Tallai et al. [57] tested CrTiN, AlTiN, AlCrN and two TiN PVD coatings on HSS form taps for generating internal threads in 40CrMnMo7 tool steel. The authors reported that AlCrN performed better than the other coatings. Although the AlCrN coated taps had a lower wear intensity and torque, this behaviour of the coating was not explained with respect to the forming process. The wear pattern or mechanism was not mentioned in this publication.

Landeta et al. [6] concluded that TiN coated HSS form taps produced " OK" threads up to 5000 holes while machining HR 45 micro-alloyed steel. TiN coating wear occurred on the crest at the lobe region. Abrasive wear on the lobes generated higher torque in tapping.

Bhowmick et al. [4] tested the performance of DLC coating with uncoated HSS cut taps under various lubrication conditions. DLC coatings prolonged tapping life and lowered the steady average torque during tapping which indicated that DLC prevented Al adhesion. Significant thermal softening of work material was observed when machining with HSS taps under dry machining because of higher temperatures generated. This is attributed to higher friction between sliding contact surfaces between the tool and workpiece. Lower torque and higher subsurface hardness (than bulk hardness) were due to the low COF of DLC in both flood lubrication and fatty acid MQL conditions.

DLC coatings on carbide cut taps showed the highest performance due to the lowest torque generated in the machining of the AlSi9Cu3 alloy [65]. Smoother chips indicated the lowest or minimal BUE on the tool. Hence, DLC coatings have lowest tendency for BUE in low-speed cut tapping of nearly eutectic Al- Si alloys. Even though the egg-shell effect, associated with a hard surface on a relatively soft material, deteriorated the cutting edge, there was minimal wear on the DLC coated carbide cut taps. No tool failure was observed up to 1100 holes and the tool life was not estimated [65].

Self lubrication mechanisms in hard coatings such as DLC are responsible for extremely low friction coefficients. The interfacial transfer layer generated upon sliding have very low shear strength [66]. This phenomenon makes DLC coatings very popular for aluminum alloy applications.

Carvalho et al. [27] observed that TiN coating performed better for smaller diameter holes compared to uncoated HSS form taps during tapping of AM60 magnesium alloy. Thrust force and torque reduced as the hole diameter increased. An optical inspection of the thread profile showed that the saw shaped crest was formed by the TiN coated tap due to the ploughing effect. The coating's high coefficient of friction led to increased adhesion of work material to the tap. This caused ploughing of the material during the tool's displacement.

Srivastava et al. [43] performed tapping in two foam casting aluminum alloys containing 6-7 % Si (% weight). TiN coated HSS taps generated lower average torque than uncoated HSS form taps. Abrasive wear of the taps was related to the primary silicon particles and hard intermetallic phases which were either iron-rich or copper-

rich. AA-356 alloy had fewer but larger primary silicon particles than the AA 319 alloy. These particles were found to be shattered on the surface of drilled holes. This drilled hole surface condition caused greater abrasive wear in the machining of AA-356 alloys.

The literature review on the application of PVD coating on taps highlights a limited understanding of the coating's tribological behaviour in internal thread generation processes. Moreover, only a few researchers have investigated PVD coating performance in form tapping. In general, abrasive wear resistant coatings on the HSS substrate of form taps is very popular for machining ductile grades of steel and aluminum-silicon alloys in industry. Considering the growing popularity of form taps in the automotive industry, there hasn't been much research on the development of PVD coatings for form tapping high silicon content aluminum alloys. The current research will focus on studying the performance of various PVD coatings in the threading of Al-12 % Si alloys for automotive applications.

2.9 Metal working fluids in machining Al-Si alloys

Metal Working Fluid (MWF) acts both as a coolant and lubricant in machining processes to improve the tribological conditions at the tool-workpiece and chip-tool interfaces. The major functions of MWFs in machining are the following — to reduce heat generation by reducing friction between tool and workpiece, to improve the chip removal from the cutting zone, to avoid thermal damage of work material and to reduce tool wear [67],[47],[68].

Tapping is one of final finishing processes which is mostly used in engine block manufacturing. This process is highly dependent on the preceding drilling performed

on the workpiece. Since drilling and form tapping of aluminum silicon die-cast alloys must be performed with MWFs due to the higher tendency of Aluminum adhesion; it is imperative to determine a sustainable, eco-friendly and efficient MWF performance comparable to the existing commercial MWFs [69],[4].

Formulation of commercial, mineral-based MWFs with anti-wear and extreme pressure additives has been a favoured practice in industry to enhance the lubrication performance in machining [70]. Anti-wear additives reduce abrasion between the sliding surfaces by physisorption and extreme pressure additives generate adsorption layers that prevent micro-welding at surface asperity contacts [68]. Fromentin et al. [22] concluded that oil with additives based on sulphur performed better than oils with chlorine during form tapping. The high temperature generated at the lobe region of a form thread created favourable conditions for chemical reactions to form chemically adsorbed layers of sulphates and sulphonates. The good anti-friction behaviour of these layers in form tapping reduced torque. In the recent past, applications of mineral oils in the machining industry has become challenging due to growing awareness of its disadvantages such as limited biodegradability, toxicity, poor disposal management, pre-mature ageing due to microbial contamination, high cost of maintenance and operational hazards [68]. These negative effects of mineral oil based MWFs pose a serious threat to the environment and industry.

Recently, a novel gel-based coolant known as a Superabsorbent coolant (SAC) was developed, which has proven to be very effective in turning and milling operations [71]. SAC is an emulsion of superabsorbent polymer in which graphite nanoparticles were

suspended. Superabsorbent polymer (SAP) is a type of material which can absorb liquids up to several hundred times its weight. The sedimentation of nanoparticles over a period and the subsequent liberation of nanoparticles into the environment might pose an environmental hazard depending on the nanoparticles used in the MWF. This separation of nanoparticles from the solvent might alter the lubricity and thermal conductivity of the fluid. The addition of superabsorbent polymer stabilizes the solution by enhancing the penetration of nanoparticles in the porous network of the polymer. Thus, the SAP maintains the required lubricity and cooling effect in the high-temperature plastic deformation zone during machining. This new MWF was noted to be environmentally friendly since its gel-based nature reduces flood coolant requirements. It is operator friendly due to low evaporation and consequently less exposure. This novel MWF has never been tested in drilling and tapping applications.

Vegetable oil-based lubricant such as jatropha, rapeseed and sunflower oil are increasingly considered as sustainable MWFs in machining due to their high lubricity, low operator hazards, environmental-compatibility, longer service life, and low maintenance costs [72],[73],[74],[67]. Generally, vegetable oil consists of Triacylglycerides, which are glycerol molecules with three long chains of fatty acids bonded through an ester linkage. High polarity of fatty acids in vegetable oil can be attributed to its stronger interaction with metallic surfaces, which provides a high strength boundary film to reduce both friction and wear. The triglyceride structure of the sunflower oil, with higher level of poly-unsaturation, has poor oxidation stability. The unsaturated double bonds in the fatty acids are active sites for oxidation when in

contact with metals that act as a catalyst even at room temperature. Auto-oxidation can be initiated by free radicals formed out of the removal of a hydrogen atom from the methylene group next to a double bond. These free radicals react with oxygen to form peroxy radicals that then attack another fatty acid, generating more free radicals and thus propagating the oxidation process [75]. The rapid degradation of vegetable oil due to low oxidation stability is the major hindrance to its use in the field of machining. Fox and Stachowiak [75] suggested that antioxidants such as peroxide decomposers and radical scavengers can be added to the lubricant to reduce peroxide accumulation and oxidation of double bonds. Most publications recommend the use of ZDDP with antioxidants, but ZDDP acts as an antagonist to antioxidants. In fact, Asaduakas et al. [76] observed that neat vegetable oil performed better than neat oils with antioxidants, because under such a combination, the wear was greater than neat oils in a four-ball wear test.

Evaluation of MWFs for subsequent operations, such as drilling and tapping processes, provide a complete understanding of the tribological conditions for formulating the correct lubricants and coolants [73]. Belluco and Chiffre [73] reported that the tapping operation will be uncontrolled if the drilled hole diameter is inconsistent. This could be attributed to the poor performance of MWF in the drilling process. The authors stated that BUE formation and adhesion on the drill often leads to oversized drilled holes and consequent reduction in tapping torque. Bhowmick et al. [4] reported BUE and chip clogging in the flutes as common problems associated with poor lubrication. Cut tapping of 316 stainless steel with additive enriched vegetable oil,

produced strain hardening similar to that of mineral oil [74]. This vegetable oil with additives performed well in the tapping tests considering its environmental compatibility and comparable performance to mineral oils. In the past, several researchers concluded that MWF reduced interfacial friction which lowered the torque but did not affect thrust force [6],[22],[4]. Srivastava et al. [43] demonstrated superior performance of high concentration MWF in significantly reducing tapping torque during the machining of AA-319 and AA-A356 aluminum-silicon alloys. Bhowmick et al. [4] concluded that high temperature generation promoted excessive Al adhesion during cut tapping of 319 Al alloys with HSS taps. The temperature rise was attributed to high COF between the two contact surfaces. The application of minimum quantity lubrication with sulphur and phosphorous based additives significantly reduced adhesion.

There is a lack of research literature on MWFs for Al-12Si alloy form tapping. Most comparative studies evaluated the performance of additive enriched vegetable oils with respect to mineral oil-based MWFs. In order to fully explore sustainable alternatives for commercial MWFs, a pure vegetable oil in water emulsion and SAC could be studied for form tapping applications.

Chapter 3. Experimental Procedure

3.1 Workpiece properties and preparation

The workpiece material used in this experimentation was ADC-12, which is a die-cast Al-12Si alloy of JIS grade for engine block application. This Al-12Si alloy has undergone T6 solution heat treatment (artificial aging). Its chemical composition and mechanical properties are equivalent to A383 aluminum alloy. The chemical composition and mechanical properties of this alloy was given in Table 1 and Table 2 [77]. The microstructure of this alloy was studied using optical microscopy. It was observed that the α-Al matrix consisted of coarse primary Si precipitates, plate shaped eutectic Si and several intermetallic phases (see Fig.7). The flat surface was prepared by facing the ingots for the actual drilling and tapping tests. Every ingot was drilled and tapped in a zig-zag pattern to get a maximum of 360 holes (see Fig.9). A height of 45 mm from the largest face of the ingot was kept untouched to avoid any interference with porosity during tapping.

Table 1—Chemical Composition of die-casting ADC12 Aluminum-Silicon alloy

Chemical Composition									
Element	Cu	Si	Mg	Zn	Fe	Mn	Ni	Pb	Sn	Al
Weight%	1-4	10-12	~0.3	~2.5	~1.3	~0.5	~0.5	~0.2	~0.3	Rest

Table 2—Mechanical Properties of die-casting ADC12 Aluminum-Silicon alloy [77]

Mechanical Properties					
Yield Strength (0.2% offset)(MPa)	Ultimate Tensile Strength(MPa)	Hardness (BHN)	Young's modulus(GPa)	Elongation (% in 50 mm)	Poisson ratio
152	310	80	71	2-4	0.33

Fig.9: Workpiece preparation

3.2 Tooling selection

Based on industry requirement and past literature review of form taps for machining Al-Si alloys, a standard bottoming M8 HSS form tap of standard tool steel grade was used for the entire experimentation (see Fig.10). Table 3 presents the specifications of the drill and form tap provided by the industry partner. Several PVD coatings were tested on the form taps. The detailed information about the selected coatings has been provided in Chapter 5.

(a)   (b)
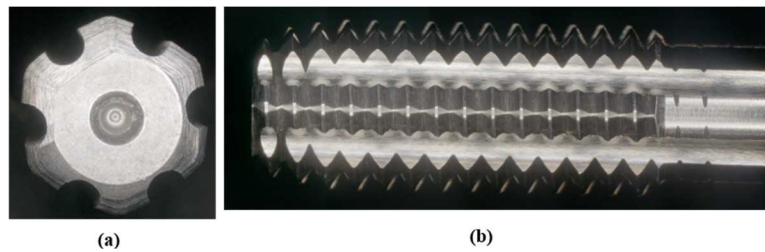
Fig.10: (a) Side view of M8 x 1.25 form tap, (b) top view

Table 3—Specifications of the drill and form tap

Drill	Tap
Type: Metric, no coolant through	Type: Metric, Bottoming Form tap, 3 threads chamfer, 6H
Material: Coated Carbide (TiAlN)	Material: uncoated and coated High-Speed Steel
Diameter: 7.35 mm	Diameter: 8 mm
Point Angle: 135 °	Pitch: 1.25 mm
Flutes: 2 (straight)	Grooves: 6, straight
Flute length: 54 mm	Thread height: 74.12%
Make: Guhring	Make: Balax

3.3 Process parameters

In order to replicate the exact machining conditions of the industry, the machining process parameters, were restricted to those suggested by the industry partner for both drilling and form tapping tests (see Table 4). The drilling speed was slightly improved to reduce aluminum adhesion. The drill hole diameter for a M8 form tap was controlled such that the thread height was almost 74 %. Drill hole depth was kept larger than thread hole depth so that the chamfered threads of the form tap could be accommodated once the desired threaded length of hole was obtained. Feed of the form tap is a very important parameter for avoiding any pitch error. The product of spindle speed and pitch gives the feed for the tapping process. A floating type tap holder with a quick-change adapter was provided by the industry partner to compensate axially for any synchronous error between spindle speed and feed during tapping. The industrial practice for drilling and tapping operations is flood lubrication for this work material. A commercial MWF—Castrol Hysol™ MB 50 was employed for experimentation in this research.

<p align="center">Table 4—Process parameters for drilling and form tapping</p>

Parameters	Drilling	Form-tapping
Nominal diameter, mm	7.35	8
Hole Depth, mm	25	19
Spindle speed, RPM	3960	1000
Feed rate, mm/min	1188	1250
Flood-MWF	Castrol Hysol™ MB 50	9-10 % (emulsion concentration)

3.4 Fixture Development

In this research, a considerable amount of time and effort was spent developing a fixture for easy and accurate handling of workpiece and form taps. An account of the

challenges that required the development of several fixtures will be provided later. In addition, the advantages of each fixture in terms of its functionality and design will be stated below.

Fig.11 shows the fixture for holding the aluminum ingots on the machine table of the horizontal CNC machine. The length and shape of an ingot posed serious clamping and pre-processing issues in the CNC. Since the ingot was much longer than the machine table, a fixture table was designed to provide a stable and larger clamping surface. The trapezoidal surface of the ingot was very uneven, and the machining of multiple faces was required to get a flat surface for drilling and tapping. The fixture was designed for the ingot's push-fit arrangement along with three locking screws underneath the fixture table. This design reduced initial setup and pre-processing time from 40 minutes to 10 minutes. Only the front side facing operation was required for the tests.

(a) (b)
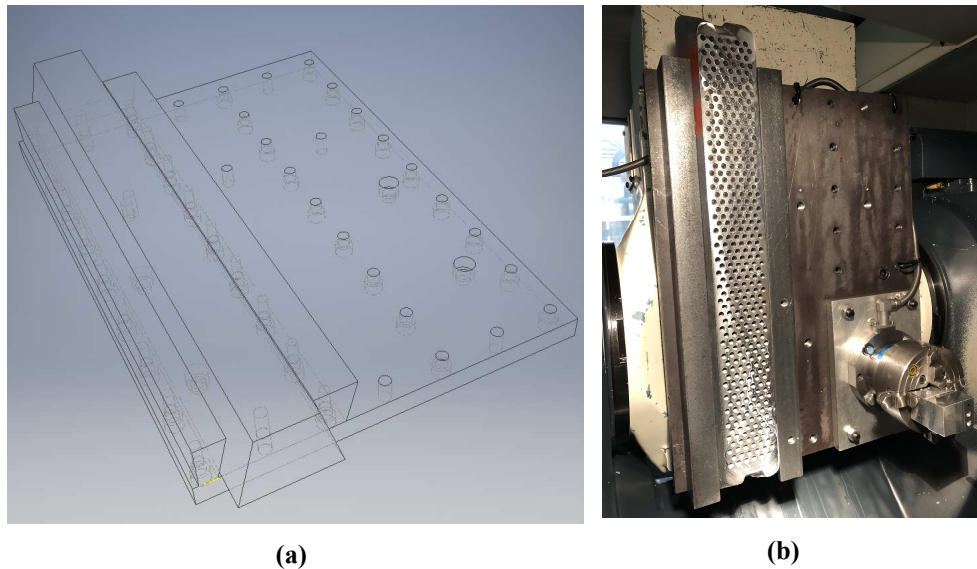
Fig.11: (a) Design of workpiece fixture, (b) application of fixture in tests.

Fig.12 shows the floating holder connector for fixing the floating type tap holder to the HSK A100 weldon-shank type tool holder. This floating type tool holder was provided from industry to axially compensate for any synchronous error between feed and spindle speed. A simple customization of a cylindrical shaft allowed the weldon-shank holder to be assembled with the floating tool holder.
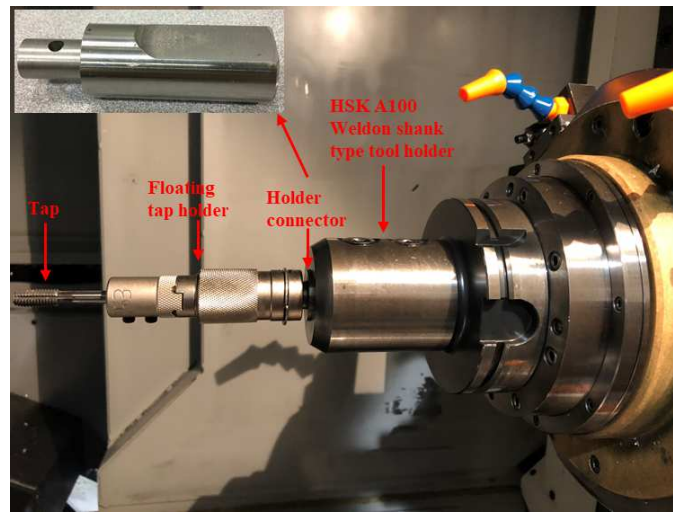
Fig.12: Floating holder connector

One of the most critical fixtures developed in this research was the fixation unit for tool-wear measurement (see Fig.13). Linear wear measurement using optical microscopy repeatedly demanded positional accuracy of the chamfered threads during the entire testing process. The fixture was designed in such a way that the v-shaped locating pin could be positioned over a groove, arresting any rotational motion of the tap. This feature of the fixture enabled very accurate positioning of the centre point of the crest over the lobe . This point of reference was used for measuring wear on the crest of second and third chamfered threads. The detailed methodology of linear wear measurement is provided in Chapter 4.
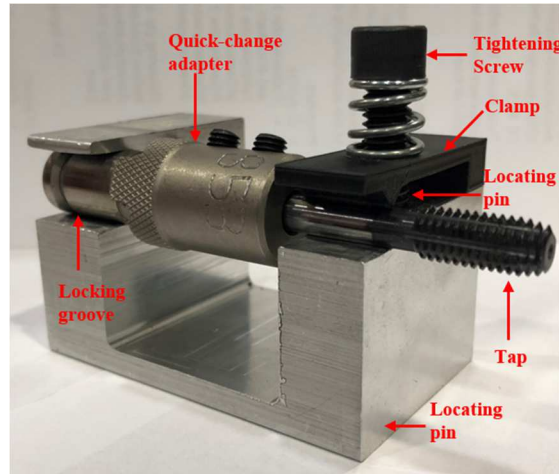
Fig.13: Fixture for tool wear measurement

Fig.14 shows a simple fixture designed for easy clamping of the tool during SEM. Since the tool was longer than the diameter of the SEM table, the tool overhang was repeatedly lifting the tool from the table. As working distances in SEM are kept very small in the range of 10 mm, proper clamping of the tool was indispensable for the security of the detector. A modified 3D printed stud promptly solved this issue.
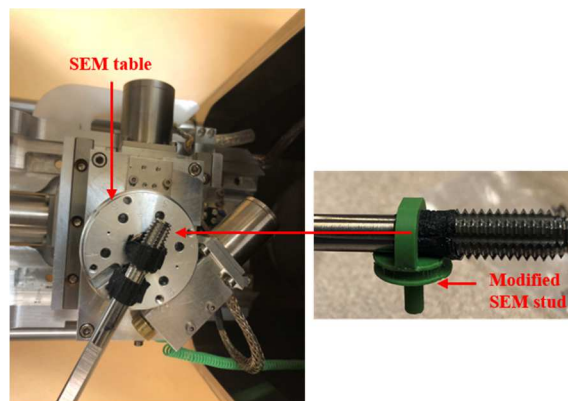
Fig.14: Tool fixture for SEM table

3.5 Experimental Setup

The drilling and tapping tests were performed on a Makino M56, 5-axis CNC milling centre with spindle power of 52.4 kW and a maximum spindle speed of 15000

RPM. Fig.15 shows the horizontal machining setup which ensured swift evacuation of chips during drilling under flood lubrication conditions. Initially, facing was performed to generate a flat surface on the aluminum ingot. Then, an optimized zig-zag pattern for drilling was selected by considering two important factors. First, drills and taps must not interact with the pores in the ingots, thereby providing enough clearance. Second, the maximum number of holes must be machined since drilling and tapping tests are material intensive and uneconomical processes. A total of 360 holes were machined on every ingot. A floating type tap holder, mounted on an HSK A100 Weldon-shank holder, was selected for the tapping tests to provide any axial compensation required during tapping.
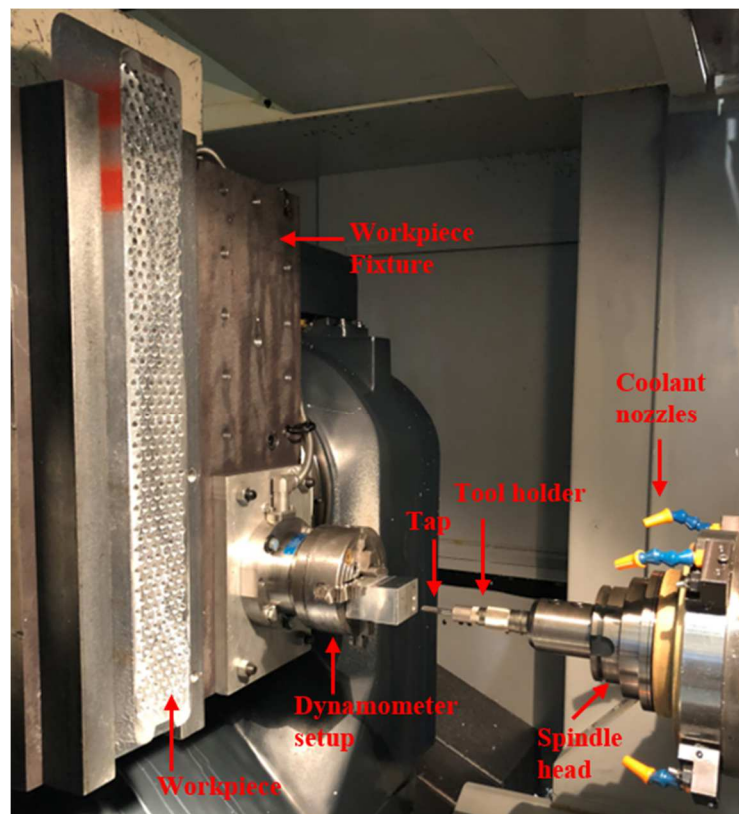
Fig.15: Experimental setup for drilling and tapping tests in the horizontal CNC machine

Fig.16 shows the dynamometer setup for measuring torque during the drilling and tapping processes. A smaller block of workpiece material was mounted on a 9272 Kistler stationary 4-component dynamometer. The dynamometer was rigidly fixed to the workpiece fixture. It is recommended by Kistler to measure forces at the centre of the dynamometer to obtain the most accurate results. The block on the torque dynamometer was shifted every time to get the centre position of the dynamometer for recording torque. The sampling rate was fixed at 5000 Hz. The force data was collected via a DAQ card and processed using National Instruments LabView 2014 software. The forces and tool wear were measured after every 360 holes. The mean and maximum torque for the forward motion of the tap cycle has been analyzed in this study.
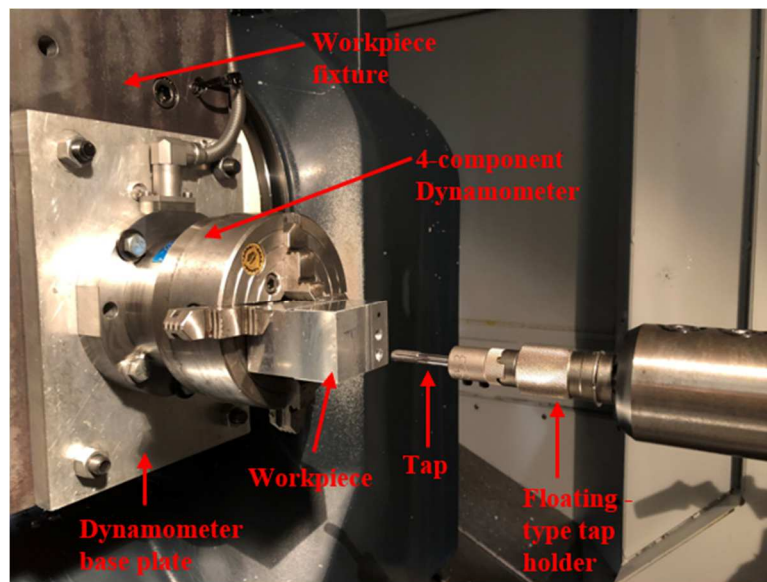
Fig.16: Dynamometer setup

The two methods for quantifying tool wear in this study are linear and volumetric wear measurements on the crest of a tap's thread. A Keyence VHX 5000 digital microscope was used to measure the wear on the crest. A fixture was designed for tool

inspection under this microscope to locate the maximum diameter point on the crest. The volumetric wear measurement was performed using Alicona Infinite Focus equipment which is based on white light interferometry with focused variation. The 3-jaw chuck with rotational control unit on the Alicona equipment was used for inspecting volumetric wear of the second and third chamfered threads. A detailed description of both linear and volumetric wear measurements is given in Chapter 4. The pre-tapped hole diameter was frequently checked with a Zeiss Prismo Coordinate measuring machine (CMM). Surface morphology of the worn tool was inspected with scanning electron microscopy (SEM). Elemental analysis was performed to investigate coating wear patterns. SEM was performed on TESCAN-VEGA II LSU SEM and JEOL 6610LV SEM at 20kV. Elemental maps were processed using the INCA Software from Oxford Instruments. An ISO thread plug gauge of M8 x 1.25 mm dimensions was used to periodically check the condition of internal threads.

Chapter 4. Study on wear mechanism and wear measurement methods

The objectives of this study are as follows:

❖ Investigate the failure modes and establish the dominant wear mechanisms of uncoated HSS roll form tap for machining die-cast Al-12Si alloy.

❖ Propose and develop wear measurement methodology specifically for form taps.

❖ Develop a performance criterion for a short machining test to perform comparative wear study on form taps.

4.1 Necessity for a wear measurement methodology

There has been limited research on the wear of form taps in the previous literature. There is no concrete literature which investigated the tool life of a form tool. Landeta et al. [6] conducted an extensive study on the tool wear of TiN coated HSS-E M10* 1.5 roll form taps of three different types – 5 pitch chamfer- hexagonal shaped lobes without oil grooves, 3 pitch chamfer-pentagonal shaped lobes with oil grooves, and 3 pitch chamfer-pentagonal shaped-without oil grooves. The taps were measured at five different stages after every 1000 threads and up to 5000 threads. These taps were obtained from industry for measuring wear. A wear measurement system was developed where linear measurement of the wear on the crest was recorded for every lobe of threads. This research indicated that the tool wear on form taps requires huge workpiece materials and machining time. As such, there were few tool life and tool wear studies in past literature. Section 2.7 provided a description of the different approaches developed by several researchers for wear measurement on taps.

The reasons to develop a wear measurement methodology for form taps are given below as follows:

- ❖ No ISO standard for wear measurement on form and cut taps.

- ❖ Limited research on measuring tap wear and wear measuring methodology.

- ❖ Previous research on tool-life study of form taps is inadequate.

- ❖ Absence of a wear failure criterion for the maximum wear limit on taps.

- ❖ To maintain the quality of threaded holes by conforming to geometrical tolerances.

- ❖ To predict periodic inspection cycle of internal threads produced in mass production by a screw plug gauge.

- ❖ To prevent scrap or rework of the parts, since a threading is one of the last finishing processes.

- ❖ Need for an easy, repeatable and accurate wear measuring system.

In this study, a performance criterion for the form taps will be developed for the following reasons:

- ❖ To establish a wear mechanism of the form taps in machining Al-12Si alloys which is absent in the past literature.

- ❖ To understand wear propagation and to quantify wear on both crest and flanks of a thread on the tap.

4.2 Preliminary Study of standards

In order to study the metric form taps, ISO 68-1: 1998 (see Fig.17) relates the pitch and the fundamental triangle height to obtain the basic dimensions of the internal thread such as major, minor and pitch diameters [78]. The fundamental deviations and tolerances specified in ISO 965-1 are applied to the basic dimensions as given in ISO 68-1:1998 [79].
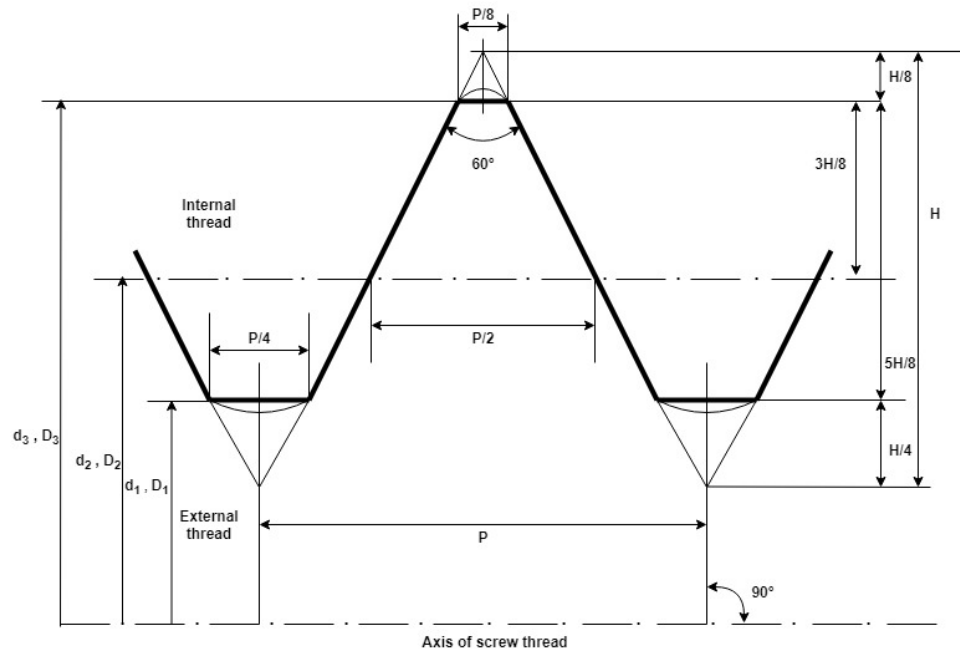
Fig.17: Basic profile of a metric screw thread[78]

As per ISO 1502:1996, the internal threads can be inspected with either a screw plug gauge or a plain-cylindrical plug gauge. The most popular gauge in the industry is the screw plug gauge [80]. A GO-screw plug gauge checks the minimum pitch diameter, considering the errors in flank angles and form deviations that might cause an apparent reduction in pitch diameter of the internal thread on the workpiece. In addition, this gauge checks the minimum major diameter and straight flank length to

ensure that rounding at the root does not affect the thread flanks. A NOT-GO screw plug gauge checks the maximum pitch diameter only and should not penetrate the thread more than two turns for an acceptable (OK) part.

The GO plug gauge is responsible for checking the minimum minor diameter and the NOT-GO plug gauge checks the maximum condition of the minor diameter. As the plain plug gauge checks only one feature compared to the screw plug gauge, the industry relies more on screw plug gauges to check internal threads.

Table 5—Design parameters of the form tap under study

M8*1.25 mm form tap, Form C type (2.5 threads), 10° chamfer, 6H	Basic Dimension	Tolerance	Actual Dimension (Min to Max)
Major diameter (D)	8	+0.024	8.110 to 8.134
Pitch Diameter (D2)	7.188	+0.020	7.248 to 7.268
Minor Diameter (D1)	6.647	+0.091	6.647 to 6.556
Pitch (P)	1.25	+/- 0.010	

4.3 Setting failure criterion based on Taylor's Principle of gauge design

According to Taylor's principle of Gauge design, the Go gauge should check maximum material condition and as many dimensions as possible. The Not Go Gauge should check the minimum material condition of the part. ISO 965-1:1998 suggests a tolerance of 160 μm on the pitch diameter of internal threads [79]. Based on Taylor's principle (ISO 1502: 1996) and M8*1.25 roll form tap design parameters, the internal threads should be checked for the following parameters to produce acceptable quality threaded holes.

For a 6H Tolerance Grade,

Tolerance on Pitch diameter for internal threads = 160μm.

GO gauge condition: Minimum limit of pitch diameter = 7.348 mm

NOT-GO gauge condition: Maximum limit of pitch diameter = 7.188 mm

Generally, the manufacturer sets conservative tolerances on tap pitch diameter to produce threads within the above ISO standard tolerances for 6H. These limits are incorporated in the "class of fit" for metric taps with 6H tolerance grade which is usually D8, D9, D10 for the M8 x 1.25 roll form tap. Each D limit is +0.013 mm as shown below. In the above case of the given tap, the manufacturer has reduced tolerances conservatively from 26 μm to 20 μm based on customer's requirements for the pitch diameter. This tolerance assures that the tap will produce internal threads with the GO and NOT-GO gauge conditions. The manufacturer assures that this tolerance on the pitch diameter of the tap will produce parts within the given tolerances as per ISO standards. Hence, the wear failure criterion for M8*1.25 form taps can be based on the manufacturing tolerances given below (see Fig.18).

Maximum acceptable pitch diameter of Tap = 7.268 mm

Minimum acceptable pitch diameter of Tap = 7.248 mm
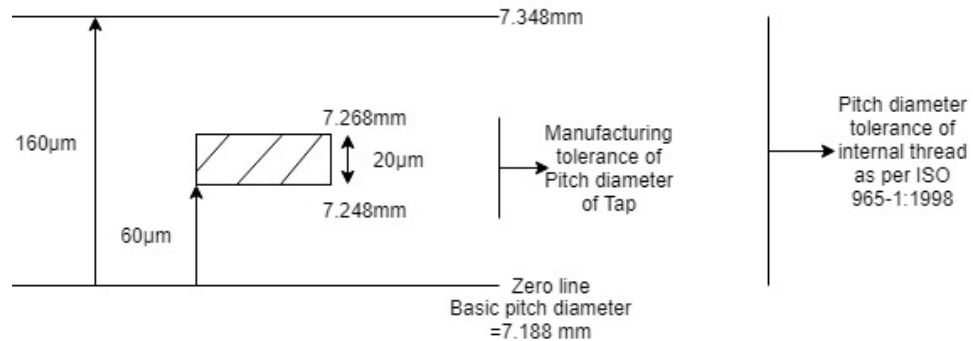
Fig.18: Tolerance zones for the pitch diameter of internal threads [80]

4.4 Description of the proposed wear measurement methodologies

Based on the literature review conducted on wear measurement method for form taps (see Section 2.7), two methods have been introduced in this research to quantify the wear. The "Linear wear" method measures the wear on the crest of the chamfered threads by optical inspection. The reference point for measurement was the centre point of the lobe with the maximum diameter. The wear on both the rake and relief edge was measured along the crest from the reference point (see Fig.19) [6] by using the fixture (Fig.13) developed for linear wear analysis using an optical microscope.

(a)   **(b)**
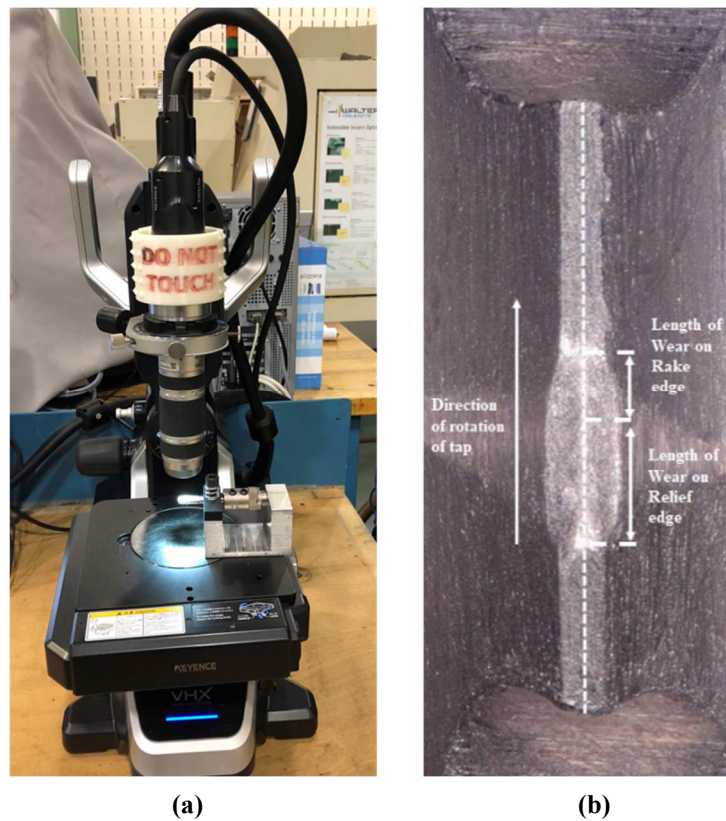
Fig.19: (a) Keyence VHX 5000 (b)Measurements on the top view of the crest

The "Volumetric wear" method quantifies the wear on the entire chamfered thread by aligning surface datasets of both new (reference) and worn taps (measured). Then,

the difference in the volume of the measured and reference surface datasets is measured (see Fig.20). The surface datasets were collected using Alicona Infinite focus equipment, which uses white light interferometry to generate the datasets. The tolerance for defect detection was maintained at 6 μm for all the difference measurements made. The volume of peaks above and below the reference surfaces gives the build-up volume and wear volume respectively.

Table 6—Proposed wear measurement methodology

|	Method 1- Linear	Method 2- Volumetric
Equipment and settings	Keyence VHX 5000 optical digital microscope, 100x, Glare Removal, Depth focus Mode, No tilt.	Alicona Infinite focus microscope, 5x lens, Real 3D scan- 60 deg., Tilt of 8.5 deg., Ring and Coaxial Lights
Fixture	Customized fixture locking oil grooves on the shank of form tap.	Self-centering 3-jaw chuck-automated rotation control.
Procedure	1. Place tap on the fixture to orient the highest point (mid-point or maximum diameter) of thread along the axis of the objective. 2. Scan the chamfered threads on only one particular lobe side. 3. Locate the midpoint using Assist tools in the microscope for the first three threads. 4. Considering the midpoint as reference, measure tool wear on the crest along the both the rake and relief edges.	1. Real 3D scan of 60 degrees is required to cover one row of threads. Consider only one lobe side for measurement in both fresh and new tap. 2. Convert the Real 3D scan to surface dataset in Alicona. 3. Use the Difference Measurement suite in Alicona to align the datasets with simple, automatic alignments until the relative displacements of aligned dataset is minimal. 4. Calculate the volumetric differences by setting the tolerance for defect detection.
Advantages	1. Easy fixturing helps locate the maximum diameter point at the same position always. 2. Very quick measurement on Keyence VHX 5000 microscope. 3. Targeting only one particular lobe side for each chamfered thread, which has maximum wear, reduces the number of measurements. 4. Repeatability of this measurement is as good as flank wear measurement on cutting inserts	1. Automatic alignments based on RGB color contrast and XYZ positions ensure maximum alignment. 2. No positional error during fixation. 3. Mean deviation in the aligned datasets are generally low. 4. Statistical analysis is based on ISO 8785:1998
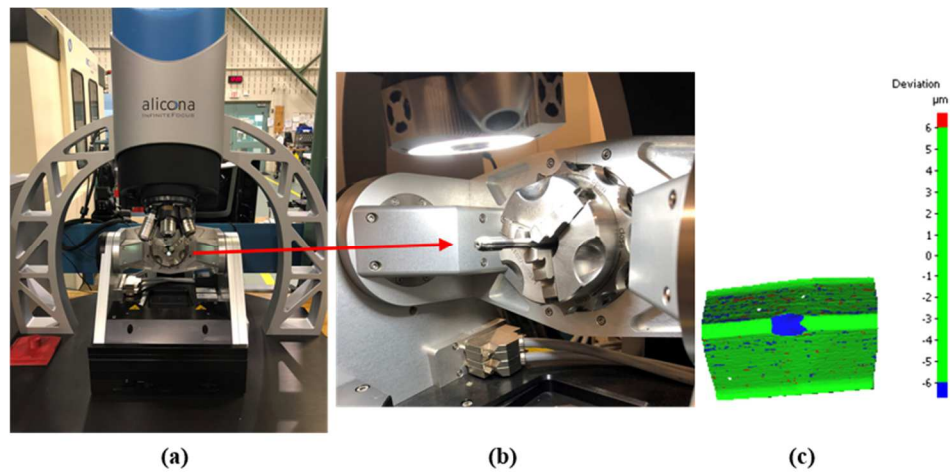
Fig.20: (a)Alicona Infinite focus, (b)3D scanning of tool, (c)volumetric difference of aligned datasets

4.5 Experimental methodology

- ❖ A progressive wear study was performed for the uncoated form tap. Mean torque monitoring, wear measurements, optical inspection, SEM & EDS of worn regions, thread gauging, and pre-tapped hole diameter checks were performed at the following stages—360, 1080, 2160, 3240 and 4320 holes.

- ❖ Linear wear measurements were conducted for the second thread whereas the volumetric wear measurements were performed for both second and third threads.

- ❖ A validation test was performed to confirm the torque trend and wear pattern, but it was limited to 2160 holes.

- ❖ Initiation of wear after 120 holes, and propagation of wear after 1080, 2160, 3240, 4320 holes were studied by analyzing the worn region using SEM and EDS.

4.6 Results and discussion

4.6.1 Evaluation of torque

In Fig.21, the torque response was significantly different for the first threaded hole and the 4320th hole which indicated change in tangential forces due to the change in tribological conditions caused by wear. In fact, the mean tapping torque varied by 23.2 % for the 4320th hole from the first hole as shown in Fig.21. The crest of the second thread was plucked-out at the lobe, which has resulted in the torque increment. However, the torque responses of 1080th , 2160th , 3240th and 4320th hole do not differ much, and the mean torque for the 4320th hole is 31 % higher than that of the 1080th hole.
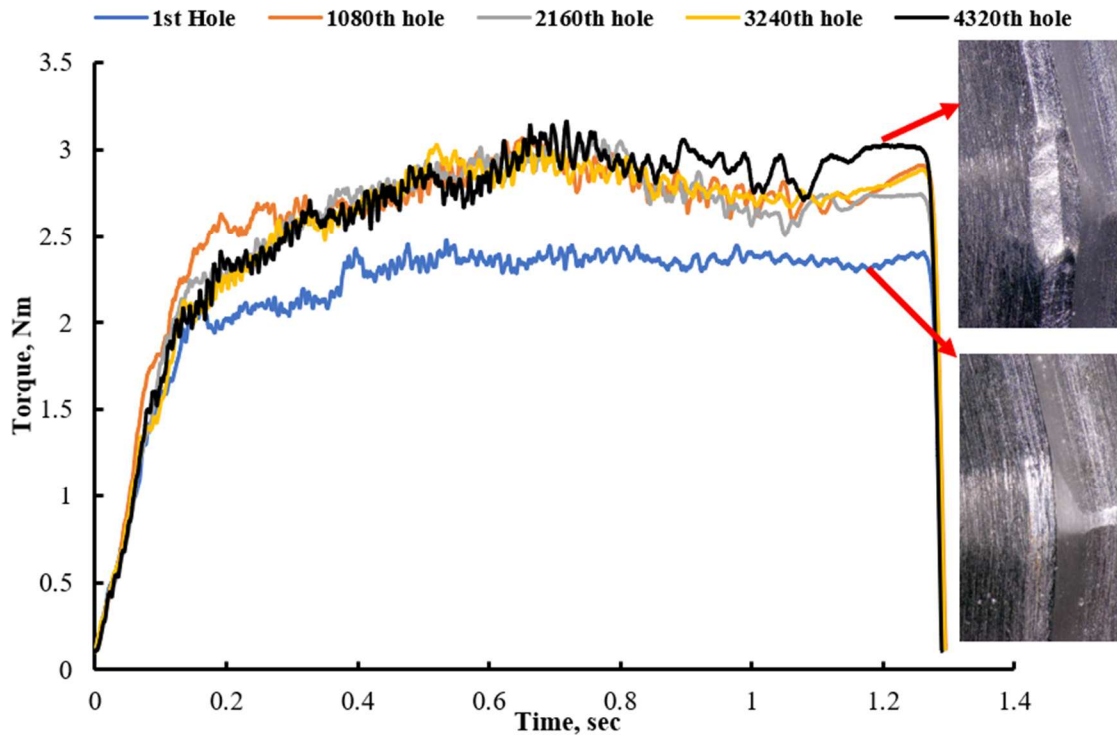
Fig.21: Time based forward torque response in tapping.

It can be observed in Fig.22 that the mean torque becomes stable after tapping 1800 holes to 4320 holes. A hypothesis might be derived that the tool wear is progressive but minimal on the crest of the second chamfered threads, and it reaches a steady wear region. The minimal torque variation is an indication of steady wear growing on the crest of the second thread. Fig.23 shows the mean torque variation of test-2 which is a repeatability test for the main test (test-1). This test proves that the torque variation due to progressive wear on the second thread follows a similar trend as the main test. Therefore, it can be concluded that the torque variation becomes minimal in the steady wear region beyond tapping of the 2160 holes.

A comparative study on the role of MWFs on the forming torque was investigated. It was observed that mineral oil had a better performance than vegetable oil and gel-based coolant. A detailed discussion of the results of this study has been provided in the Appendix B.
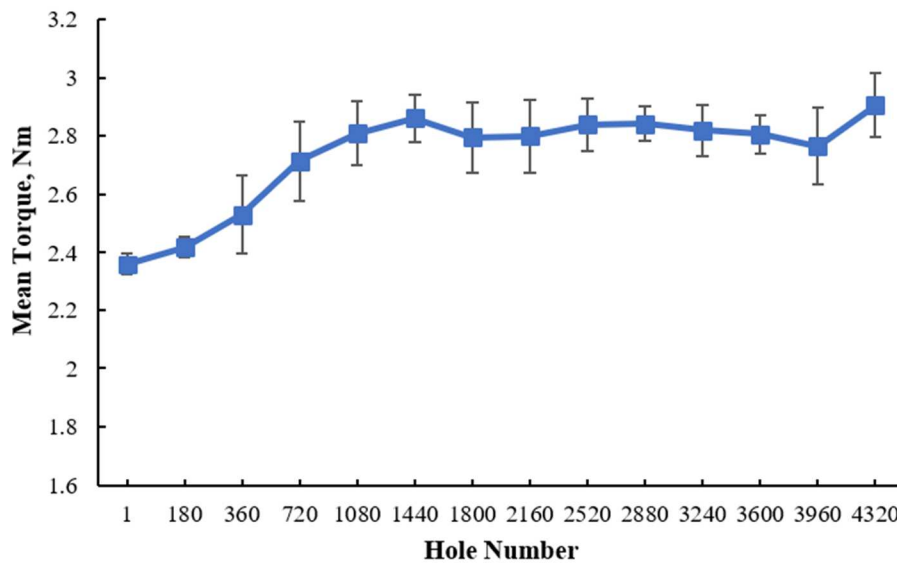
Fig.22: Mean torque of forward motion
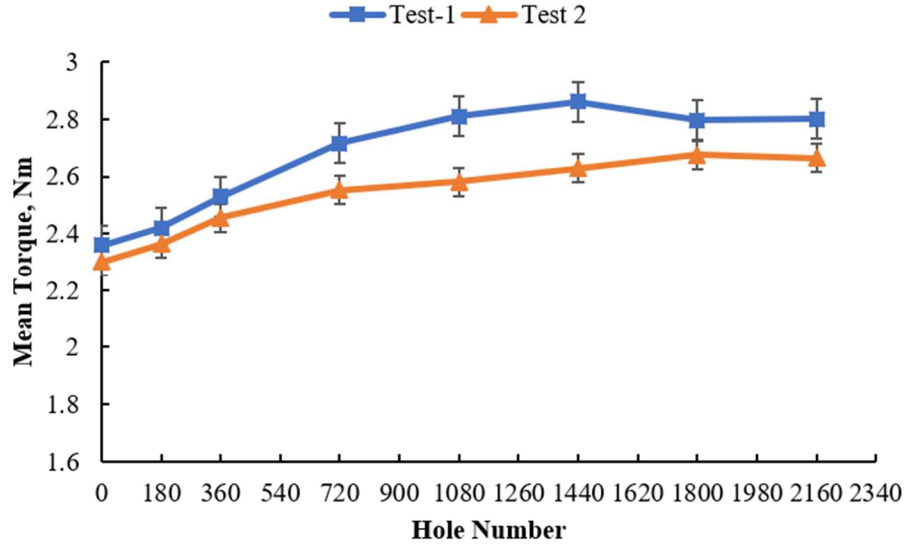
Fig.23: Mean torque of repeatability Test-2

4.6.2 Volumetric Wear Analysis

Fig.24 shows the volumetric wear comparison of the second and third threads of the tap after machining 1020th, 2160th, 3240th and 4320th holes with respect to the tap at new condition. The adhesion of aluminum material to the tap's crest and flank surface is prominently witnessed as a build-up and wear is mostly localized on the lobe of the second thread. A high tendency of aluminum adhesion to the tool's surface is expected during tapping of aluminum alloys [4]. The reference surface is the tap in new condition. Comparison of the measured surface with the reference surface showed that the volume of adhered material above the reference surface fluctuated at different stages. However, the wear volume below the set tolerance of 6 μm, was gradually increasing with further machining. Wear on the lobe of the second thread chiefly

contributed to the progressive volumetric wear. The third chamfered thread had minor

wear on the crest, and major wear on the flank neighbouring its lobe.
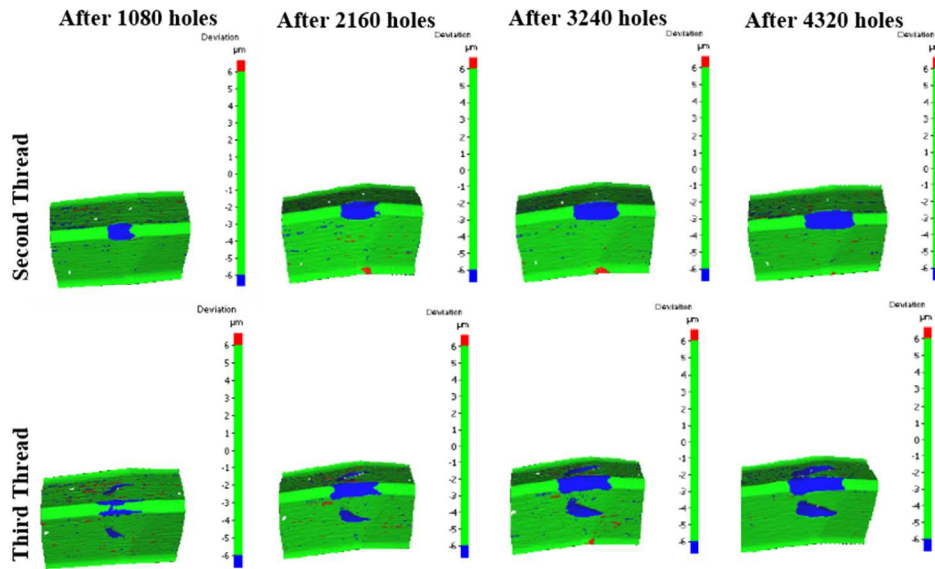
Fig.24: Volumetric wear progression of second and third threads at different stages
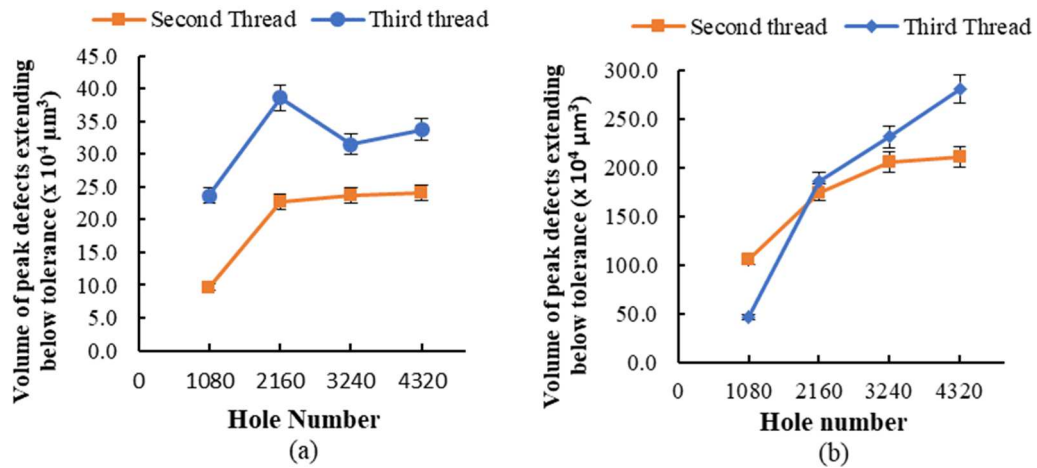
Fig.25: (a) Volume of build-up material and (b) volume of wear for 2nd and 3rd threads

The wear initiation of the second thread as well as the third thread was focused in

the repeatability test, Test-2. Fig.26 shows comparison of the worn tap and a new tap

with respect to the second thread. After tapping the 120th hole, the first instance of wear

at the rake edge of the Crest's lobe was detected, and the wear progressed very quickly to the relief side of crest within the tapping of 2160 holes. In the case of the third thread, wear on the relief initiated around the 720th hole and progressed slowly up to the 2160th hole. The volumetric wear on the third thread progressed faster than the second thread beyond 2160th hole which was also established in the test-1 as shown above in Fig.25(b).
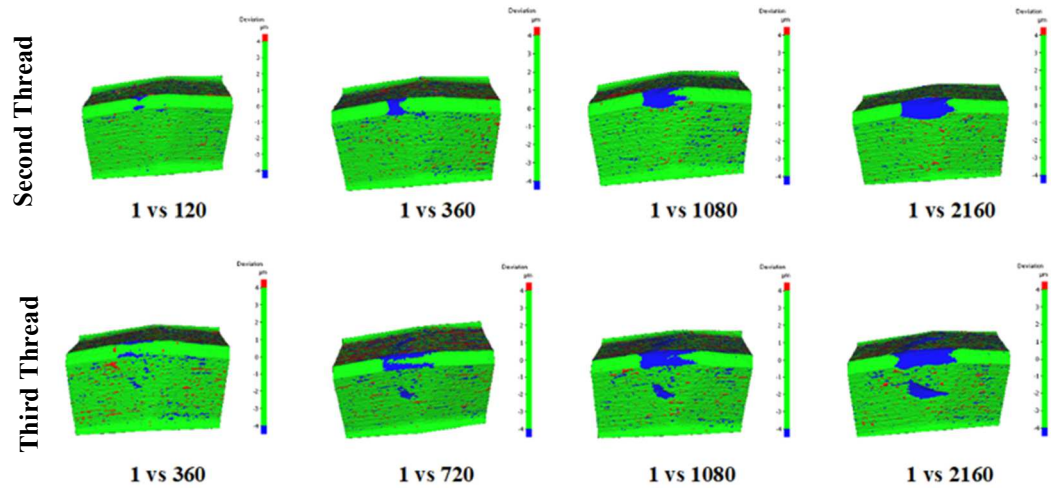
Fig.26: Volumetric wear progression of second and third threads of the Test-2

4.6.3 Linear wear analysis

The linear wear measurement method is focused on providing detailed wear analysis of the second thread. The wear on both rake and relief edge was measured along the crest from the reference point (see Fig.19(b)). Fig.27 shows that the total wear on the crest progressed gradually with the increase in threaded holes. It was observed from the tool wear curve that the wear on the rake edge began earlier on than the relief edge. After machining 2160 holes, linear wear on the rake and relief edges is similar. Beyond this machining stage, the rake edge wear reached its maximum on the lobe and

wear on the relief side progressed gradually. As the rake side of lobe was worn, the relief side of lobe on the crest needed to perform plastic work for forming the thread up to the second thread's requirement, in addition to the elastic recovery work. It is important to understand that the relief side of lobe is responsible for restricting elastic recovery. Hence, under such harsh condition during forming, the relief edge wear was more severe than the rake edge wear on the crest of the second chamfered thread. Careful observation of the wear curve for relief edge showed that wear stabilized beyond tapping of 2160 holes. The total wear on the crest, localized over the lobe, tends to grow steadily and a steady state regime of wear for the second thread can be observed. This steady state of wear confirmed the minimal variation of mean torque after tapping 2160 holes as shown in Fig.22.
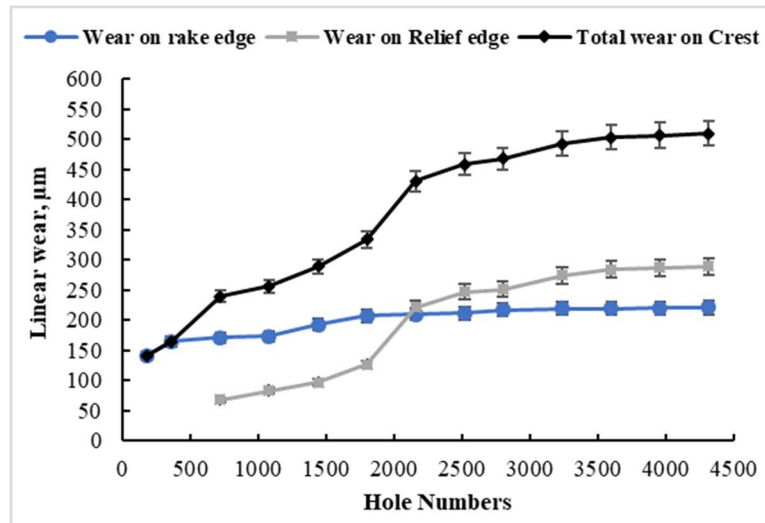
Fig.27: Linear wear curve for the second thread

4.6.4 Wear mechanism

Fig.28 shows the gradual progression of wear at the lobe region of the second thread's crest. After tapping the 120th hole, the first instance of pluck-out was observed

on the second thread. The lobe at this crest was severely worn after finishing 4320 holes. Wear initiated at the rake edge of the crest near the lobe and very slowly advanced over the lobe towards the relief side. This wear progression direction can be understood by the geometry of form taps [25]. Once the leading face F3 along the rake edges starts plucking out, the plastic work required from these leading faces is incomplete. Consequently, the central faces F4, F5, and F6 have to counter the elastic recovery as well as perform the extra plastic work. Contact forces tend to increase for this region and the chamfered threads become susceptible to tool wear due to greater metal to metal contact followed by adhesion [32]. Wear progression is discussed in the following paragraphs.
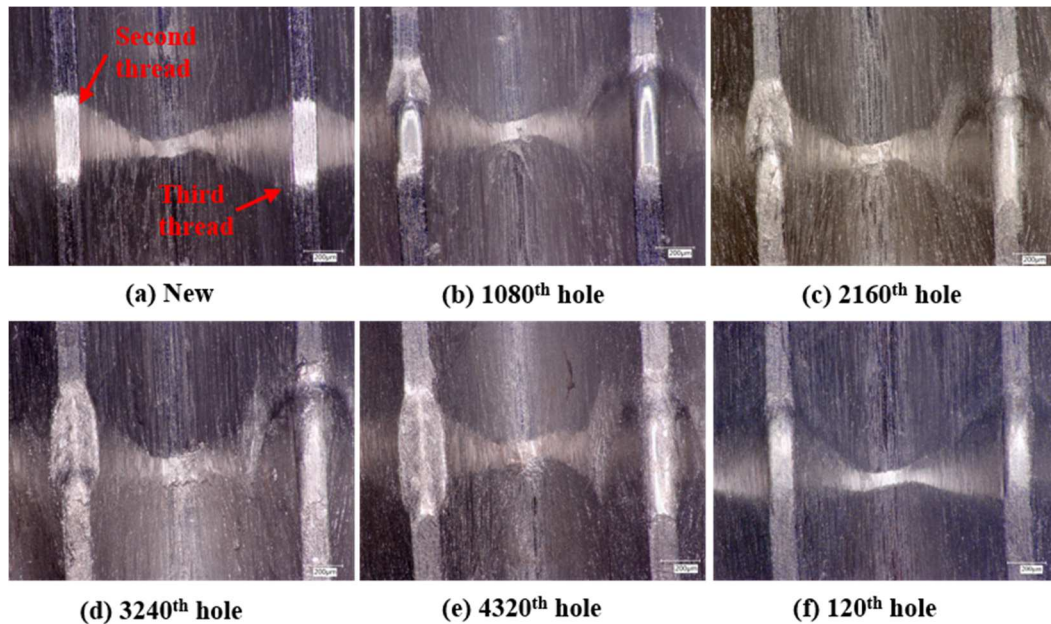
Fig.28: Wear progression on the second and third threads (at 200x)

4.6.4.1 Initiation of wear after tapping 120 holes

SEM was performed on the worn region of the crest of the tap's second thread after tapping 120 holes. Fig.29 (a) shows the wear initiation region on the rake edge of the second thread's crest. The plucking marks on the rake edge as shown in the Fig.29(a) indicate that tool material was removed along the direction of the tool's rotation. The continuous built-up layer of Al-Si alloy at this wear initiation, as shown in the Fig.29 (b), provides evidence of a micro-level pluck-out at the crest, due to aluminum adhering to the tool's surface and breaking away along with the tool material from the rake. This region was under high normal load, and the nature of any build-up, at this region, would be to slowly pluck-out the tool material along with its removal from the tap's surface during tapping. The presence of Al build-up is confirmed by the EDS elemental map shown in Fig.30(a). Fig.29(c) shows the secondary wear mechanism to be abrasion along the F3 face. These abrasion grooves are caused by highly coarse Si precipitates embedded in the α-Al matrix. EDS spectrum maps of the abraded grooves indicated the adhesion of the alloy, and the crack seen in Fig.30(b) indicated the tearing away of these adhered layers from the tap's surface.
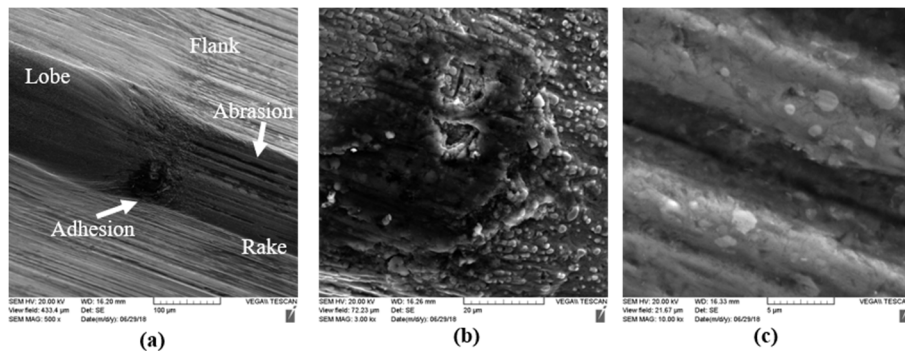
Fig.29: SEM images of crest of second thread after 120 holes, (a) critical region, (b) Al adhesion, (c) abrasion grooves on rake
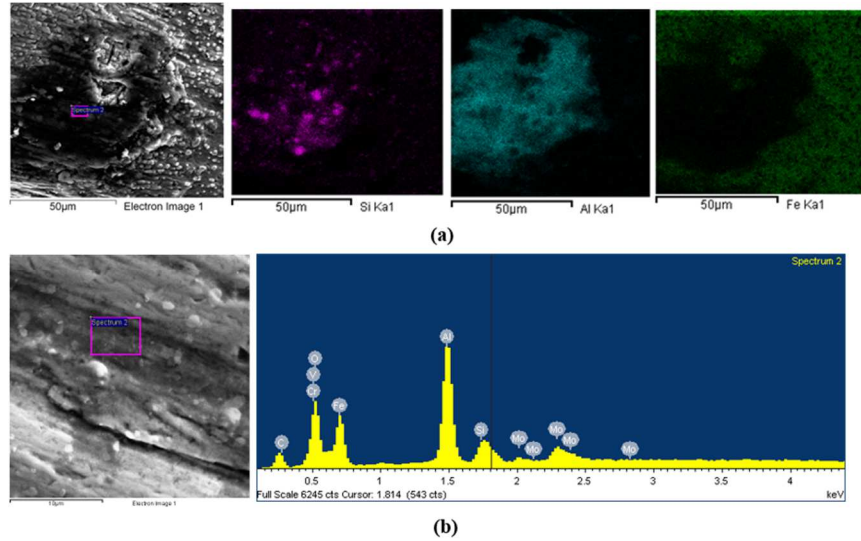
Fig.30: EDS analysis on the rake edge of second thread after 120 holes (a) elemental map of Al build-up, (b) spectrum map at abrasion mark

4.6.4.2 Wear progression after tapping 1080 holes

After tapping 1080 holes, the pluck-out on the crest of the second thread had progressed towards the relief edge (see Fig.31(a)). As stated earlier, this wear progression is along the direction of tap's rotation. Forming requirement has been transferred towards the relief side due to failure of the rake side face F3 to carry out the needed contribution to form the threads. Fig.32 shows the traces of the work material on different areas of the worn region on the second thread. SEM investigation on the third thread's crest (see Fig.31(b)) revealed a similar pattern of build-up layer formation on the rake edge of the crest. Elemental mapping (see Fig.33) of the build-up layer confirmed the presence of Al and Si at the rake edge on the crest. In addition, a high amount of abrasion was noticed on either flank neighbouring the lobe of the third thread. The direction of the abrasion marks is quite different from the grinding marks

on the flanks as seen in the Fig.31(c). In fact, this direction is along the plastic flow of material during forming along the lobe relief angle on the flanks. It is worth mentioning that no abrasion mark was observed on the flanks of the second thread. The condition of the third thread indicates that it carried out extra plastic work to fulfill its contribution in forming the threads. Thus, the forming load is being transferred to the third thread and tangential forces are increased on the contact surfaces of the third thread. This is consistent with the increase in torque as shown in Fig.21. It can be inferred that greater forming loads have caused higher abrasion of the third thread due to the presence of silicon precipitates in the alloy during forming.

(a)   **(b)**   **(c)**
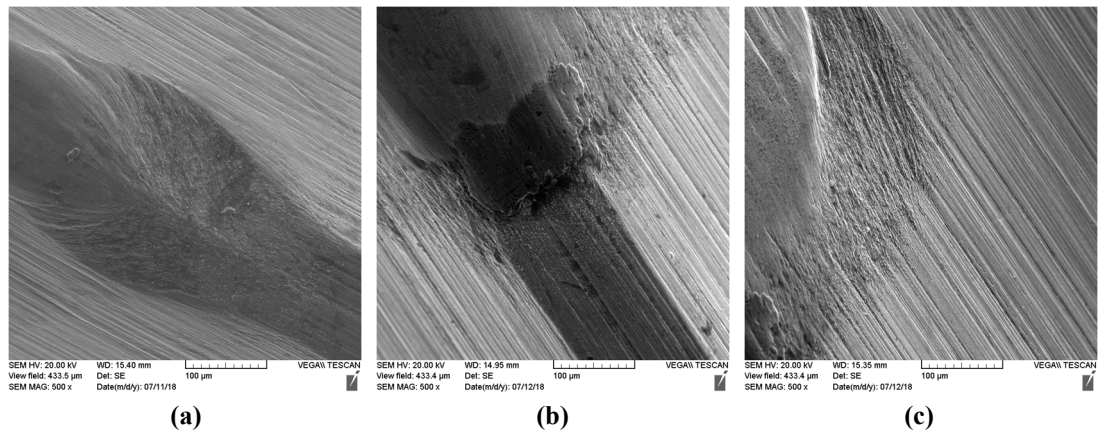
Fig.31: SEM images (a) crest of second thread, (b) crest and (c) flank of third thread
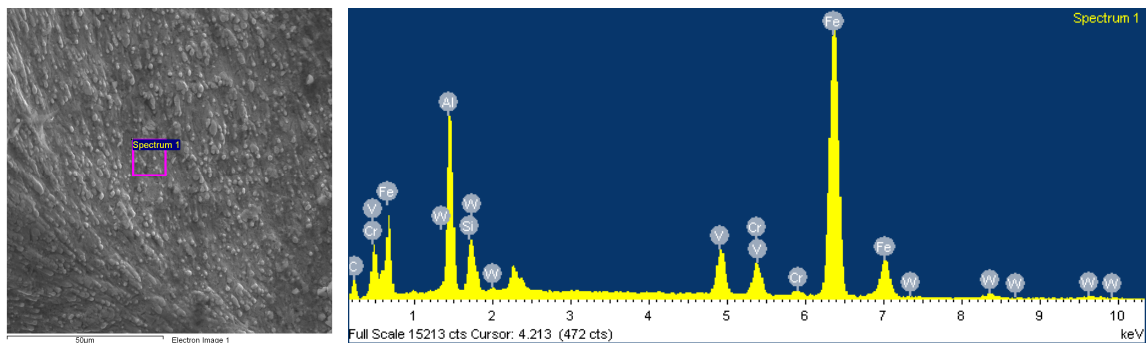
Fig.32: Spectrum map on the worn lobe of second thread after 1080 holes
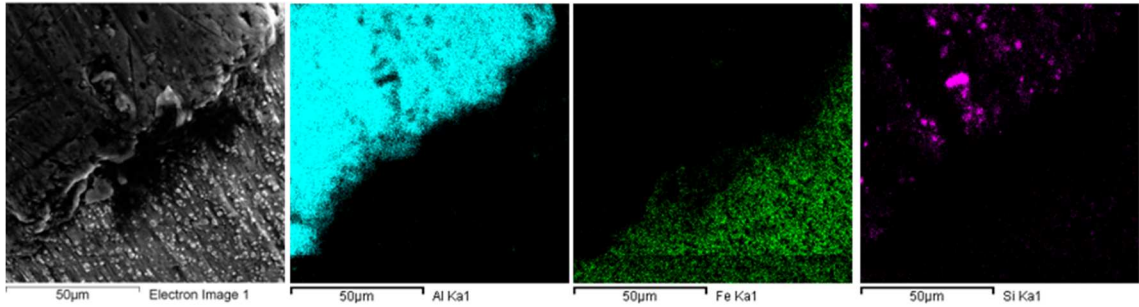
Fig.33: Elemental map of crest of third thread after 1080 holes

4.6.4.3 Wear progression after tapping 2160 holes

SEM images of the second thread as shown in the Fig.34(a) suggested that the pluck-out has progressed further on the lobe. The high trace of Al (Fig.35(a)) on the plucked region of the crest confirmed the primary wear mechanism to be adhesion of Al, followed by removal of build-up layer. In case of the third thread, the presence of a build-up layer can be observed in Fig.34(b). As seen earlier in Fig.30(b) for the second thread, the deposited build-up layer on the third thread's rake gets torn apart during forming (Fig.34(c) and Fig.35(c)).
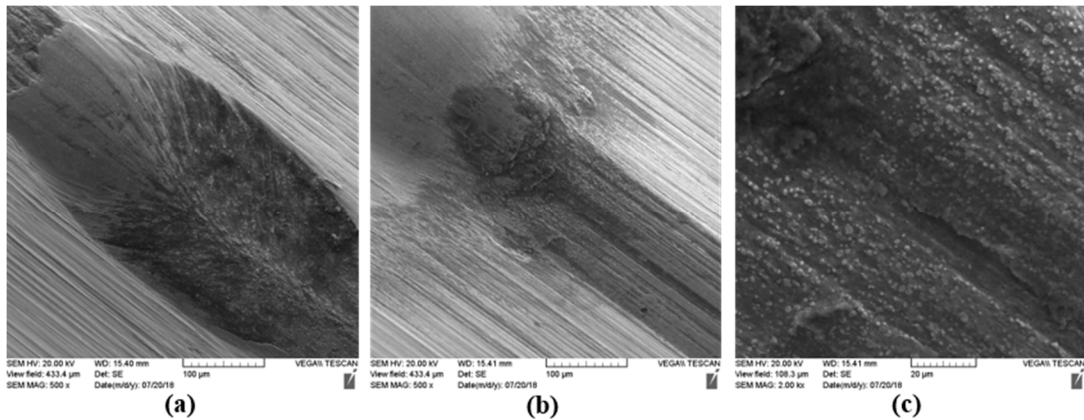
Fig.34: SEM images (a) crest of second, (b) crest of the third, (c) rake of third threads

Elemental maps from EDS analysis on the flank of the third thread, (Fig.35(b)) show Al adhering to this region too. It was observed in the element maps of Al that the Al was adhering to the grooves and covering it, which indicates that both adhesion and abrasion are responsible for wearing out the third thread's flanks.
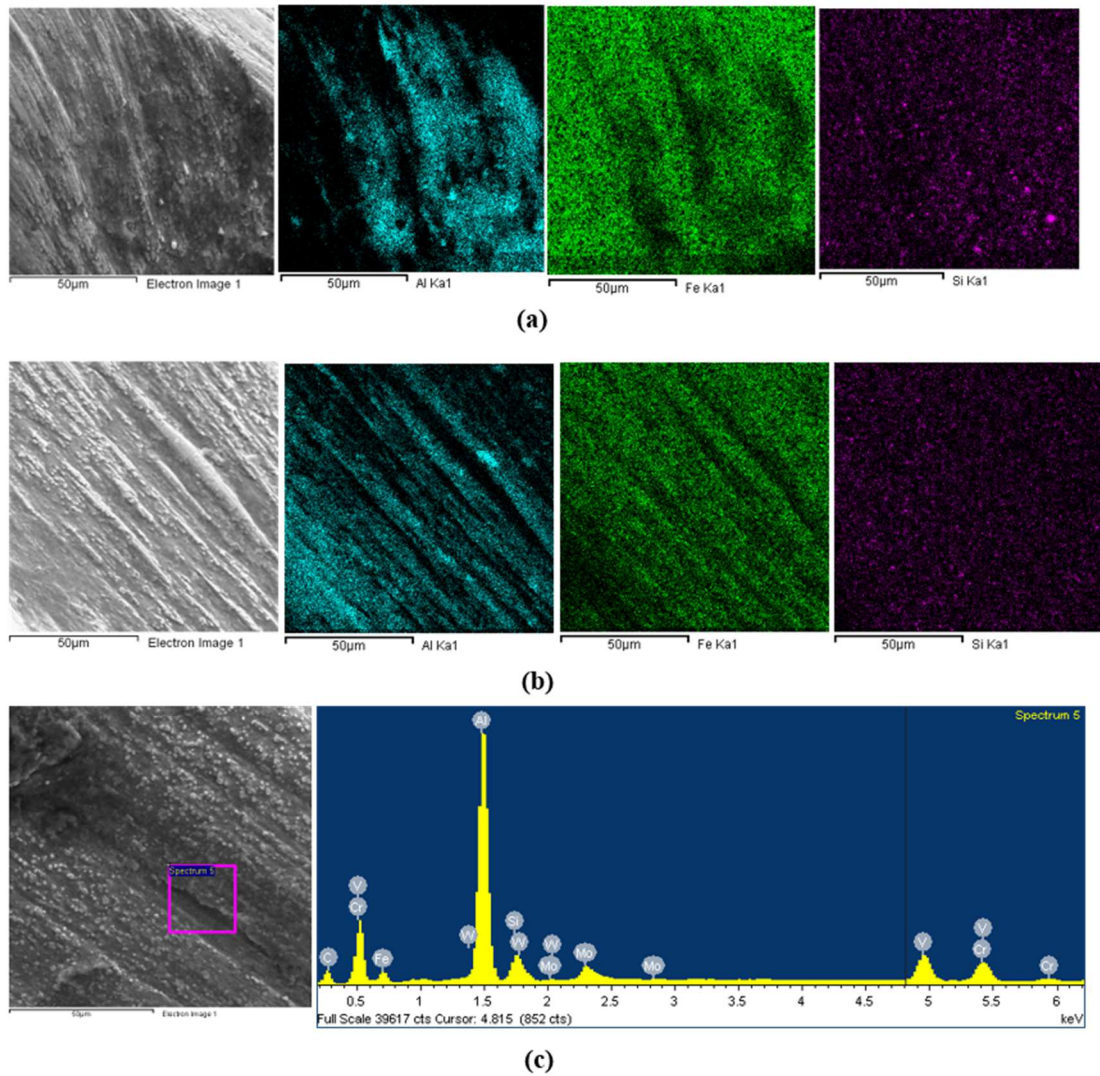
Fig.35: After 2160 holes, elemental maps of crest-(a) second, (b)third threads, (c) spectrum map third thread's crest

4.6.4.4 Wear progression after tapping 4320 holes

After tapping 4320 holes, the second thread's lobe was severely worn out from its crest as seen in Fig.36(a). Elemental maps of the build-layer from Fig.37(a) suggested that wear had progressed to the relief side which led to the partial failure of the second thread.
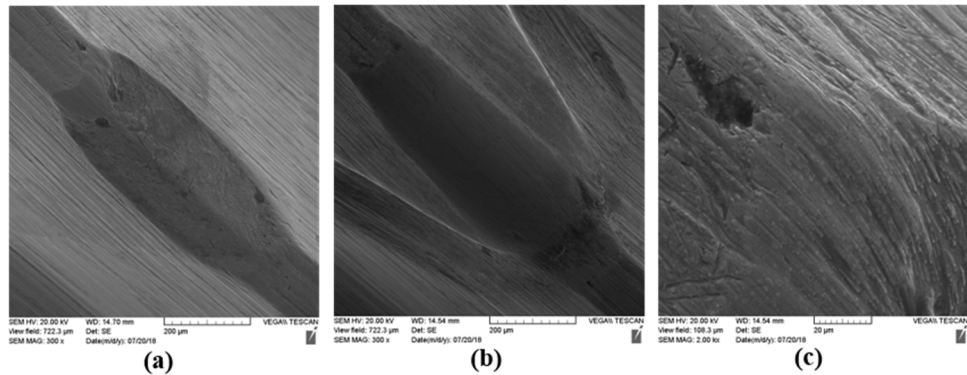
Fig.36: SEM images of second thread's (a) crest and (c) relief, (b) crest of third thread
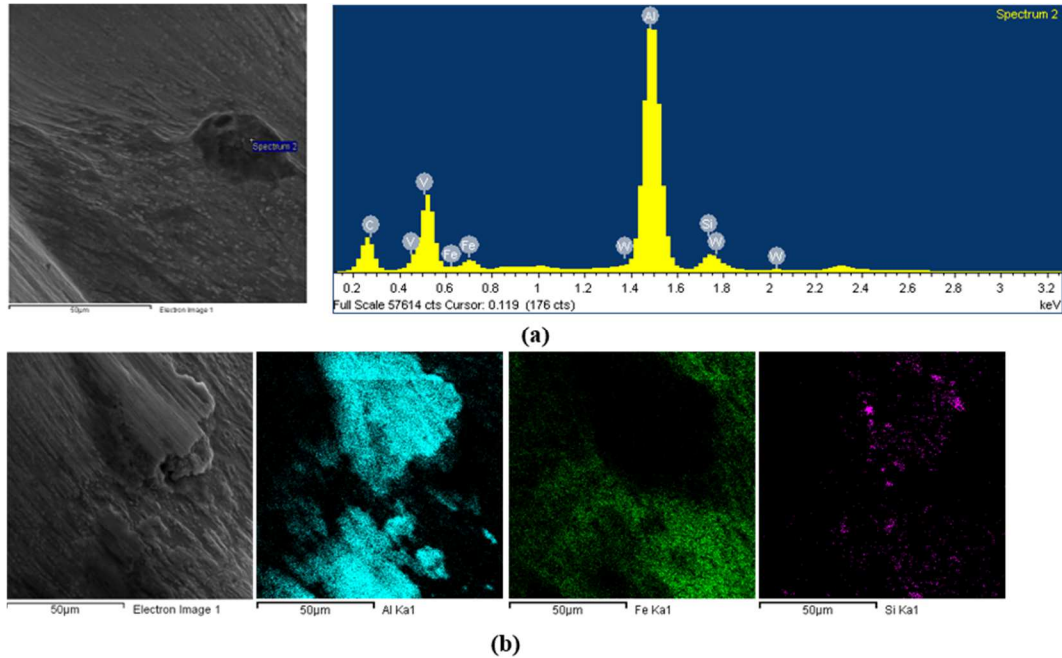
Fig.37: After 4320 holes (a)spectrum map of crest of 2nd thread, (b)elemental map of 3rd thread

Fig.36(b) showed the surface of the third thread in the lobe region where abrasion on the flanks had become very prominent. The small hole in Fig.36(c) indicated the unstable nature of the Al layer adhered on the third thread's crest. Removal of tool material from the crest is imminent with the removal of the build-up layer. A huge build-up was observed on the rake edge of the crest as shown in the Fig.37(b) which confirmed that wear on the third thread's crest followed the same pattern as that of the second thread.

Although the flanks of the second thread have minimal or no wear, it is important to understand the reason for the development of flank wear on the third thread only. The plastic work required by the tap's second thread in forming the threaded groove is delegated to the tap's third thread due to the second thread's significant wear. Leading rake faces of the third thread undergo extra plastic deformation. The flank faces near the lobe (F4, F5), including the lobe (F6) are expected to restrict the elastic recovery of deformed material [25]. In this case the amount of elastic recovery is proportional to the amount of plastic deformation undergone by the previous leading faces of the third thread [25]. Also, the direction of elastic recovery is normal to the surface. Hence, faces F4, F5 and F6 of the third thread are under higher contact pressure due to the increased elastic recovery. As normal load over these faces becomes higher, volumetric wear also increases due to abrasion as per the Archard's equation [37],[45]. Hence, the overall volumetric wear of the third thread is considerably higher after tapping 4320 holes , since the flank faces have rapidly deteriorated. This is clearly observed in Fig.25(b) above.

An important observation on the lobe face F6 of the second thread's crest was the presence of micro-grooves in random directions on the worn surface. Even though the worn surface appears to be smoothly worn, at high magnification, micro-level abrasion grooves on rake side of lobe were visible, as seen in Fig.38(a) and (b). Fig.38(c) showed that the plucked-out region appeared to be smooth on the relief side of the lobe as traces of Al adhesion covered these micro-grooves. The generation of micro-grooves on the surface is related to the loose abrasive particles trapped as wear debris in the lubricant film between the two sliding surfaces [50],[49]. This abrasive wear debris must have scored the surface at a very micro-scale during the process. The randomness of micro-grooves was evidence of the loose abrasive particles present in the wear debris.

(a)   (b)   (c)
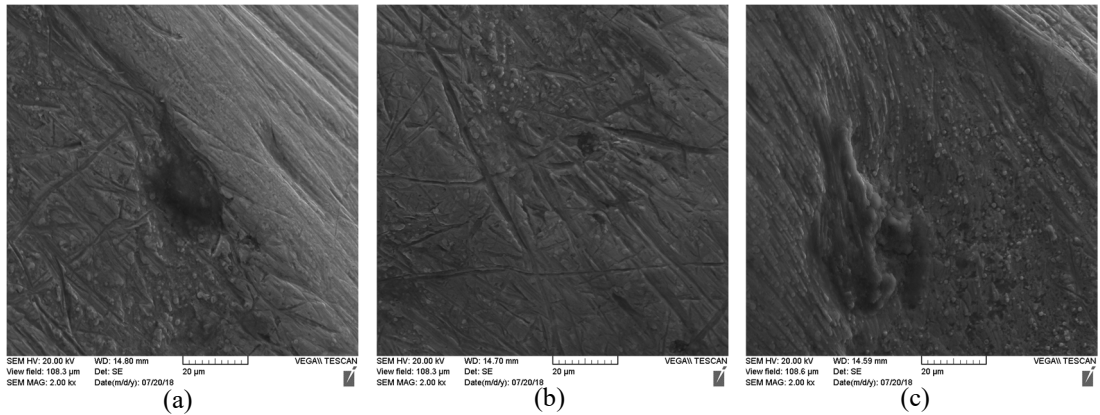
Fig.38: SEM images of second thread's crest (F6) showing micro-grooves (a)&(b) rake, (c) relief

As such, the crests of the chamfered threads undergo a very complex wear mechanism, which involves plucking out caused by removal of adhered Al build-up from the surface, distinct grooves on the rake faces of crest due to abrasion and micro-grooves on the lobe face due to abrasive wear debris. In case of the flanks, abrasion was primarily the cause of wear.

4.6.5 Radial wear of the lobe

After 4320 holes of tapping, the change in the lobe's radius of the second thread with respect to the same in the new tap was significant. Fig.39 shows the cross-section views of the tap's second thread where the lobe was nearly worn from the crest after tapping 4320 holes. Fig.39 consists of all cross sections compared to the new condition for the second thread only. The lobe region has been flattened and lost its functional shape. Further machining with the same tap might cause further removal of tool material from the crest. Hence, it will be unnecessary to proceed after 4320 holes. Difference in the radial wear of the lobe could be marked as the limiting parameter for linear wear. Beyond a certain radial wear of 0.0726 mm, the expected linear wear should be reached which can make the lobe of the second thread severely worn or flattened. This metric is indicative of the second thread's inability to perform its expected plastic work.
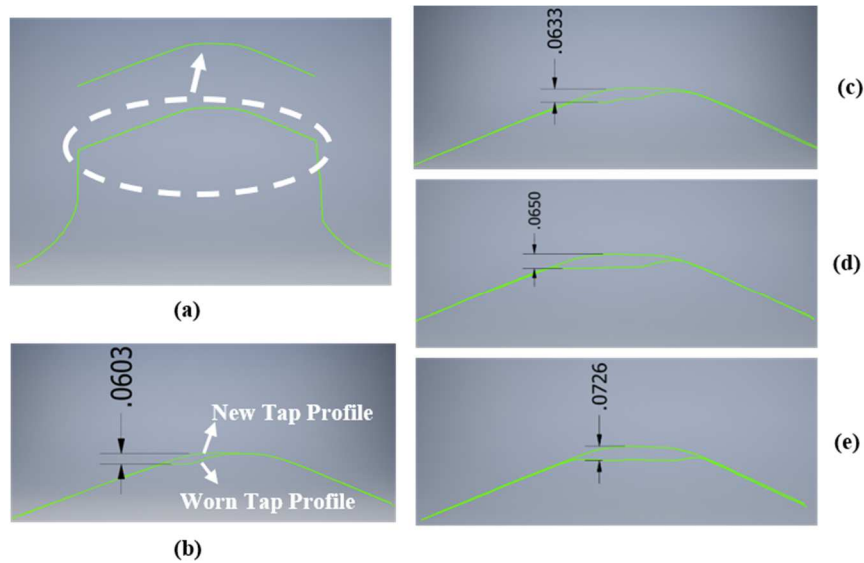
Fig.39: Radial wear of second thread's crest shown by profile comparison of (a) new tap with the same after (b)1080, (c)2160, (d)3240, (e)4320 holes

4.6.6 Forming energy

The total forming energy required in form tapping can be calculated by measuring the area under the time-based torque response for the forward motion. Piska et al. [64] compared the specific forming energy for the tribological condition of the PVD coated taps at initial and final stages of tapping. In this research, the uncoated tap underwent significant wear upon tapping of 4320 holes. In addition to the mean torque, the time domain signal of the forward torque response could be useful in measuring the forming energy. The torque is proportional to the tangential force acting on each thread. The tangential force is based on the force components in the X, Y, Z directions. Each force component depends on the frictional and normal forces developed on each thread of the tap [25]. Therefore, friction and normal forces on the contact areas during plastic deformation are responsible for the total forming energy. At high normal load present in forming, the real area of contact increases between the mating surfaces. This results in an increase in welded junctions and hence, increased wear rate due to adhesion. It is well known that the frictional force is proportional to the area of real contact. With increased metallic contact at mating surfaces, the frictional force tends to increase over the crest and flank surfaces of each thread. For every chamfered thread, the area of the flank and crest surrounding the lobe (F4, F5 and F6) is supposed to counter the elastic recovery only. As discussed earlier, progressive wear caused these neighbouring areas of the lobe to contribute to plastic deformation for that thread in addition to restraining elastic recovery. This change in the responsibility of chamfered thread's functional

areas could cause higher frictional force, and hence higher tangential forces during the forming of threads on the workpiece.

Also, the total forming energy can be divided into the work done by plastic deformation, elastic recovery and losses. Since, the 4320th threaded hole was found to be in good condition when checked by a standard ISO 6H thread screw gauge, the form tap was performing the required plastic deformation and elastic recovery in forming the threads. However, the change in the area under the torque curves for first and 4320th hole as shown in Fig.40 suggested that losses during forming have increased. This could be correlated to the partial inability of chamfered threads to perform plastic work due to gradual wear and the transfer of plastic work to the successive threads. Beyond the chamfered threads, the threads are responsible only for guiding the tap forward and prevent minimal elastic recovery. As the wear progressed on the chamfered threads, the trailing threads start performing some part of plastic deformation which increased the tangential forces. Thus, torque tends to increase gradually as the threads on the tap become worn on its functional surfaces. As shown in Table 7, the increasing trend of specific forming was an indication of wear growth on the tap's crest and flanks.

Table 7—Specific forming energy during form tapping

Hole number	Forming Energy (J)	Specific forming energy (J/mm^3)
1st	2.787	0.032
2160th	3.277	0.037
4320th	3.353	0.038
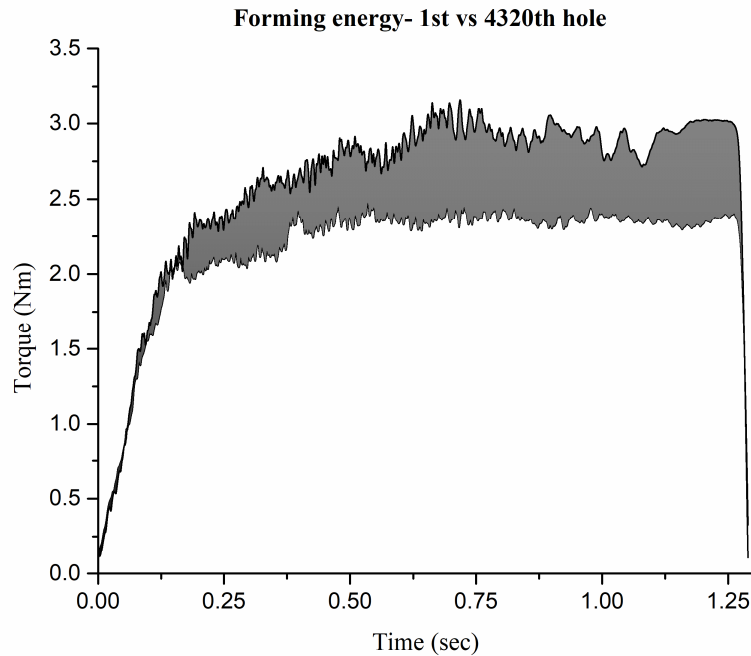
Fig.40: Shaded area represents forming energy

4.7 Conclusion

In the current work, the wear mechanism of form taps in threading Al-Si alloy with high Si contents (about 12%) was studied. Different methods were used to measure the wear of the tap threads. The following conclusions can be drawn from this work:

1. Wear on the crest of second thread at the rake edge initiates after tapping of 120 holes. It gradually propagates to the crest on the relief edge with increasing number of threaded holes. The presence of Al build-up and pluck-out on the crest are the major causes of tool wear. This phenomenon is also observed on the third thread's crest at a later stage. Thus, the primary wear mechanism for tapping of Al-Si alloy with an uncoated HSS tap could be stated as adhesion of aluminum to the tool's surface.

2. Grooving abrasion on the flank neighbouring the lobe of the third thread was caused by the hard Si precipitates embedded in the Al-matrix. Traces of Al on the grooves and tear marks inside the grooves indicated that the flank's surface deteriorated by both adhesion and abrasion.

3. The flank region neighbouring the lobe of the third thread conducts extra plastic deformation as the second thread becomes worn out, resulting in greater contact pressure and increase in abrasion wear.

4. Micro-grooving on the lobe in random directions was caused by abrasive wear debris generated during the process. Major grooving abrasion marks on the rake side of the crest were caused by hard Si precipitates embedded in the Al Matrix. Thus, abrasion wear is the second major wear mechanism that needs to be prevented during forming.

5. The linear wear measurement is only useful for a detailed wear study on a particular thread's crest, but it is time consuming. Since it is optically inspected, wear on the flanks cannot be measured due to the steep angle of this surface. However, the volumetric wear measurement method is useful for calculating wear volume on the entire surface of the worn thread and for understanding the wear propagation. This accounts for both abrasion wear and adhesion wear volumes.

6. Monitoring of mean torque for form tapping of Al-Si alloy with uncoated HSS roll form tap can be limited to 2160 threaded holes. This stage of the form tap marks the onset of a steady wear region of the second chamfered thread. The variation of

torque beyond this stage is minimal as the wear growth over the second thread is minimally and steadily increasing with further machining.

7. After 4320 holes, the formed threads were found to conform to ISO standards upon gauging with an ISO metric screw thread gauge. In the chamfered zone of the form tap, the second thread was significantly worn at the crest, but the third thread was still producing good threads despite its wear. It can be concluded that successive threads get worn one after another, and at some point, the formed thread will have unsatisfactory quality.

8. Short tests may be adopted to compare performance of different designs, tap coatings or optimization of process parameters. The current study recommends 2160 holes for the form tapping of an Al-Si alloy with an uncoated HSS roll form tap.

Chapter 5. Performance of PVD coatings in improving tool life

Based on the conclusions drawn from Chapter 4, the application of PVD coatings was explored to improve the performance of the HSS tap in machining Al-12Si alloy. The tap geometry, process parameters and the machining setup in this study were kept the same as in the previous study. The objectives of this study were as follows:

- ❖ Examine the performance of selected PVD coatings using preliminary (short) machining tests.

- ❖ Investigate the performance of an effective coating using progressive wear tests.

- ❖ Comparative analysis of the effective coating with the uncoated and coated tap provided by the industry partner.

- ❖ Investigate the feasibility of accelerated performance tests for form taps.

5.1 Selection of PVD coatings for machining of Al-Si alloy

The major wear mechanism of Al-12Si alloy machining with uncoated HSS tap was determined in Chapter 4 to be the combination of both abrasion wear and adhesion wear. Selection of PVD coatings was based on the following findings from the literature and the previous chapter:

- ❖ Abrasion wear due to the high content of silicon in the aluminum alloy required harder surface coatings on the tool. TiCN, TiAlN, DLC, TiAlN+C, TiB_2 are examples of hard coatings.

- ❖ Adhesion wear due to high sticking tendency of aluminum required coatings that have good anti-seizure and lubricious properties. ZrN, CrN, MoS_2 and DLC are favourable coatings for aluminum alloy machining.

❖ Coating recommendations from industry, coating suppliers and MMRI coating facility were also considered for preliminary tests. Table 8 shows the characteristics of the selected coatings as listed by the suppliers.

Table 8—Characteristics of the selected coatings

Composition	Supplier	Coating Name	Hardness	Thickness (μm)	Coefficient of friction
CrN	Richter Precision	Titankote C3	2000-2200 HV	1-5	0.35
TiCN	Richter Precision	Titankote C5B	2800-3200HV	1-5	0.3
DLC *(DLC-2)	Richter Precision	Titankote C10	5000-9000 HV	0.5-2.5	0.1
ZrN *(ZrN-2)	Richter Precision	Titankote C8	2300-2500	1-5	0.35
MoS₂ (DCD coating)	Richter Precision	Tribo-Kote S	-	0.5-1.0	0.08-0.1
TiB2 *(TiB2-2)	Cemecon	CC Aluspeed	4000 HV	1.3-2.7	-
TiAlN + C	Cemecon	CCPlus C	3300 HV	2-4	-
TiB2 *(TiB2-1)	Kyocera	Aluspeed	4000 HV	1.3-2.7	-
TiAlN	MMRI	-	35-40 GPa (nano-hardness)	1-2	0.4-0.5
TiAlN *(TiAlN-2)	MMRI	-	35-40 GPa (nano-hardness)	10-12	0.4-0.5
ZrN	Industry partner	-	20 GPa (nano-hardness)	1-4	0.35
DLC *(DLC-1)	Industry partner	-	-	-	-

Note: * denotes the name given to coating which have been supplied from more than one coating supplier.

5.2 Experimental Methodology

❖ This study was divided into Phase I and Phase II. Phase I consists of the preliminary tests of 12 select coatings to identify the better performing coatings. Phase II consists of the progressive wear study of these identified coatings.

❖ In Phase I, the preliminary shorts tests were limited to the machining of 360 holes. Drilling and tapping were conducted with the same process parameters as in Table 4. These tests were designed to eliminate the poorly performing

coatings as the quantity of work material was limited. Torque was monitored and wear on the chamfered threads was inspected by optical microscopy, SEM and EDS. The severity of coating delamination and subsequently substrate exposure served as a criterion for coating elimination. Wear measurements were not possible due to minimal wear of taps after machining only 360 holes.

❖ In Phase II, the progressive wear study of the identified coatings was limited to the machining of 2160 holes initially. Torque and volumetric wear were monitored for each coating. Linear wear measurement was not possible due to minimal wear on the crest. If coating delamination occurred for the entire lobe of either chamfered threads, then the coated tap would not be machined further. After 2160 holes, only one coating was effective and hence, it was further machined up to 4320 holes.

❖ A comparative performance study of the effective coating with the uncoated and ZrN (used by industry partner) was done. Torque, volumetric wear, optical microscopy, SEM and EDS data were analyzed to identify the wear pattern and wear failure modes.

5.3 Results and discussion: Phase I

5.3.1 Evaluation of torque

The mean torque was monitored for each coated tap after producing 60 holes. In Fig.41, the mean torque varied between 2 Nm to 3.3 Nm for all 12 coatings. The TiAlN-2 coating had the highest mean torque of 3.3Nm of all coatings. This is attributed to its higher thickness of almost 12 μm. The internal hole diameter after drilling was found

to be within the required value. Therefore, drill diameter had no influence on such high torque values for the TiAlN-2 coating. Out of 12 coatings, the mean torque for 11 coatings ranged between 2 Nm to 2.8 Nm. The average of mean torque for the uncoated tap was 2.53 Nm. Hence, these 11 coatings performed similarly to the uncoated tap with respect to torque. The average of mean torque for the tapping tests with the DLC-1 coating was 2.14 Nm. Generally, DLC coatings have a very low coefficient of friction [4]. Thus, the torque generated in the tapping tests of the DLC-1 coating indicated lowest frictional forces. However, the optical inspection of DLC-1 after 360 holes showed very severe delamination (see Fig.46).
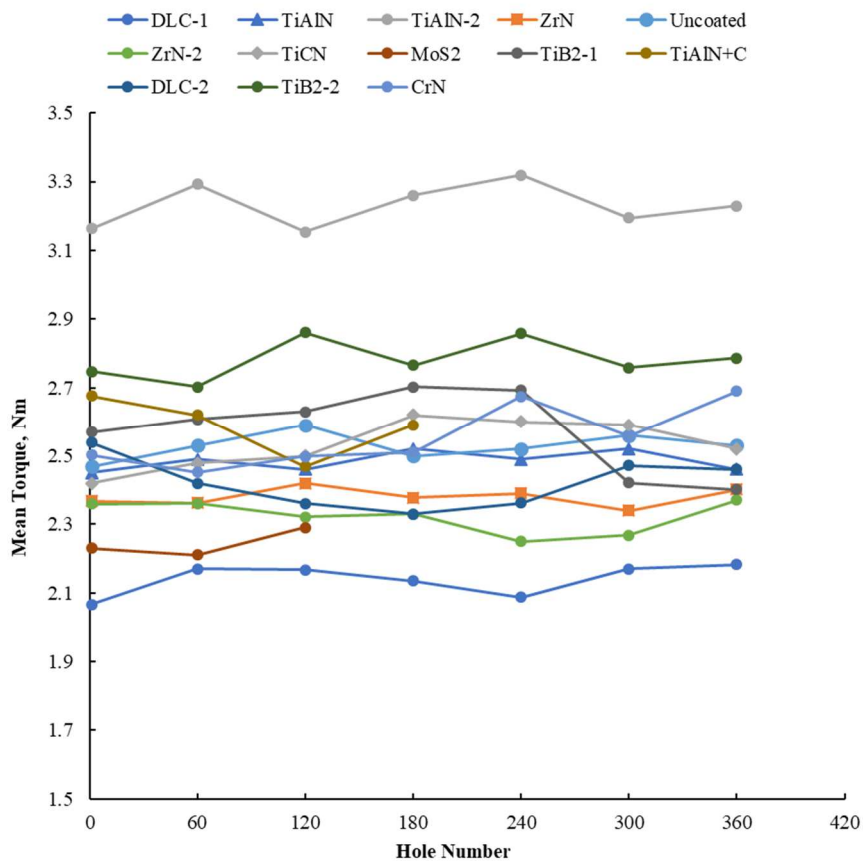
Fig.41: Mean torque of the selected PVD coatings in the preliminary tests.

Among the hard coatings, TiAlN and TiCN had performed better than the TiAlN+C coating in terms of mean torque. In Fig.42, TiCN performed very similarly to the uncoated tap, whereas the TiAlN coating showed lower torque generation. Although the ZrN coating exhibited a lower torque trend than rest of the coatings, it had the worst coating delamination. This is discussed in the next section.
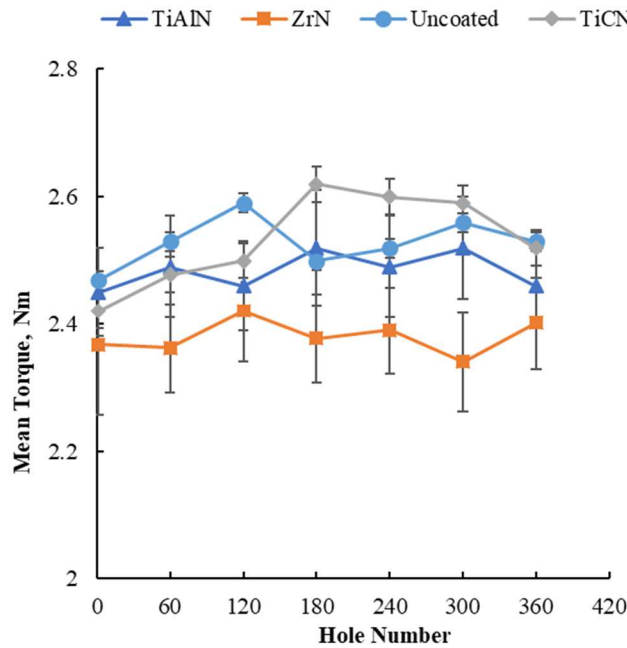
Fig.42: Mean torque of TiAlN and TiCN coatings

5.3.2 Wear assessment by optical and electron microscopy

The assessment of wear was restricted to the second and third chamfered threads based on the conclusions of Chapter 4. The lobe region of a thread was found to be the most affected in the previous chapter. Therefore, the optical inspection was performed on the crest of second and chamfered threads.

Although aluminum adhesion on the crest was clearly visible under an optical microscope, the condition of the coating could not be properly investigated. As such, extensive SEM and EDS were performed in this coating study to observe wear of the coated taps. Substrate exposure, flaking of coating, aluminum adhesion, abrasion grooves, micro level pluck-out, and coating cracks were clearly visible. There was no micro-grooving abrasion observed on the crest as the application of hard surface coatings prevented it. A record of the observations is shown below for ZrN, TiAlN, and TiCN, since these were less worn than the rest of the coatings.

The findings of the preliminary tests for each coating are provided in Table 9. Both DLC coatings suffered severely in form tapping of Al-12Si alloys. Almost the entire lobe of the chamfered threads was delaminated, and substrate exposure was severe for both DLC coated taps. Since these DLC coatings are super-hard coatings deposited on a softer HSS substrate, the DLC coating suffered a brittle fracture and subsequent flaking of the coating [81],[41],[62]. ZrN coatings suffered severe Al adhesion on the crest's rake and substrate exposure was localized along the edges of the crest. The presence of severe grooving abrasion on the rake suggested that ZrN could not prevent abrasion in high silicon content aluminum alloys (see Fig.43). TiCN and TiAlN performed much better than ZrN in preventing abrasion (see Fig.45 and Fig.46). Also, minimal aluminum adhesion was noticed upon elemental mapping in EDS. In the case of TiAlN coating, there was a minor region along the rake edge of the crest where coating was removed from its inter-layer. EDS analysis of this region (see Fig.44) showed that there was no substrate exposure on the rake. Cracks were present on the

coating in this region. Since TiAlN is a multi-layer coating, the interlayers prevent any crack propagation through the coating (along the thickness). This prolongs the coating's adhesion with substrate even if the surface layers generated cracks and fractured [61]. Coating removal layer by layer will be a much better outcome than complete flaking away from the coating-substrate system's interface.

Table 9 summarizes all observations for CrN, TiB$_2$-1, TiB$_2$-2, TiAlN+C, DLC-1, DLC-2, MoS$_2$, TiAlN-2 and ZrN-2 coatings. These coatings performed poorly in form tapping of Al-12Si alloys. Therefore, it was decided not to proceed further with these coatings.

Table 9—Summary of observations in the preliminary tests

Coating	Mean Torque range (Nm)	Observations
ZrN	2.22-2.5	Substrate exposure, chipping at rake edge, Al build-up on crest, grooving abrasion on crest and flanks neighboring lobe.
TiCN	2.48-2.73	No substrate exposure, minor pluck-out at rake edge, coating delamination from inter-layer, No wear on flanks
TiAlN	2.42-2.58	Minor pluck-out, minor delamination on the flanks. Cracks along the region where coating was removed from inter-layers.
DLC-1	2.06-2.18	Severe substrate exposure from crest (lobe), Al build-up on crest and flanks, no pluck-outs on rake edge.
TiAlN-2	3.05- 3.29	Substrate exposure along the rake edges, coating flaking off from the inter-layer, Al build-up on crest before lobe.
CrN	2.5-2.69	No observable wear on second thread. Third Thread-Al adhesion on the crest along the rake edge, micro level pluck-out and substrate exposure on the crest along the relief edge.
DLC-2	2.33-2.53	Substrate exposure on the crest along rake edge, coating delamination on crest and flanks neighboring lobe, Al adhesion on crest.
TiB$_2$-1	2.4-2.56	Substrate exposure, pluck-outs along the rake edge, Al adhesion on crest.
ZrN-2	2.25-2.37	Severe substrate exposure of full lobe on the crest (lobe region),Grooving abrasion on flanks.
TiAlN+C	2.46-2.67	Severe substrate exposure at pluck-out region of rake edges after 180 holes
TiB2-2	2.7-2.86	Large pluck-outs on crest along the rake edges.
MoS$_2$	2.23-2.29	Large pluck-outs on crest along the rake edges, Severe delamination.
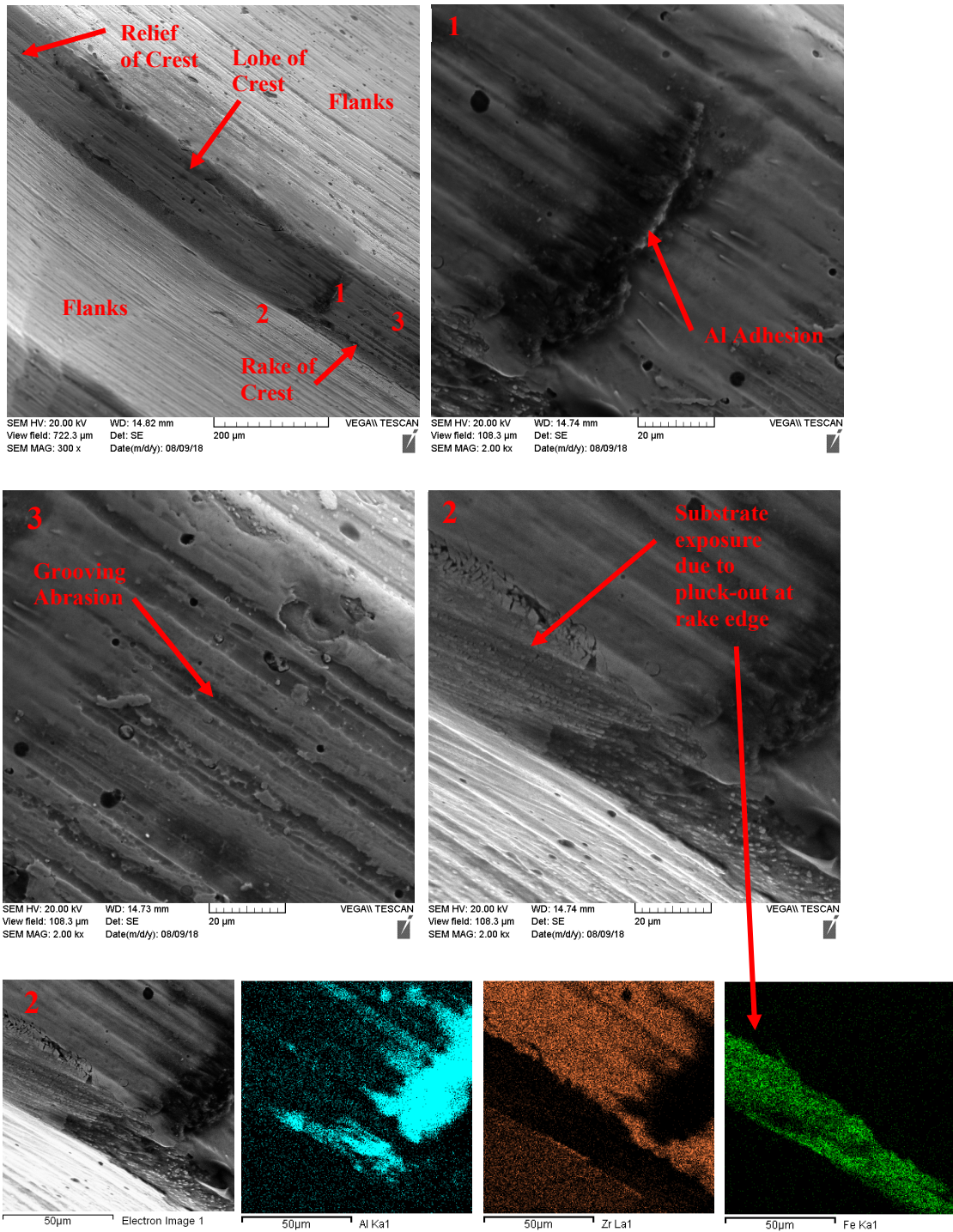
Fig.43: SEM and EDS of the ZrN coated tap showing the wear on second thread's crest after 360 holes.
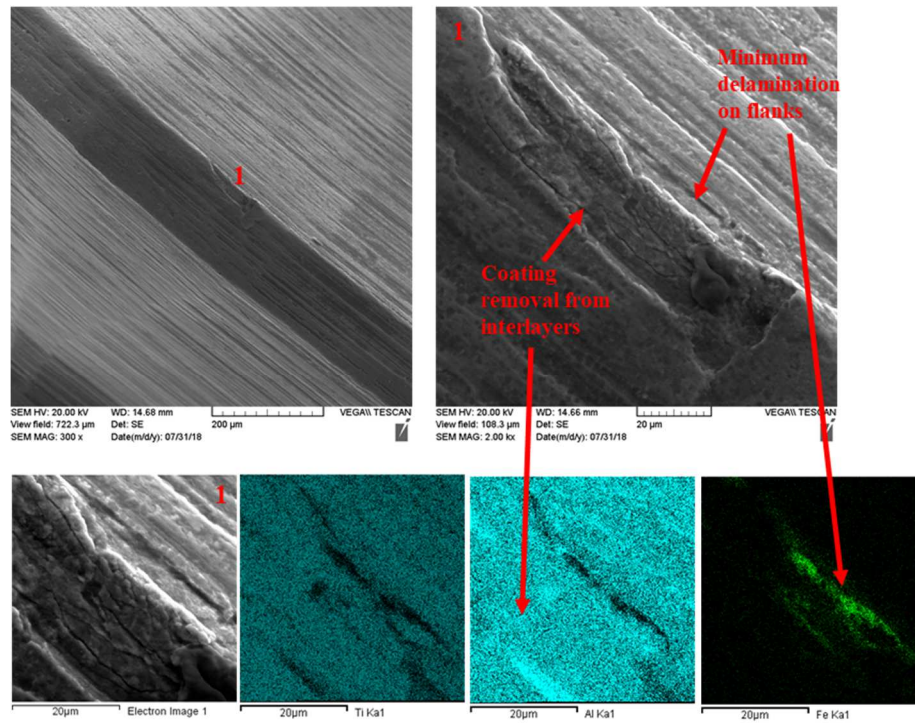
Fig.44: SEM and EDS of the TiAlN coated tap showing the wear on second thread's crest - 360 holes.
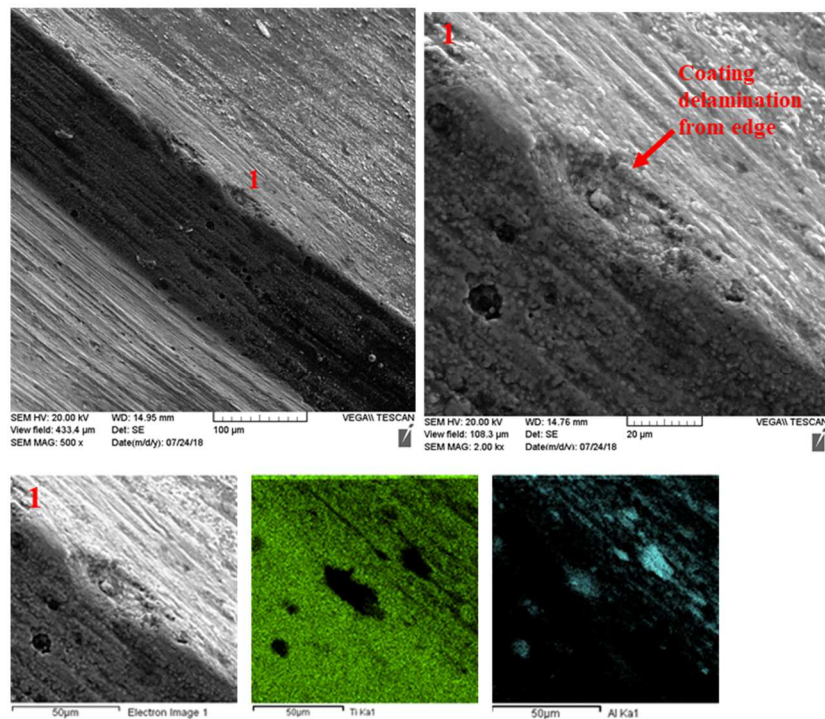
Fig.45: SEM and EDS of the TiCN coated tap showing the wear on second thread's crest- 360 holes.
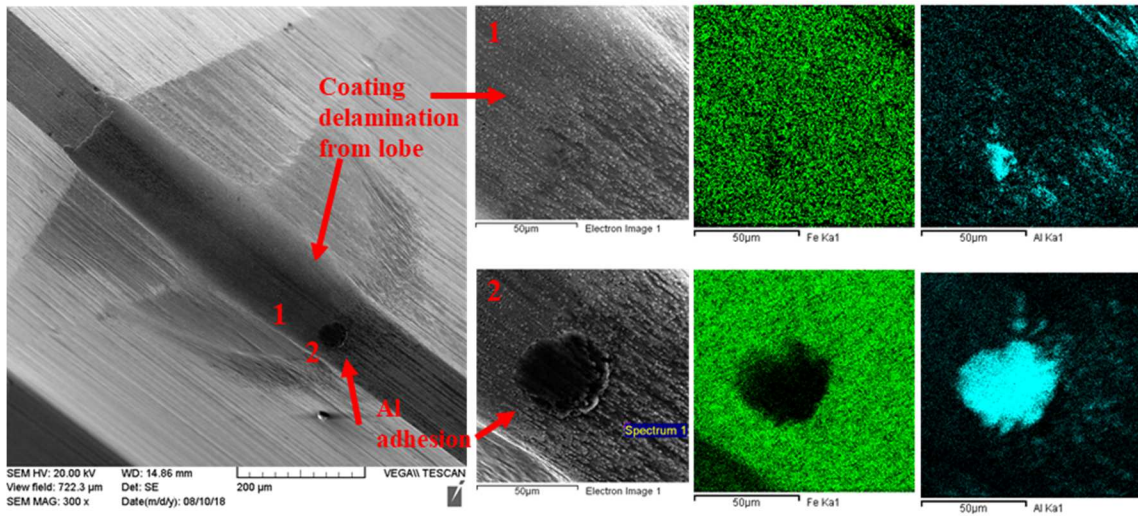
Fig.46: SEM and EDS of the DLC coated tap showing the wear on second thread's crest- 360 holes.

5.3.3 Evaluation of drilled and tapped hole condition

The drilled hole dimeter was checked at intermediate stages of each short test with the CMM (see Appendix A). All holes were found to have a drilled hole diameter within the advised tolerance of 22 microns. There was no influence of hole diameter on the tapping torque results for the thick TiAlN-2 coating.

The thread holes were inspected with an ISO M8 x 1.25 screw plug gauge. All threaded holes were found to be good on both Go and No-Go limits. This indicated that pitch diameter and nominal diameter of the threaded holes are within the expected tolerances (see Appendix A).

5.4 Conclusion of Phase I

The conclusions drawn from the preliminary tests are the following:

❖ The critical wear region on the uncoated tap was found in the previous chapter to be the area over the N-M edge. Wear initiation of the coated taps was also localized at the critical region of crest along the rake edge as shown in Fig.47.
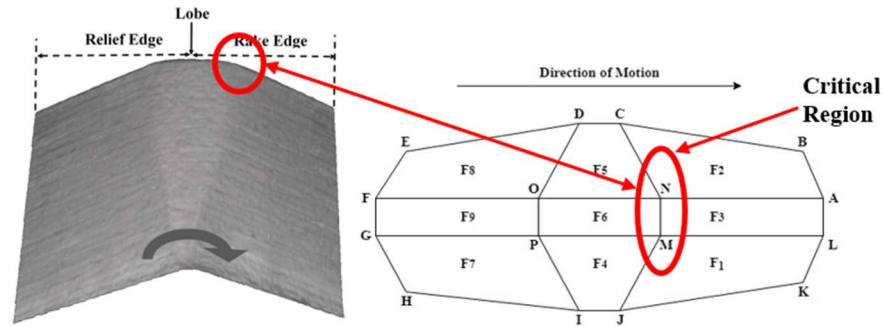
Fig.47: Critical region of the chamfered thread

❖ The majority of the coatings such as ZrN, CrN, TiB2, DLC failed at this region by pluck-out due to severe Al adhesion and subsequently coating delamination. Substrate exposure on the crest's lobe of chamfered threads was severe. Abrasion grooves present on the crest indicated that these coatings did not provide the expected abrasion resistance.

❖ TiCN and TiAlN performed very well compared to ZrN coating (used by the industry partner). Minimal pluck-out along the edge and the rake of the crest was observed after 360 holes. Minor abrasion marks on the crest were observed but no substrate exposure occurred in the grooves.

❖ At this stage, TiAlN and TiCN could be identified as better performing coatings for form tapping of Al-12Si alloys. In order to fully assess the coating's resistance to abrasion and adhesion wear, further machining was planned with these two coatings.

5.5 Results and discussion: Phase II

The wear pattern and failure modes of TiAlN and TiCN could not be established with the short preliminary test. Hence, the progressive wear study was designed to investigate the wear behaviour of TiCN and TiAlN coatings. A comparative study was provided with respect to the ZrN coated and uncoated tap to analyze the improvement of tribological conditions in the form tapping of Al-12Si alloys. In addition, this study also investigated the possibility of any common wear pattern of coatings for this tapping process condition.

5.5.1 Evaluation of torque

The mean torque was monitored in the progressive wear study after producing every 360 holes. Fig.48 showed the mean torque trend for TiAlN, TiCN and ZrN coatings to be slowly increasing upon further machining. This behaviour was expected as the wear on the coatings gradually increased. ZrN had consistently generated marginally lower torque than TiCN and TiAlN. This was attributed to its lower coefficient of friction than TiCN and TiAlN. In comparison to the uncoated tap, all coated taps generated lower torque at an early stage up to 2160 holes. Beyond this state, significant coating delamination at the lobe and severe substrate exposure was witnessed in TiCN (see Fig.56). A detailed discussion of this coated tap's performance will be provided in the next section. Considering the severe wear of TiCN after 2160 holes, there was no further machining with this coated tap.
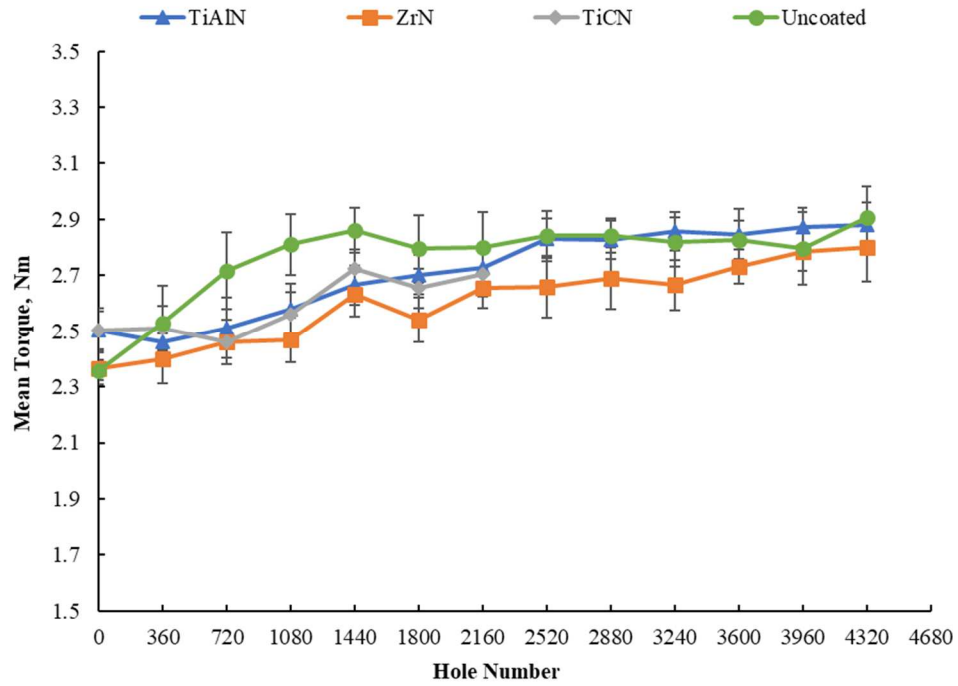
Fig.48: Mean torque of the TiAlN, ZrN and TiCN in the progressive wear tests

In the case of TiAlN, the mean torque steadily increased up to 2520 holes. Beyond this stage, the mean torque trend for this coating is very similar to the uncoated tap. This is due to coating delamination progressing with machining gradually exposing the substrate. After 4320 holes, the uncoated tap showed severe wear on the lobe of the second and third threads. On the contrary, the TiAlN coated tap did not suffer severe substrate wear for the chamfered threads. Hence, it could be inferred from the mean torque evaluation that TiAlN coating could delay substrate wear on the lobes of the chamfered threads.

5.5.2 Volumetric wear analysis

Fig.49 shows volumetric wear progression of the second and third threads on the coated taps after producing 1080, 2160, 3240 and 4320 holes, respectively. The ZrN coated tap was the most worn on the chamfered threads in comparison with other coated taps. If every stage of the three coated taps is compared in terms of wear, the ZrN coating performed the worst. TiCN showed higher wear region than TiAlN at both 1080th and 2160th hole conditions. The TiAlN coating performed the best among the three coatings. The wear on the second thread of the TiAlN coated tap was localized along the edges of the crest. In case of its third thread, the wear initiated at the edges and progressed gradually over the rest area of the lobe. The flanks of its third thread had negligible wear. In the same region of the ZrN coated taps, the wear was more severe than in the other coated taps. Abrasion wear was identified as the wear mode for the flanks of the third thread in Chapter 4. Thus, the TiAlN coating was effective in preventing abrasion wear.

Fig. 50 shows the volumetric wear trends for the second thread of the selected coatings. TiCN performed similar to the ZrN coated tap. The TiAlN coated tap has the lowest wear volume compared to ZrN and TiCN coatings for the second thread. It reduced the wear of the second thread significantly more than the uncoated tap. This could be attributed to the least substrate wear on the lobes of TiAlN coated tap after producing 4320 holes. In case of the uncoated tap, the lobe of the second thread became severely worn after 4320 holes (see Fig. 36 (a)).
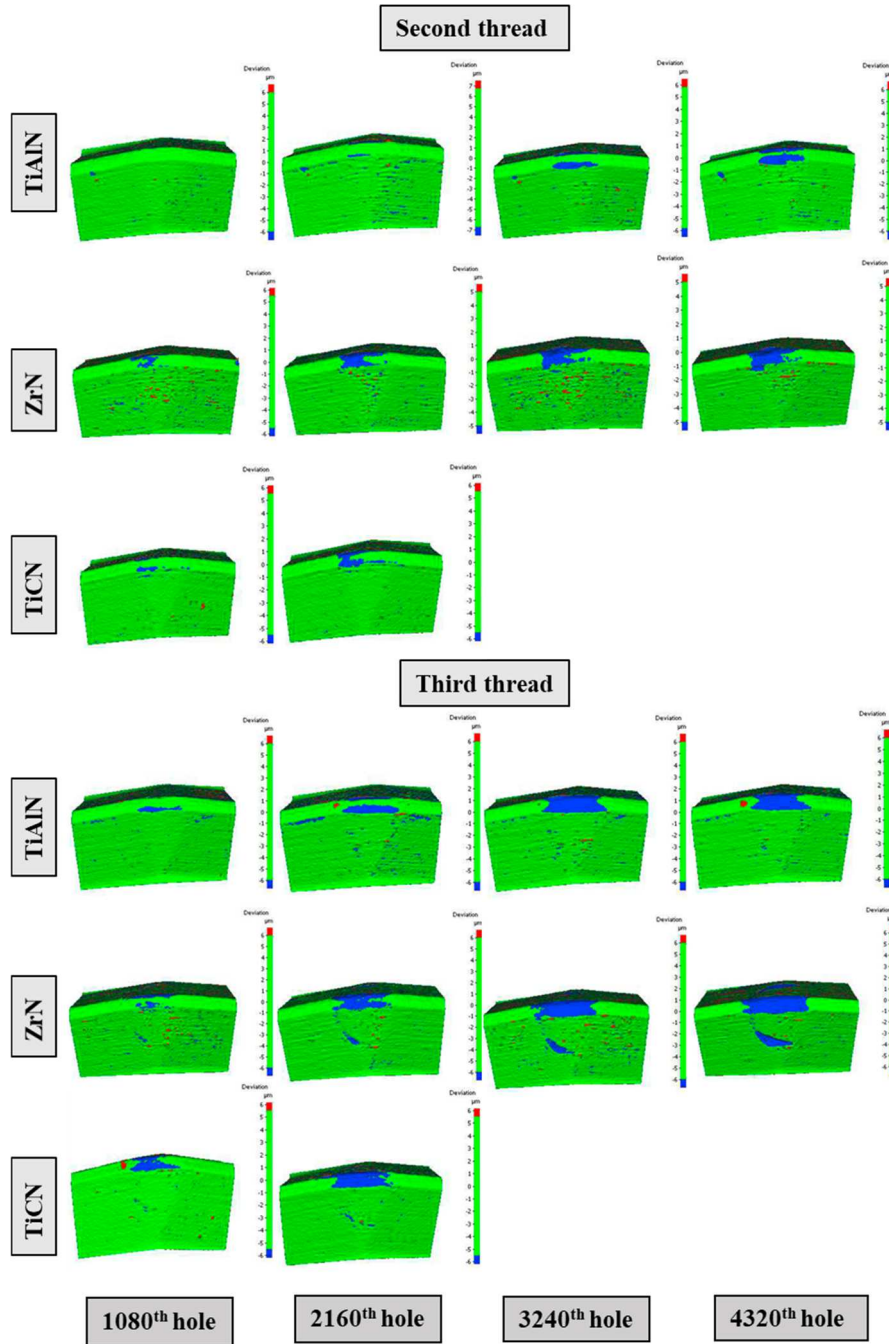
Fig.49: Volumetric wear progression of second and third threads in the progressive wear tests
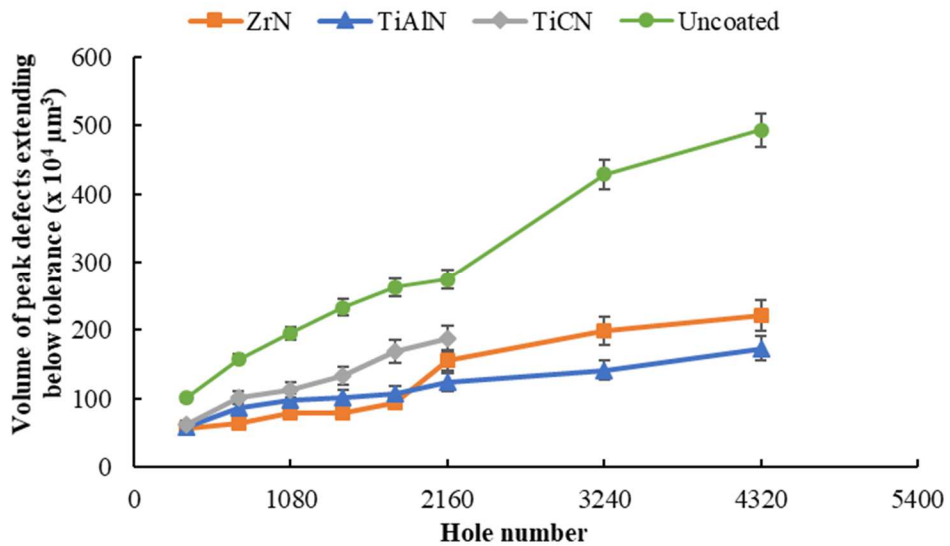
Fig.50: Volumetric wear progression for second thread of the TiCN, TiAlN, ZrN coated taps
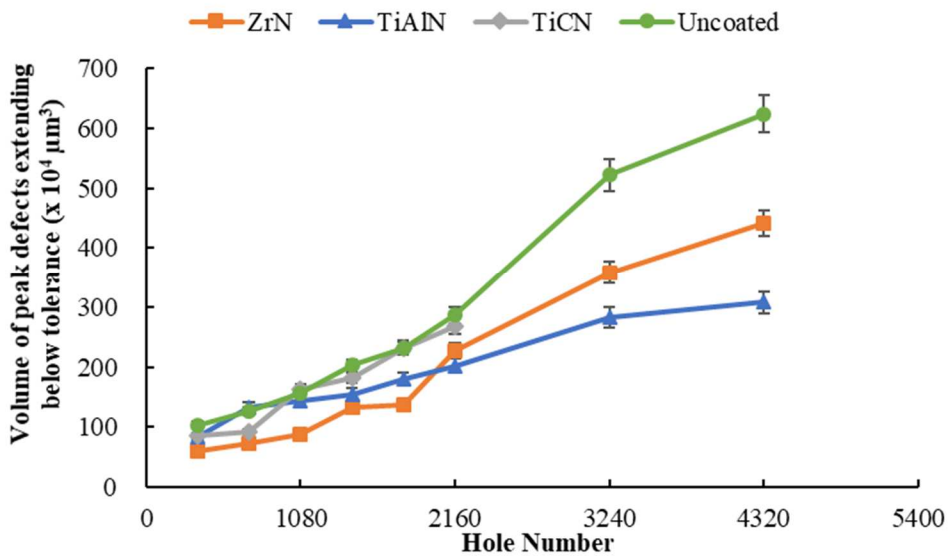
Fig.51: Volumetric wear progression for third thread of the TiCN, TiAlN, ZrN coated taps

In Fig. 51, volumetric wear trends for the third thread are provided for all three coated taps. The wear progression on the third thread was similar to the second thread. The TiAlN coated tap had the lowest wear on the lobe of its third thread. Statistically,

if the volumetric wear of the second and third threads of the TiAlN coated tap is compared to the uncoated tap, there is an almost 284 % and 202 % reduction in wear after 4320 holes are produced.

There was another interesting trend observed in the volumetric wear analysis of the chamfered threads. The third thread had marginally higher volumetric wear than the second thread for the same coated tap. In the case of the chamfered threads of the uncoated tap, there was significantly more wear on the lobe of the second thread than on its third thread. It is important to note here that minimal substrate wear occurred on the lobes of the coated taps after producing 4320 holes. Hence, coating delamination chiefly contributed to the volumetric wear data of most coatings except ZrN. This observation indicated that coating delamination is higher for the third thread than the second thread. Although the plastic work contribution of each chamfered thread is unknown, it can be inferred that the third thread must have experienced different loading conditions than the second thread. This was an important finding in the progressive wear study, which warranted another research study on the impact of tap geometry on the loading conditions of the chamfered threads.

5.5.3 Wear evaluation of the ZrN coated tap

A detailed discussion of the wear behaviour of ZrN coating in form tapping is provided below. The wear assessment of this coated tap was conducted after producing 360, 1080, 2160, 3240 and 4320 holes. The second and third thread were investigated using SEM and EDS extensively. In Fig.52, an overview of the wear progression at the second thread's crest is shown. After producing 360 holes, it was observed that the ZrN

coating was delaminated at both edges of the crest. The coating on the central lobe region was unaffected. The inspection of the lobe after producing 1080 holes showed pluck-out at the rake edge of the crest. Fig.52(b) demonstrated evidence of severe Al adhesion at the pluck-out region of lobe after 2160 holes. The critical region progressively deteriorated due to the growth of pluck-out region. This is evident from Fig.52(c) which showed the condition of the lobe after 4320 holes.
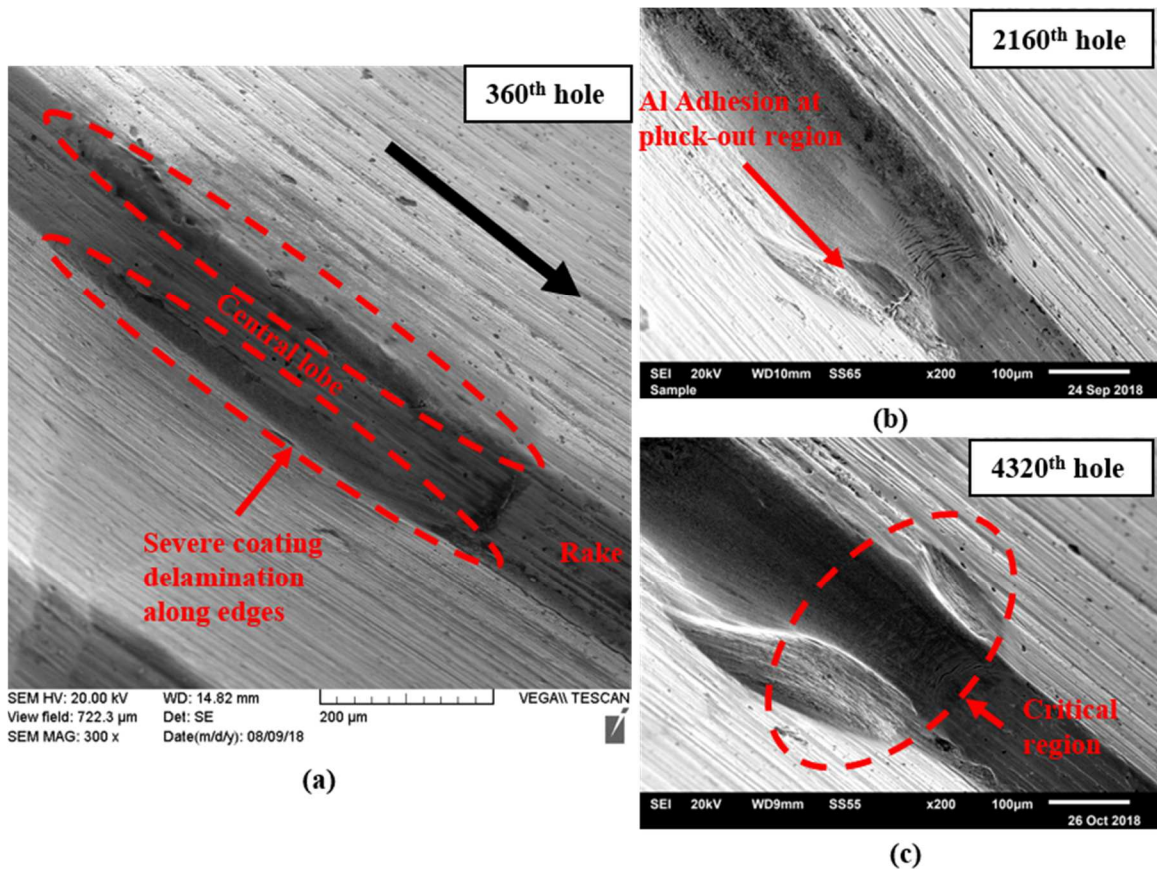
Fig.52: Overview of the crest of second thread (ZrN coated tap)

The critical region of the lobe was inspected at various stages of the progressive wear study. It was noticed that cracks on the coating originated from the fractured

edges. These cracks propagated towards the central region of lobe as machining with the coated tap progressed. Fig.53(a) showed that the development of angular cracks at initial stages of tapping along both the edges. Transverse semi-circular cracks began to form on the central region. These led to subsequent flaking of the coating in the central regions of the lobe. Fig.53(b) provides evidence of flaking from the lobe. Delamination intensified due to high Al adhesion on the lobe. The adhered Al pulls out the flaked coating from the surface of the thread (see Fig.54(c)). Adhesion of the coating to the substrate is drastically reduced once the transverse cracks are completely developed.
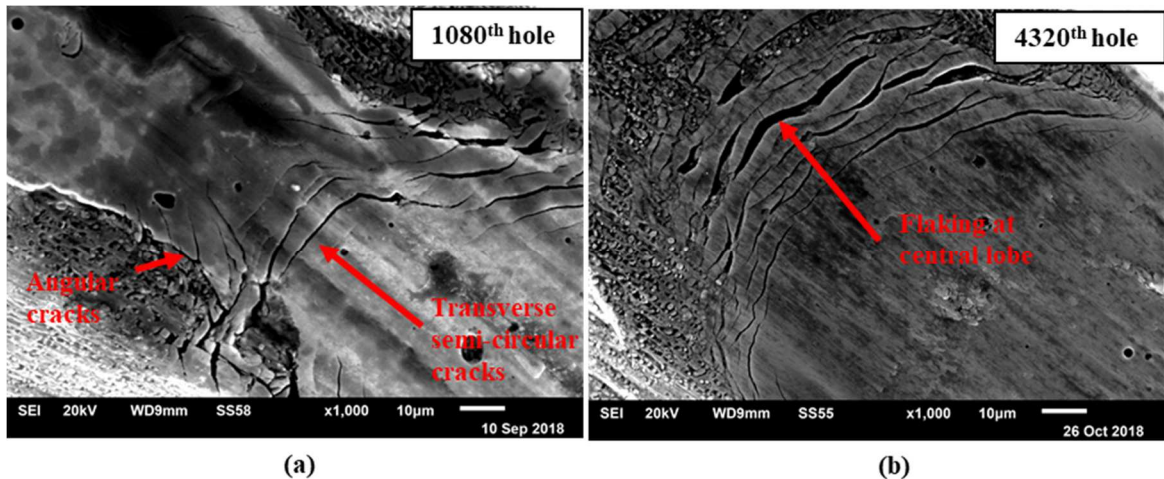
Fig.53: Critical region of the lobe after producing (a) 1080 holes and (b) 4320 holes (ZrN coated tap)

Elemental mapping of the critical region showed severe substrate exposure on the lobe after 2160 holes (see Fig.54(b) and (c)). The presence of Al adhesion on the rake edge is also evident in Fig.54(d). The coating on the crest's rake suffered severe grooving abrasion, but no substrate exposure occurred at this stage (see Fig.54(f)).

Thus, it can be emphasized that coating delamination on the second thread's lobe was the worst after 2160 holes.
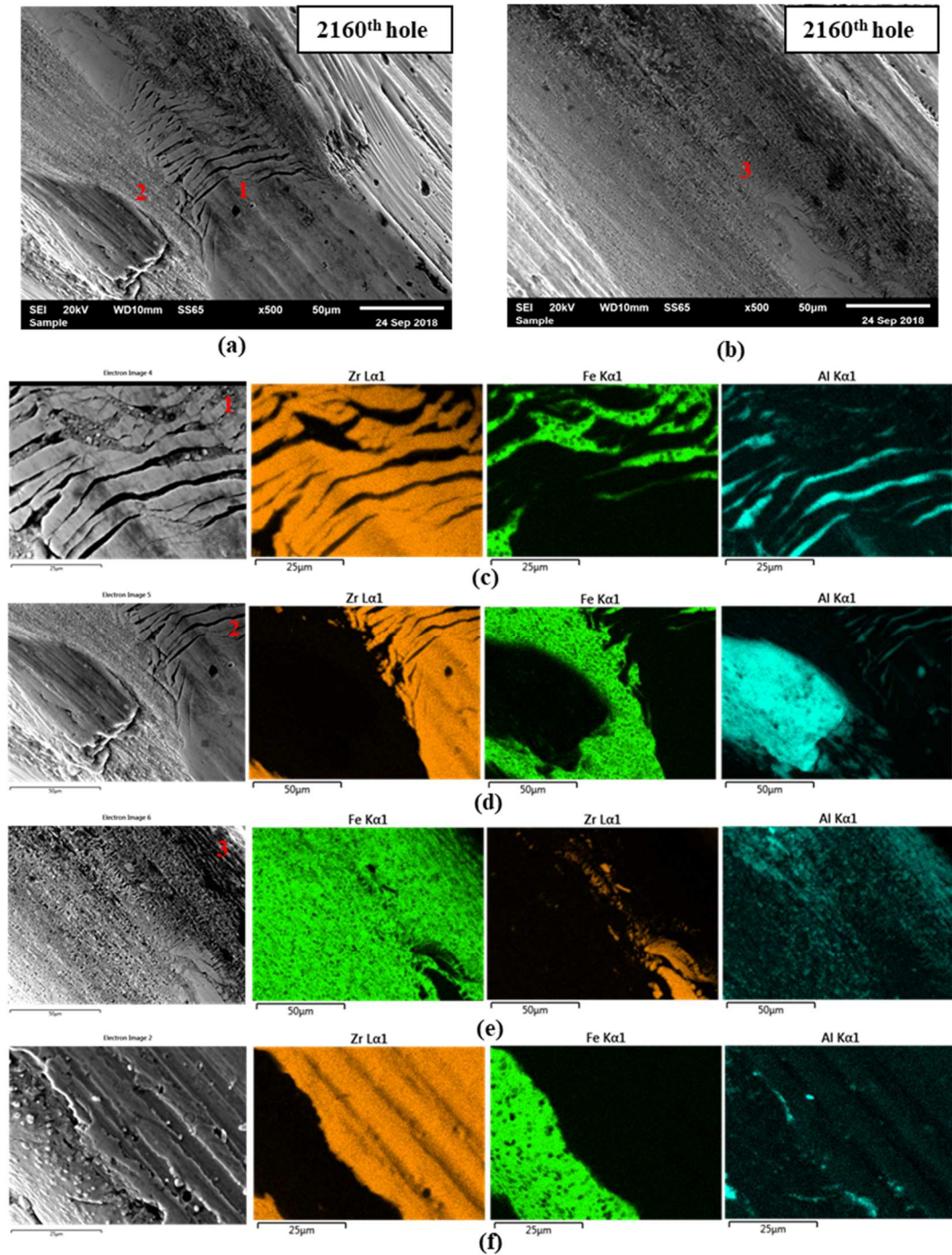
Fig.54: Elemental mapping of crest of second thread after producing 2160 holes (ZrN coated tap)

Fig.55 provides an overview of the critical region of the third thread. The wear propagation was similar to the second thread. Substrate exposure was severe on the lobe after 2160 holes. Al adhesion was consistently observed at every stage of the progressive wear study. There was no substrate wear for the third thread.
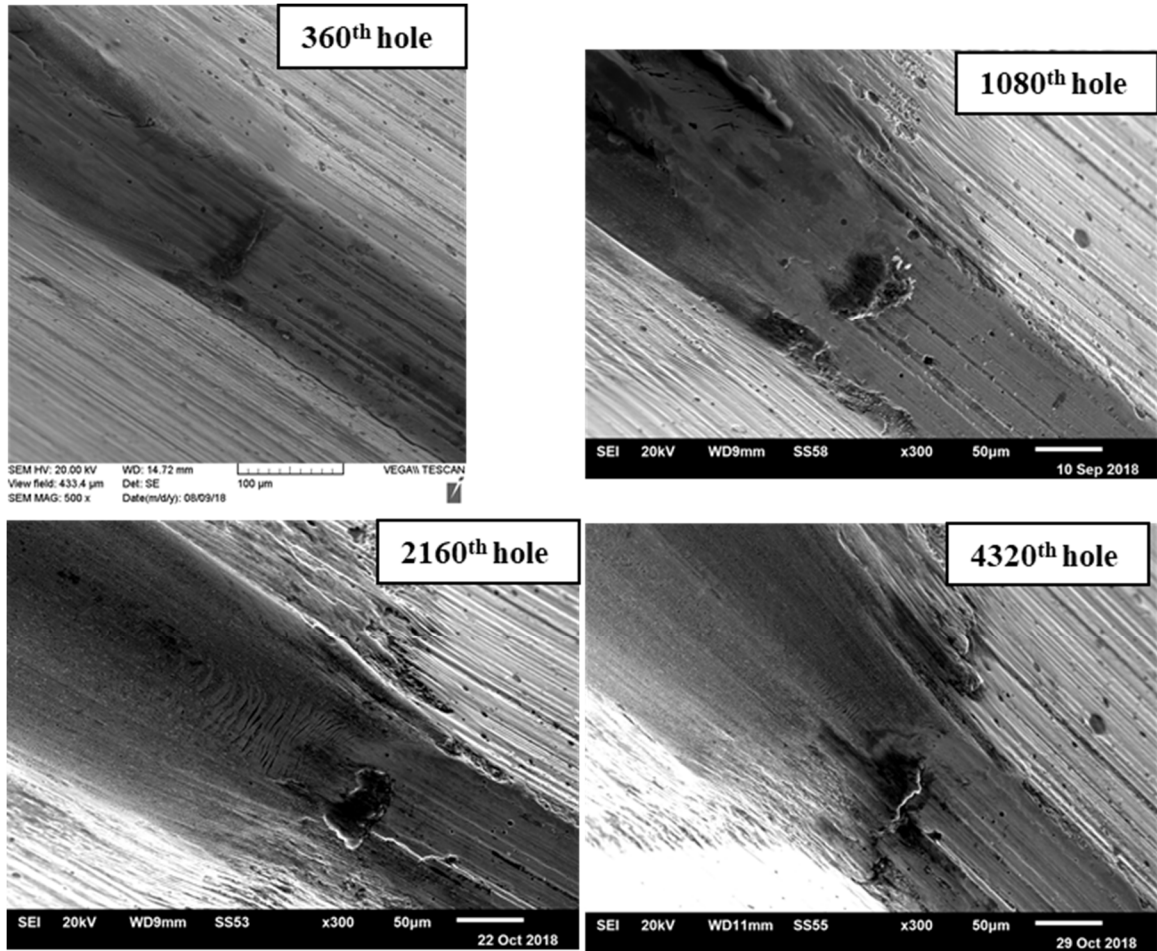
Fig.55: Overview of the critical region over the lobe of third thread (ZrN coated tap)

5.5.4 Wear evaluation of the TiCN coated tap

The wear pattern of the TiCN coated tap's chamfered threads was similar to that of the ZrN coated tap. Severe substrate exposure was observed for both lobes of the second and third threads. In Fig.56, the wear on the critical region of second thread was acute.

Pluck-out was significant on both the edges of the crest after tapping 2160 holes. At this stage, it was decided to not further proceed machining with the TiCN tap. Al adhesion on the third thread was localized in the expected critical region. The condition of the third thread's lobe was similar to the ZrN coated tap. Hence, the TiCN coating did not improve the overall performance of the tap in comparison to the ZrN coating.
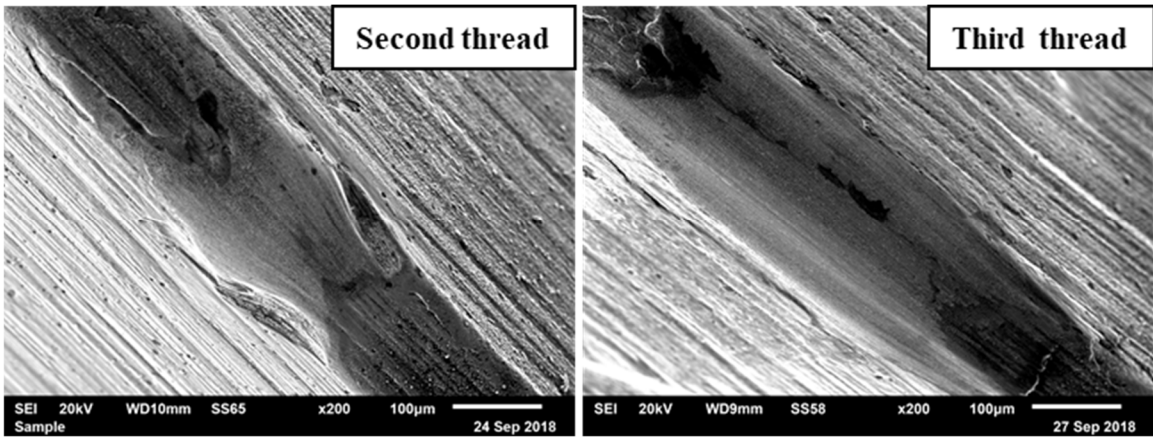
Fig.56: Lobe of TiCN coated tap after producing 2160 holes (a) second thread, (b) third thread.

5.5.5 Wear evaluation of the TiAlN coated tap

A detailed discussion of the wear behaviour of the TiAlN coated taps in machining Al-12Si alloys is provided below. Wear assessment of this coated tap was conducted after producing 360, 1080, 2160, 3240 and 4320 holes. The crests of second and third threads were investigated with SEM and EDS extensively.

An overview of the wear on the second thread's crest is shown in Fig.57. Coating wear initiated after 360 holes. Minor coating delamination started at the edge of the crest as shown in Fig.57(a). After producing 1080 holes, the delamination of the coating progressed further along the edges of the critical region on the lobe. There was considerable delamination and subsequent substrate exposure along the edges of crest

after 2160 holes. Fig.57(c) showed the condition of the lobe at this stage. The coating delamination progressed towards the central lobe region when the tap produced threaded holes from 2160 to 4320 holes (see Fig.57(d)). The coating on the second thread adhered only to the central lobe region at this stage. Unlike the ZrN coated tap which had severe substrate exposure after producing just 2160 holes, the presence of TiAlN coating on the second thread after 4320 holes indicated that the TiAlN coating adhered better to the substrate. Thus, it can be concluded that TiAlN performed better than the ZrN coating in form tapping.
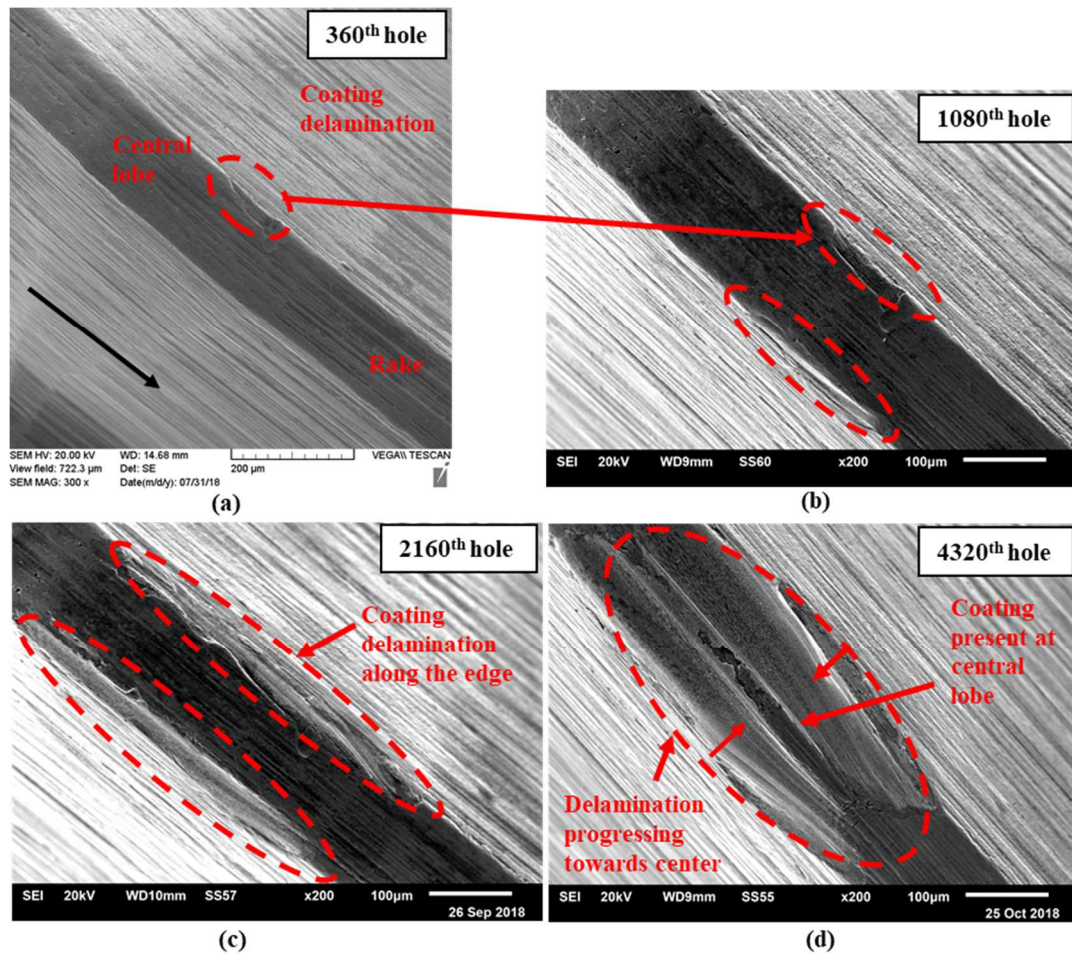
Fig.57: Overview of the crest of second thread (TiAlN coated tap)

The coating delamination initiated the edge of crest for almost all coatings. This could be attributed to the fact that sharp edges act as stress concentration points during the sliding contact [82],[60]. The coating from the tool's edge fractures when the maximum equivalent stress over the edge is greater than the coating film's yield stress [60]. Thus, wear initiation of the coating can be delayed if the edge sharpness of the tap's thread is optimized without compromising the required thread geometry.

Elemental mapping of the critical region provided very interesting observations. Fig.58(a) and (d), shows layer by layer removal of the TiAlN coating on the worn edges with very minor substrate exposure. Such wear behaviour of the coating was observed along the edges at different stages namely 360, 1080 holes and 4320 holes. If a surface layer of the coating developed any cracks, the layer underneath prevents crack propagation through the coating [62], [61]. As such, the TiAlN coating adhered to the substrate for a greater period of machining. The adhered Al along the exposed edge was observed on the second threads (see Fig.58(b)). The removal of this adhered Al during machining also facilitated coating delamination from the tool surface [4]. SEM investigations along the lobe's edge showed formation of angular cracks (see Fig.58(c)). This behaviour of the TiAlN coating was similar to ZrN and TiCN coatings. Also, transverse semi-circular cracks were seen on the central region of the lobe as shown in Fig.58(d).
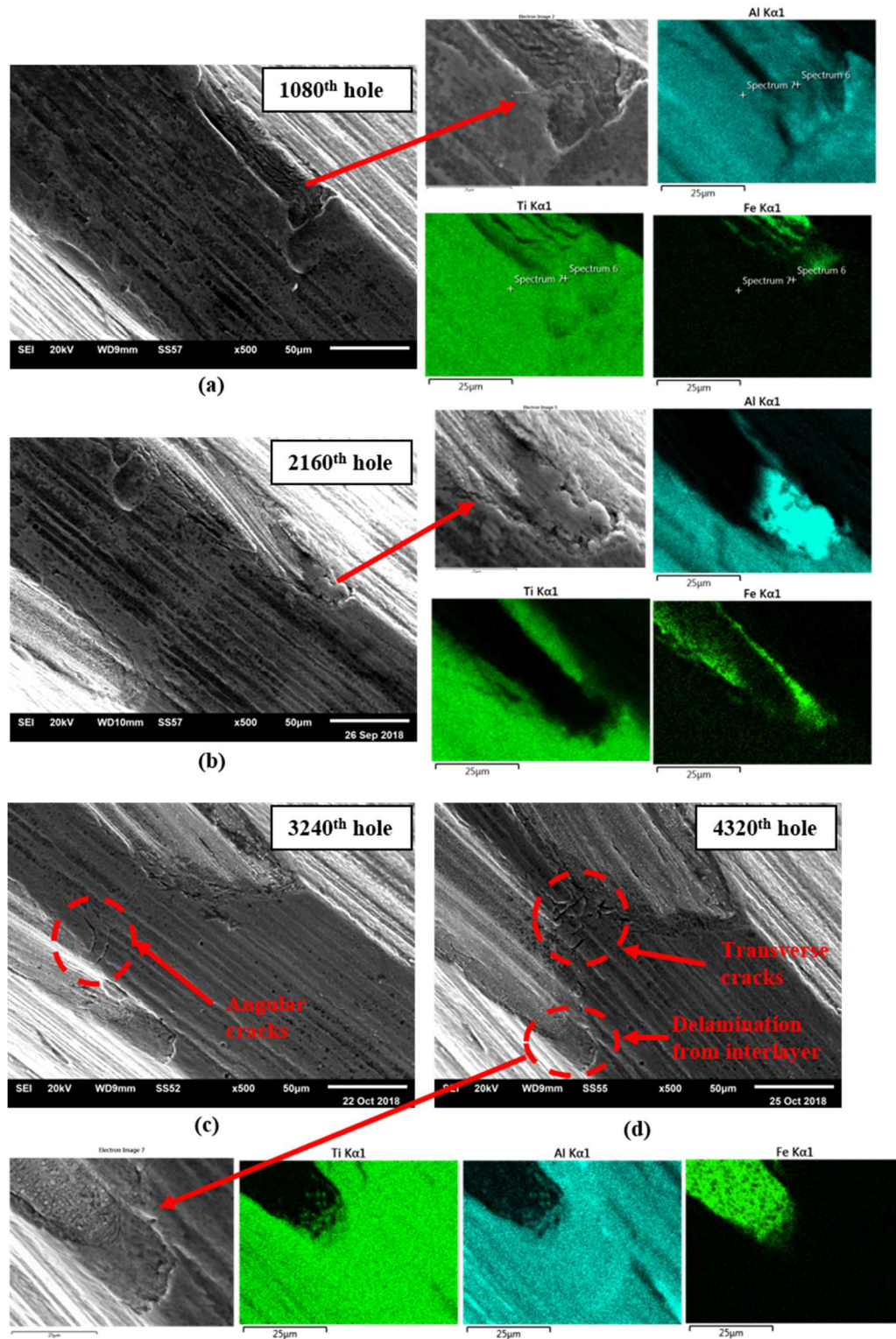
Fig.58: SEM and EDS analysis of the critical region on second thread (TiAlN coated tap)

Generation of angular cracks was detected along the edges at an initial stage of 1080 holes (see Fig.59(a)). These cracks propagated towards the central region of the lobe upon further machining. This is evident from the cracks that developed on the edges of the coated tap after 2160 and 3240 holes, as shown in Fig.59(b) and (c) respectively. Inward crack propagation from both the fractured coating edges led to the development of transverse semi-circular cracks over the central lobe region [83]. Further machining with the coated tap up to 4320 holes caused fracture of the coating and subsequent flaking from the substrate. Fig.59(d) showed the flaking of the coating at the critical region centre.
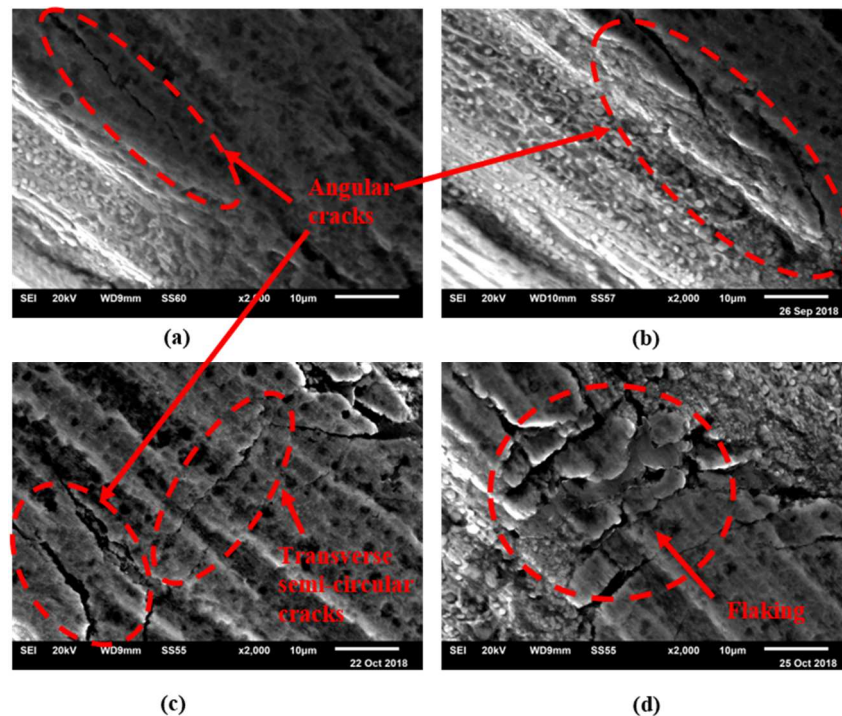
Fig.59: Crack propagation on second thread's lobe after (a)1080, (b)2160, (c)3240, (d)4320 holes (TiAlN coated tap)

A coating system which consists of a thin hard coating on a relatively softer substrate usually experiences buckling failure of the coating [84],[62]. This results in poor adhesion of the coating with the substrate. Buckling failure of coating occurs when the substrate deforms under high compressive stresses, causing interfacial cracks in the hard coating [62],[85]. This condition could be initiated by any existing interfacial defects. Fractured edges along the crest are nucleation sites for cracks which leads to buckling failure of the coatings. This failure mode was commonly observed in the hard coatings studied in this research.

Fig.59(a) showed that the TiAlN coating was able to provide greater abrasion wear resistance, since grooving abrasion was significantly reduced on the lobe of the crest. Unlike the ZrN coating which showed higher substrate exposure on the lobe after 2160 holes, the TiAlN coated tap was effective in protecting the substrate beyond this stage. After producing 4320 holes, the presence of the TiAlN coating at the central region indicated that tool life of the tap could be extended (see Fig.60). The second thread of the TiAlN coated tap suffered minimal substrate wear compared with the uncoated and ZrN coated taps.
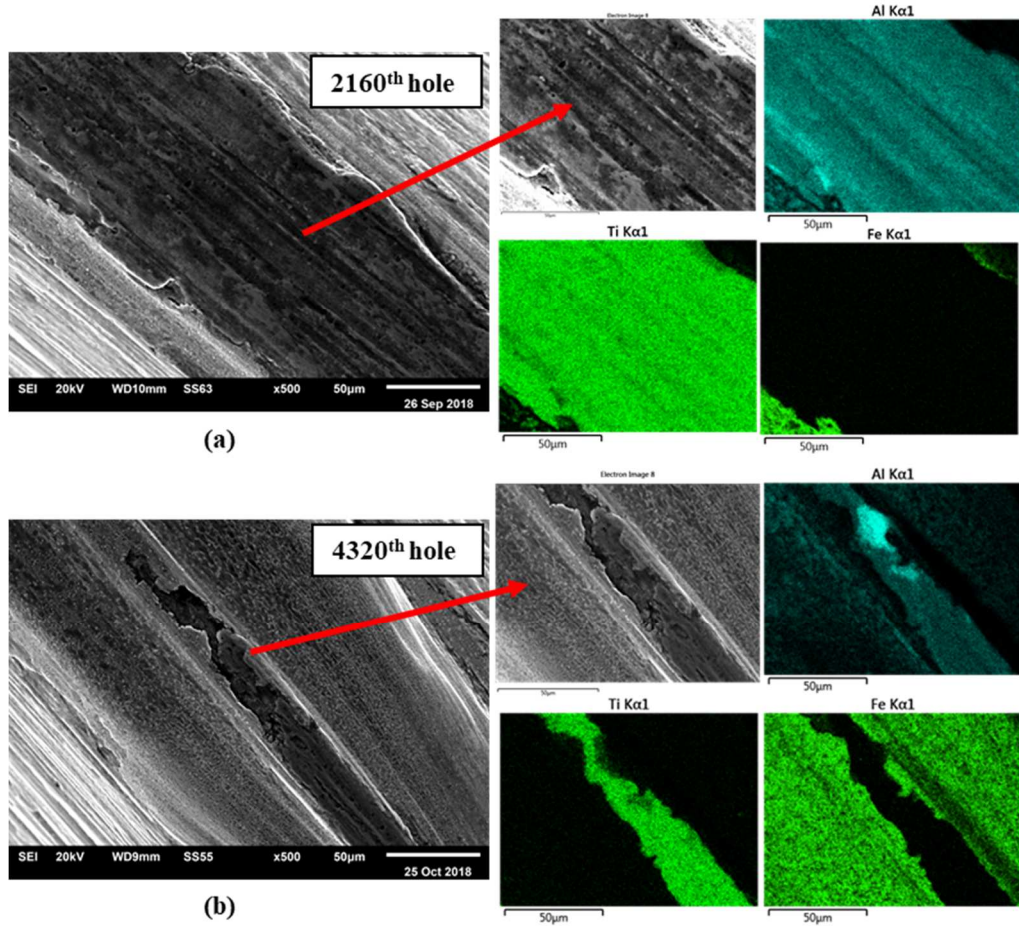
Fig.60: Central region of lobe at (a) 2160th and (b) 4320th hole condition (TiAlN coated tap)

SEM and EDS analysis of the third thread revealed that the wear pattern is similar to the second thread. After 1080 holes, coating delamination was observed along the edge of the lobe. Aluminum adhesion was noticed on the rake of the crest at every stage of the study. Fig.61(e) showed severe substrate exposure occurred at the central region of lobe after 4320 holes. In case of the ZrN coated tap, the coating on third thread was severely worn by 2160 holes. Hence, the TiAlN coating showed better adhesion to the substrate.
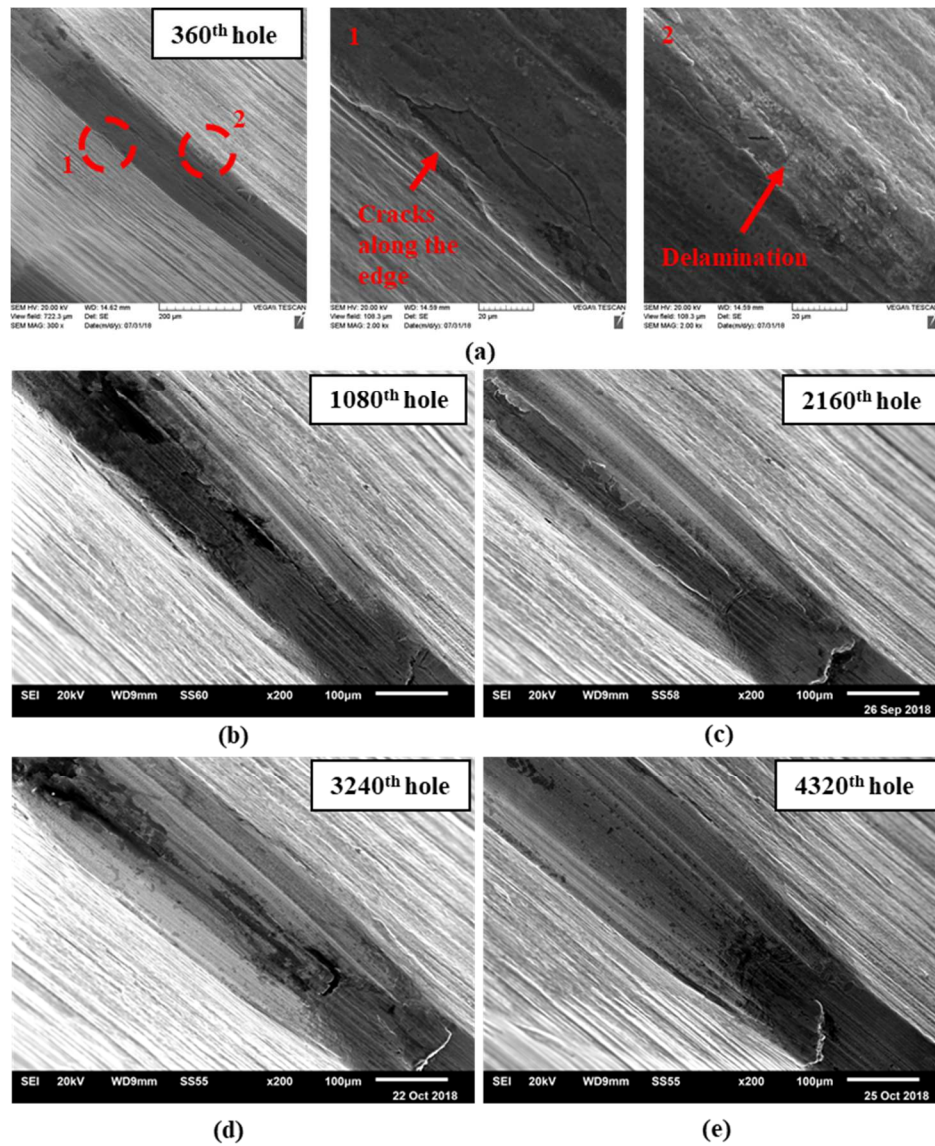
Fig.61: Overview of wear progression of third thread (TiAlN coated tap)

Wear evaluation of the chamfered threads of the TiAlN coated taps provided substantial evidence for the superior performance of this coating compared to ZrN in form tapping of Al-12Si alloy. The TiAlN coated tap showed a significant reduction in wear of the chamfered threads compared to the uncoated tap. Therefore, TiAlN is an effective coating for prolonging tool life and improving the form tap's performance.

5.5.6 Characterization of effective coating

The material characterization of TiAlN and ZrN coatings was performed to assess the mechanical properties and its influence on the wear resistance of the coating. The thickness of the coating was measured using JEOL 6610LV SEM. Fig.62 shows the coating thickness measurement for TiAlN and ZrN.
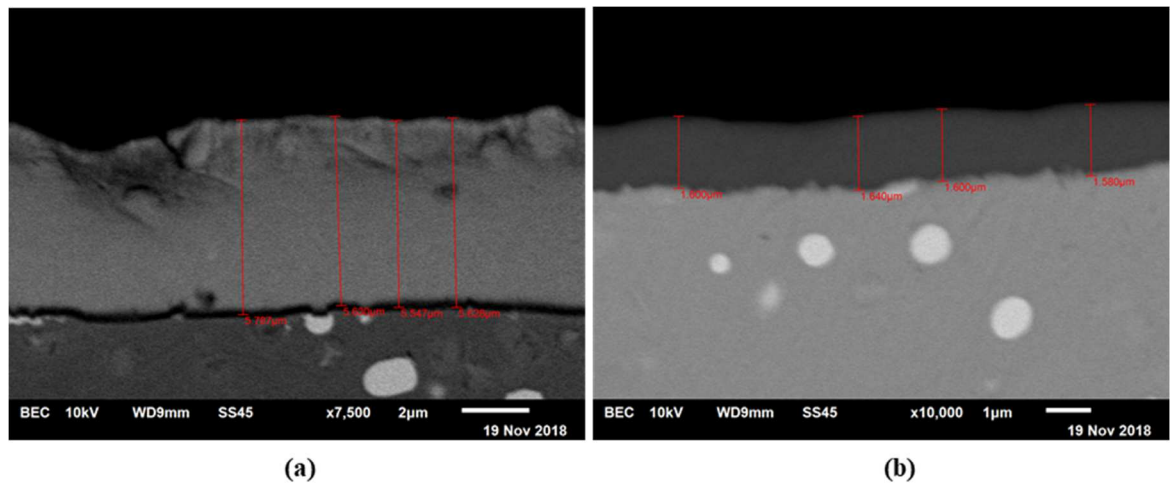
Fig.62: Coating thickness measurement (a) ZrN, (b) TiAlN

Nano-indentation was performed to measure the elastic modulus and hardness of the coatings. An Anton Paar NHT3 Nanoindentation tester was utilized to perform indentation with a Berkovich diamond indenter. In order to avoid any substrate effect, the penetration depth must not exceed 10 % of the coating thickness. Hence, the loading conditions were selected based on this principle (see Fig.63) . An attempt was made to perform scratch tests with the Anton Paar Revetest RST3 scratch tester. The scratch tests were not successful as the coated sample was too rough for a reliable measurement. Lack of coupon availability from the industry partner limited the coating characterization study.
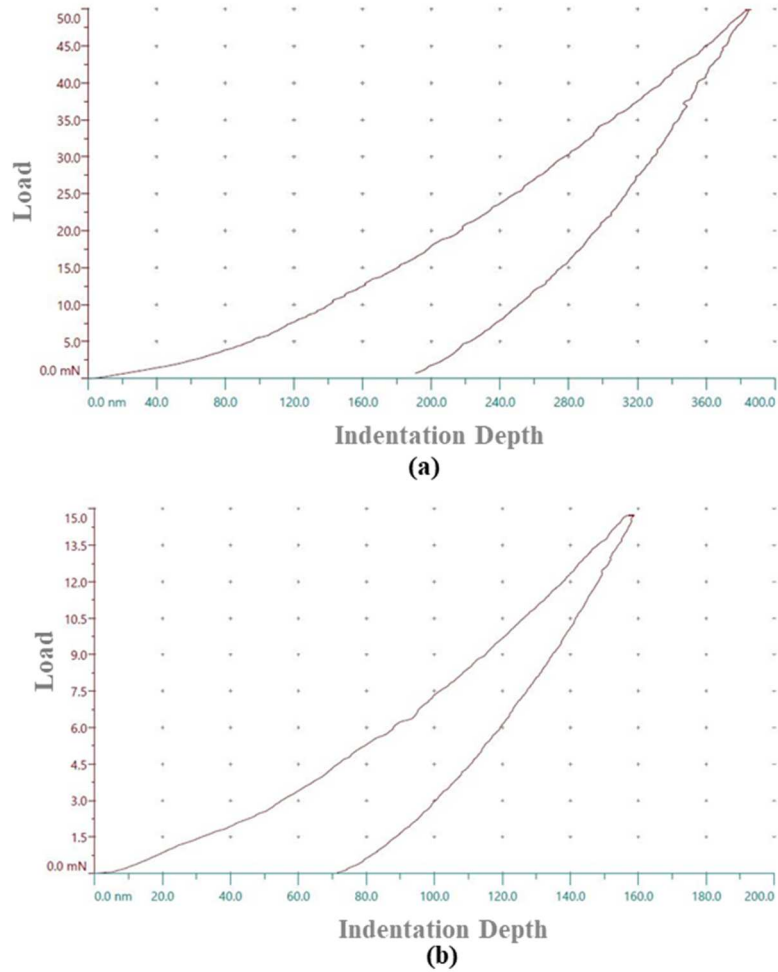
Fig.63: Load vs depth curve obtained from nanoindentation (a) ZrN, (b)TiAlN

Table 10—Mechanical properties of TiAlN and ZrN

Coating	Coating Architecture	Thickness (μm)	Hardness, H (GPa)	Elastic Modulus, E (GPa)	H/E	H^3/E^2 (GPa)
ZrN	Monolayer	5.65±0.09	24 ± 1.6	302 ± 28	0.072	0.127
TiAlN	Multilayer	1.61±0.02	38 ± 1.65	500 ± 13	0.077	0.236

The hardness of the coating directly influenced its the wear resistance [62]. Hardness is a measure of resistance to plastic deformation on the surface during sliding contacts. Hardness of HSS substrate was much improved by the TiAlN coating

116

compared to ZrN. Higher hardness could decrease wear by preventing ploughing on sliding surfaces. In this research, intense abrasion wear occurred on the crest and flanks due to very high content of silicon in the aluminum alloy. Evidences of both two and three body abrasion necessitates the requirement of a hard coating on the form tap. The TiAlN coating provided much higher hardness and better abrasion wear resistance than ZrN. Unlike ZrN coated taps, there was minimal abrasion wear on the flanks of the TiAlN coated taps.

Generally, elastic modulus tends to increase along with coating hardness. The elastic modulus of the coating should be close to the substrate value such that the coating is allowed to deflect with the substrate without crack formation [86], [87]. Buckling failure can be prevented in this case. It is nearly impossible to have high hardness and low elastic modulus for hard coatings at the same time. Therefore, a large H/E ratio is an indicator of a coating with high hardness but relatively low elastic modulus. It can also be used to characterize the fracture toughness of coating [88]. A coating with large H/E ratio can be considered a more durable coating [87]. The TiAlN coating has a higher H/E ratio than the ZrN coating.

The H^3/E^2 of a coating is an effective indicator of its resistance to plastic deformation [87]. The H^3/E^2 of TiAlN is greater than ZrN which means that the TiAlN coating provides greater load support [89].

Monolayer thin coatings are more susceptible to through coating cracks at higher mechanical loading conditions. ZrN performed worse than TiAlN since cracks propagated earlier in ZrN. The TiAlN coating's multilayered architecture provided

better adhesion of coating to the substrate, high mechanical load bearing capacity and better resistance to crack propagation [62]. As discussed earlier, crack propagation on a surface layer can be prevented by the layer underneath. Coating removal occurs layer by layer [61]. The TiAlN coating provided better adhesion and crack resistance to the substrate under high mechanical loads.

Coatings on the HSS substrate must be carefully designed to reduce any effects of elastic modulus mismatch in the coating-substrate system. AISI M2 HSS material typically has an elastic modulus of 190-210 GPa. A large difference between the elastic modulus of the coating and substrate could impact the performance of the coated tool [90]. In order to improve the wear resistance of coating, high hardness and low elastic modulus is required. A TiAlN coating on a WC-Co substrate could provide an alternative to the current coating-substrate system which might further improve the performance of this coating [90].

5.6 Wear modes and progression

 ❖ Coating delamination is first observed at the critical region of the lobe on the chamfered threads after 360 holes (see Fig.64).

 ❖ Delamination progresses rapidly along the edge after producing 1080 to 2160 holes.

 ❖ Angular cracks originate from the fractured coating edges after 1080 holes.

 ❖ Transverse semi-circular cracks develop on the central region of lobe after 2160 holes. Angular cracks tend to propagate inwards from both the edges of the crest.

❖ On further machining up to 4320 holes, intense flaking occurs on the lobe, severely exposing the substrate.

❖ This wear pattern is commonly observed for both second and third chamfered threads of a coated form tap in machining Al-12Si alloys.
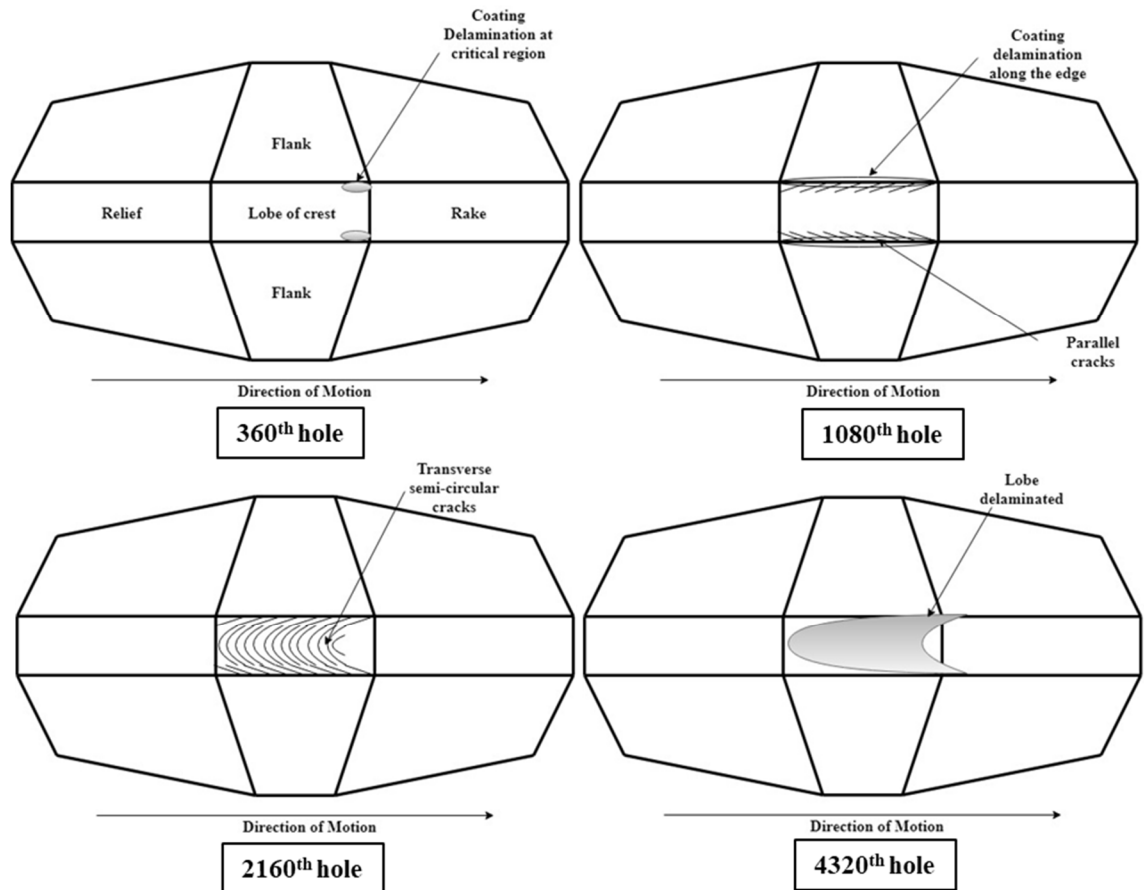
Fig.64: Common wear pattern of coated taps

5.7 Conclusion

1. The preliminary tests on coatings were effective for quickly eliminating the poorly performing coatings. Wear initiation of the coated taps occurred at the

critical region of the lobe as identified in the uncoated tap study. Severe Al adhesion at the critical region led to pluck-out of the coating from the substrate. Abrasion wear over the lobe of the crest was detected for the chamfered threads.

2. TiAlN and TiCN coatings performed very well compared to the ZrN coating in the preliminary tests. Minimal Al adhesion, abrasion and coating delamination were observed for these coatings after producing 360 holes. Therefore, the TiAlN and TiCN coated taps underwent further testing. In addition, the performance of the uncoated and ZrN coated tap was compared with the two better performing coated taps.

3. Mean torque variation of the coated taps in the progressive wear study showed a similarly increasing trend as the uncoated tap. The TiAlN coated tap had a lower average mean torque than the uncoated tap. The high torque of the uncoated tap was attributed to the greater wear on its chamfered threads.

4. Wear of the coated taps consisted of mostly coating delamination over the lobe and flanks. The reduction in volumetric wear of the chamfered threads was over 200 % for the TiAlN coated taps with respect to the uncoated tap after producing 4320 holes. This was attributed to minimal substrate wear for the TiAlN coated taps. The volumetric wear of TiCN taps was greater than TiAlN and ZrN coating after 2160 holes. Hence, the TiCN coated tap did not undergo further testing.

5. After the initiation of wear at the critical region, wear progressed along the entire edge on further machining. The edge of the crest behaved as stress

concentration points which caused fracture of the coating upon loading. Angular cracks originated from both the fractured coating edges and the transverse semi-circular cracks developed over the central region of the lobe. This led to severe subsequent flaking of the coating from the lobe. Al adhesion and pluck-out from the crest intensified coating delamination. This was a common wear pattern for all coated taps.

6. In the case of ZrN and TiCN coated taps, the chamfered thread's lobe was severely delaminated and significant substrate wear occurred at the critical region after 2160 holes. Although the substrate of TiAlN coated taps became exposed on the lobe, the delamination was most severe on the chamfered threads after 4320 holes. Therefore, the TiAlN coating was effective in delaying the delamination and preventing substrate wear at the critical regions.

7. Crack generation was attributed to the buckling failure of hard coatings. Substrate deformation due to high compressive stresses led to crack development on the hard coatings. This reduced the adhesion of hard coatings on the relatively softer substrates.

8. The TiAlN coating performed better than the other coatings for several reasons. High hardness provided superior resistance to abrasion wear for form tapping of Al-12Si alloy. The H/E ratio of TiAlN was greater than ZrN. This indicated better fracture toughness and durability of the coating. Also, the H^3/E^2 of TiAlN was greater than ZrN which showed that the TiAlN coating offered greater load support. The multilayered architecture of the TiAlN coating provided better

adhesion of the coating to the substrate and improved crack resistance under high mechanical loading conditions.

9. The TiAlN coating proved to be an effective coating for form tapping of Al-12Si alloys. It outperformed other PVD coatings, including the ZrN coating presently used in the industry. Longer tool life can be expected for HSS form taps if the coating is optimized accordingly.

10. Future wear investigations must be conducted with preliminary tests and followed by a progressive wear study. The preliminary test must be focused on detecting coating failure at the critical region. A progressive wear study must be initiated only if the coated tap does not have any delamination on the edges of the crest after the preliminary test. This approach to tool wear study will reduce material consumption, time and effort.

Chapter 6. Assessment of form taps with end of service-life condition

Based on industrial data, tool life of form taps in machining Al-12Si alloys is estimated at around 20,000 holes. This is considered to be the safe limit at which production of geometrically correct form threads can be ensured in mass-scale production setups such as the automotive industry. Although form taps have longer tool life, rapid wear of coatings on the form tap is a major challenge in industry. Process instability largely depends on the wear of the coated taps. Failure of form taps at an early stage could lead to high rework costs and scrap. As such, the coating on the tap is expected to preserve the geometry of the form tap until the end of its expected life. To fully understand the coating behaviour in this application, three M8 x 1.25 form taps that had reached end of tool-life were studied. A comparison of the wear of chamfered threads was made between the end of tool-life taps and the taps producing up to 4320 holes in this research.

6.1 Evaluation of torque

The three ZrN coated taps from industry were used to produce a certain number of holes in the same experimental setup of this research. It is important to mention that these taps were identical to the form taps studied earlier. The mean torque was monitored and recorded for analysis. In Table 11 shown below the average torque of ZrN coated taps at 20000 holes was 3.3 Nm, which was 18 % higher than the torque of the form tap after 4320 holes.

Table 11—Torque data of end of tool life taps

	ZrN - 4320 holes	ZrN - 20,000 holes	Increase in Torque (%)
Average of Mean tapping torque (Nm)	2.79 ± 0.07	3.30 ± 0.09	18.27

6.2 Inspection of thread quality and hole diameter

The internal threads produced by the three form taps were inspected by ISO M8 x 1.25 screw plug gauge to check geometrical conformity. All threads passed thread gauging tests. The internal thread's pitch diameter and nominal diameter was within the expected tolerance. This indicated that these taps produced good quality threaded holes even at the end of tool life. The drilled hole diameter was measured with CMM to eliminate any process variation due to the unexpected changes in hole diameters. All drilled holes were found to be in good condition. The results of this inspection test are included in the Appendix A.

6.3 Wear evaluation of the end of tool-life taps

SEM and EDS analysis were performed on these three ZrN coated taps to investigate the coating wear behaviour at the end of tool-life condition. An attempt was made to correlate this stage of wear with the wear pattern observed for the ZrN form taps after producing 4320 holes. The end-of-life taps were named as Tool 1, 2 and 3 for convenience.

6.3.1 Second chamfered thread

The second threads of the tool 1 ,2 and 3 were investigated for analysis of wear on the lobe of the crest. The lobe of Tool 1 was severely worn with complete coating

delamination. The crest of Tool 1 in Fig.65 was similar to the wear on uncoated tap shown in Fig.34(a). Although Tool 1 produced 20,000 holes, the comparable wear on the uncoated tap's lobe occurred after 2160 holes. Also, it should be noted that the lobe of Tool 1 is the most worn out of the three. An important conclusion could be made here with respect to the second thread of ZrN tap. With the application of ZrN coating, Tool 1 had the worst condition of the second thread at the end of tool life. Therefore, a tool life study of a coated tap could be designed based on substrate wear of the second thread reaching to the condition of Tool 1.
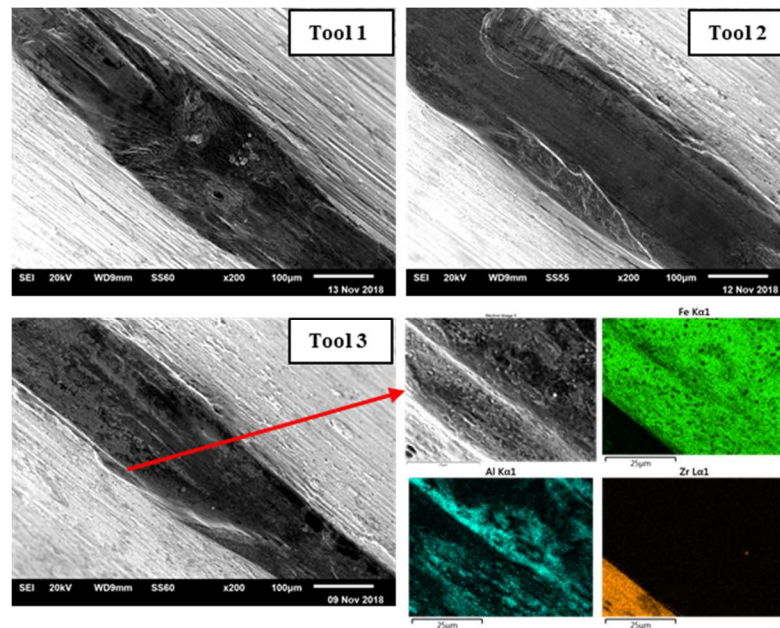
Fig.65: SEM and EDS of the second chamfered thread of Tool 1, 2 and 3

The presence of Al adhesion on the crest edge of Tool 3 indicated that severe adhesion wear was a major wear mechanism for form taps (see Fig.65). Complete coating delamination from the lobe of the crest for the second threads was expected at this stage. Abrasion grooves were detected at various locations on the crest.

6.3.2 Third chamfered thread

Tools 1, 2 and 3 had complete coating delamination from the lobe of the third threads. Elemental mapping of Tool 2 at the lobe showed total substrate exposure as seen in Fig.66. Tool 1 and Tool 2 had significant wear on the edges of the crest in the lobe region. In Fig.66, one of the edges of Tool 2 had developed a rounded shape. It could be inferred from this observation that the edges of the lobe adapt themselves such that stress concentration is minimal. Edge geometry of the thread has an impact on premature coating failure along the edges at an early stage of tool life.
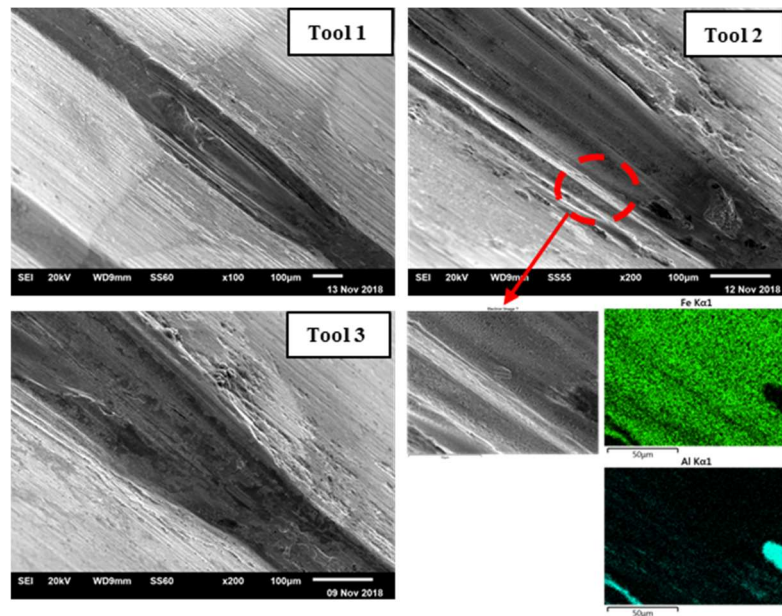
Fig.66: SEM and EDS of the third chamfered thread of Tool 1, 2 and 3

6.3.3 Coating wear on the first five threads

Tools 1, 2 and 3 had similar coating wear on the first, fourth and fifth threads. Minimal substrate wear occurred in these threads. Most coating delamination was localized over the crest's lobe. Angular cracks and flaking were observed on the lobes.

Fig.67 showed substrate exposure on first, fourth and fifth thread of Tool 1. The severity of delamination on these threads was comparatively lower than the chamfered threads. The presence of ZrN coating on the first, fourth and fifth threads at the end of tool life indicated that coating wear should be studied on the chamfered threads. Hence, the previous wear study of TiAlN coatings, based on the chamfered threads, produced convincing results.
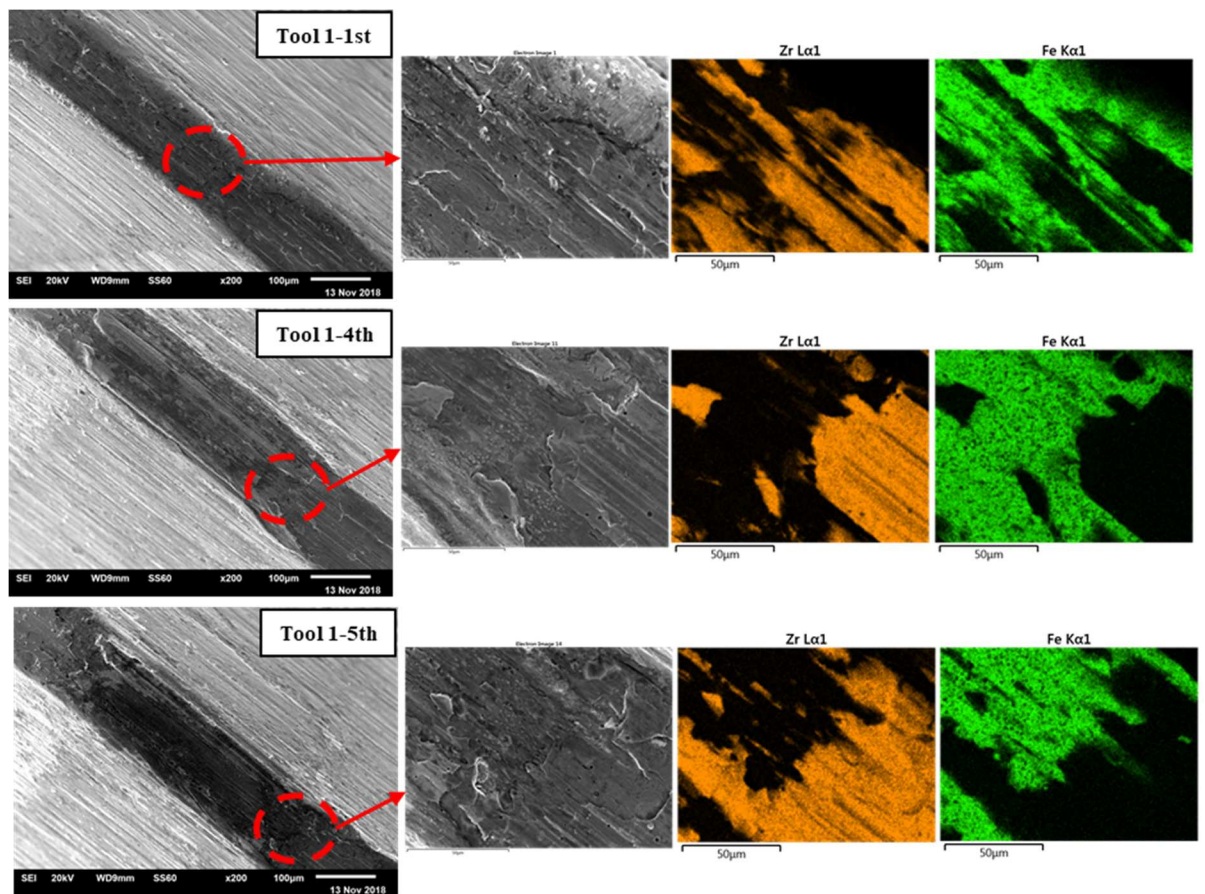
Fig.67: SEM and EDS of the first, fourth and fifth threads of Tool 1

6.4 Conclusion

1. The mean torque for form tapping could rise by 18 % at the end of tool life.

2. Threaded holes produced by Tools 1-3 were inspected. Thread gauging found all holes to be in good condition.

3. The lobes of the second and third threads were completely delaminated in the end of life taps.

4. Conclusions were drawn from the investigation of wear on second thread. A tool life study of a coated tap could be designed based on the substrate wear of the second thread reaching to the condition of Tool 1.

5. Based on observations of the third thread, it was concluded that the edge of the lobe adapts to minimize stress concentration.

6. The thread edge geometry could have an impact on premature failure of the coatings along the edge of the lobe at an early stage of tool life.

7. The severity of coating delamination is comparatively lower than the chamfered threads at the end of tool life. Hence, coating wear studies on form taps must be based on the coating performance of the chamfered threads.

Chapter 7. Conclusions and Future work

7.1 Conclusions

This research was focussed on investigating the wear mechanisms and failure modes encountered by form taps when machining Al-12Si alloy. In collaboration with the industry partner, this body of work presented a detailed discussion of the results obtained from the study on PVD surface coatings. Several key findings were concluded from the three major research studies undertaken to develop the form tap for superior performance and higher reliability. A summary of the major conclusions is provided below:

1. The wear mechanism of the uncoated tap was established as a combination of both adhesion wear and abrasion wear. Severe pluck-out occurred on the thread's crest due to the removal of aluminum build-up during tapping. Hard silicon precipitates in the α-Al matrix caused two-body abrasion wear on the flanks and crest's rake. Micro-grooving of the lobe occurred due to the wear debris generated in the process.

2. The second and third chamfered threads were identified as the most worn threads on the tap. A critical region on the lobe of the crest towards the rake was identified as the wear initiation region. Severe pluck-out was detected at this region.

3. The linear-wear measurement method was successful in the detailed wear analysis of the lobe only. The volumetric-wear measurement method accounted for total wear of the entire thread. The volumetric wear was a better performance metric as

build-up and wear volumes were measured for complex geometries. Hence, the latter method was preferred for the study on PVD coatings.

4. The key performance metrics such as the linear wear, mean torque and volumetric wear increased rapidly up to 2160 holes. Beyond 2160 to 4320 holes, the slow wear progression and minimal torque variation suggested a steady wear region of the uncoated tap. Hence, it was concluded that two stages of wear existed before and after 2160 holes for the uncoated tap.

5. Based on the results of the previous study with an uncoated tap, a progressive wear study was designed to evaluate the wear of coated taps after 1080, 2160 and 4320 holes.

6. In the next study, the preliminary tests showed wear initiation of the coated taps at the expected critical region. The TiCN and TiAlN coated taps suffered minimal coating delamination, aluminum adhesion and abrasion wear on the lobe. Hence, progressive wear of the TiCN and TiAlN was conducted. The TiCN coated tap was withdrawn after 2160 holes due to severe substrate wear on the lobe of the second thread.

7. By the 4320th hole, the volumetric wear of the TiAlN coated tap was reduced by nearly 200% and 50% when compared against the uncoated and ZrN coated taps, respectively. This significant improvement was attributed to better adhesion of the coating to the substrate. An extensive SEM and EDS investigation showed that the TiAlN coating delamination at 4320th hole was similar to the ZrN coating at 2160th

hole. Hence, the TiAlN coating delayed its delamination and prevented substrate wear on the lobe.

8. The progressive wear study revealed a common wear pattern for the coated taps. At the critical region, coating delamination initiated and then progressed rapidly along the edge of the crest with further machining. This fracture of the coating was caused by stress concentration along the edge. Angular and Transverse cracks propagated from both edges due to buckling failure of hard coatings. Subsequently, flaking was intensified by severe Al adhesion on the central region of the lobe.

9. Nano-indentation tests were conducted to compare the mechanical characteristics of TiAlN and ZrN coating. The high hardness of TiAlN provided superior resistance to abrasion wear. The H/E ratio of TiAlN was higher than ZrN which indicated better fracture toughness and durability of TiAlN. Also, the H^3/E^2 of TiAlN was higher than ZrN which showed greater load support with TiAlN. The multilayered architecture of TiAlN coating provided better coating adhesion and improved crack resistance under high mechanical loads. Since TiAlN outperformed the ZrN coating, a higher tool life of TiAlN coated taps could be expected.

10. A few taps, at the end of service, were assessed in the final study to validate several findings of the previous studies. The second thread's lobe of the uncoated tap at 2160th hole was similar into the one produced by the ZrN coated tap (Tool 1) at the end of service life. Hence, this stage of wear is taken as the maximum accepted wear for the coated form taps.

11. The investigation of the third thread revealed that the crest's edge tends to adapt its shape to reduce stress concentration. Hence, early failure of the coating on the edge was indeed due to severe stress concentration along the edge.

12. Elemental mapping of the first five threads showed complete coating-delamination of the lobes of chamfered threads only. Hence, the approach for characterizing the wear of coatings based on the analysis of chamfered threads was correct. The results provided in the previous studies are accurate and reliable.

13. This research study strongly suggests performing a short preliminary test to detect any early coating failure at the critical region and along the edges. Such short tests of just 360 holes could be effective in saving time and material during performance evaluation of coatings for form taps.

In summary, the contributions of this research included an efficient experimental setup, a reliable wear measurement method, an understanding of the established wear mechanisms, critical region and common wear pattern. Through these efforts made at the MMRI, further development of the effective coating for the form taps is expected soon.

7.2 Future work

Based on the findings and the challenges associated with this research, a few recommendations are put forward for future studies:

1. The lack of coated coupons limited the coating characterization study, which should include a Scratch test, Nano-impact test, Palmqvist toughness test,

Tribometer test and XRD. These tests will help to understand the effect of mechanical properties and friction on coating adhesion and wear resistance.

2. Coating optimization of TiAlN is needed to get the best tool performance.

3. FEA modelling is required to evaluate the stresses and friction on the lobe and edge of the crest under similar forming loads.

4. The impact of edge geometry on coating wear must be investigated.

5. The intensity of wear was different for both the second and third threads. An experiment is needed to find the contribution of plastic work done by each thread in form tapping taking into account the cold working of the material.

6. The complete focus of this research was on tool improvement. The scope of any future research should include surface integrity studies to characterize the formed thread under these process conditions.

7. A collaborative work on studying the effect of MWFs on drilling and form tapping process was conducted at MMRI (see Appendix B). The experiment was not designed to understand the impact of MWFs on the wear of form taps. Based on the wear pattern and critical region of form taps, an investigation could be performed to find a sustainable, safe and environmentally friendly MWF.

References

[1]   B. S. Shabel, D. A. Granger, and W. G. Truckner, "Friction and Wear of Aluminum-Silicon Alloys," in *ASM Handbook: Friction,Lubrication,and Wear Technology*, vol. 18, ASM International, pp. 785–794, 1992.

[2]   J. F. Su, "Characterization of Fracture and Debonding of Silicon Particles in Aluminium Silicon Alloys," University of Windsor, 2009.

[3]   A. S. M. H. Committee, "Machining of Aluminum and Aluminum Alloys," in *ASM Handbook, Volume 16, Machining*, ASM International, pp. 761–804, 1989.

[4]   S. Bhowmick, M. J. Lukitsch, and A. T. Alpas, "Tapping of Al–Si alloys with diamond-like carbon coated tools and minimum quantity lubrication," *J. Mater. Process. Technol.*, vol. 210, no. 15, pp. 2142–2153, Nov. 2010.

[5]   G. Fromentin, G. Poulachon, A. Moisan, B. Julien, and J. Giessler, "Precision and surface integrity of threads obtained by form tapping," *CIRP Ann.*, vol. 54, no. 1, pp. 519–522, 2005.

[6]   J. Fernández Landeta, A. Fernández Valdivielso, L. N. López de Lacalle, F. Girot, and J. M. Pérez Pérez, "Wear of Form Taps in Threading of Steel Cold Forged Parts," *J. Manuf. Sci. Eng.*, vol. 137, no. 3, p. 031002, Jun. 2015.

[7]   C. Warrington, S. Kapoor, and R. DeVor, "Experimental Investigation of Thread Formation in Form Tapping," *J. Manuf. Sci. Eng.*, vol. 127, no. 4, p. 829, 2005.

[8]   J. S. Agapiou, "Evaluation of the Effect of High Speed Machining on Tapping," *J. Eng. Ind.*, vol. 116, no. 4, p. 457, 1994.

[9]   L. Reithmaier and R. Sterkenburg, "Bolts and Threaded Fasteners," *Standard*

Aircraft Handbook for Mechanics and Technicians, Seventh Edition. McGraw Hill Professional, Access Engineering, 2014.

[10] E. Hong, H. Zhang, R. Katz, and J. S. Agapiou, "Non-contact inspection of internal threads of machined parts," *Int. J. Adv. Manuf. Technol.*, vol. 62, no. 1–4, pp. 221–229, 2012.

[11] A. P. S. Dogra, S. G. Kapoor, and R. E. DeVor, "Mechanistic Model for Tapping Process With Emphasis on Process Faults and Hole Geometry," *J. Manuf. Sci. Eng.*, vol. 124, no. 1, p. 18, 2002.

[12] Cm. Hwaiyu Geng PE, "Threading," in *Manufacturing Engineering Handbook, Second Edition*, McGraw Hill Professional, Access Engineering, 2016.

[13] M. Rezayi Khoshdarregi and Y. Altintas, "Generalized modeling of chip geometry and cutting forces in multi-point thread turning," *Int. J. Mach. Tools Manuf.*, vol. 98, no. September, pp. 21–32, Nov. 2015.

[14] A. Carla Araujo, J. Luis Silveira, M. B. G. Jun, S. G. Kapoor, and R. DeVor, "A model for thread milling cutting forces," *Int. J. Mach. Tools Manuf.*, vol. 46, no. 15, pp. 2057–2065, Dec. 2006.

[15] Y. Wang, C. Zhang, Y. He, L. Tao, and H. Feng, "Development and evaluation of non-contact automatic tool setting method for grinding internal screw threads," *Int. J. Adv. Manuf. Technol.*, vol. 98, no. 1–4, pp. 741–754, Sep. 2018.

[16] A. E. Reiter, B. Brunner, M. Ante, and J. Rechberger, "Investigation of several PVD coatings for blind hole tapping in austenitic stainless steel," *Surf. Coatings Technol.*, vol. 200, no. 18–19, pp. 5532–5541, May 2006.

[17]   A. G. Del Val *et al.*, "On Line Diagnosis Strategy of Thread Quality in Tapping," *Procedia Eng.*, vol. 63, pp. 208–217, 2013.

[18]   Y. Saito *et al.*, "Effect of friction at chip–tool interface on chip geometry and chip snarling in tapping process," *Int. J. Mach. Tools Manuf.*, vol. 107, pp. 60–65, 2016.

[19]   G. Benga and I. Ciupitu, "The influence of coating and tool geometry on the tool life in a thread cutting process," *Ann. DAAAM Proc.*, pp. 91–93, 2008.

[20]   T. Cao and J. W. Sutherland, "Investigation of thread tapping load characteristics through mechanistics modeling and experimentation," *Int. J. Mach. Tools Manuf.*, vol. 42, no. 14, pp. 1527–1538, Nov. 2002.

[21]   V. Ivanov and V. Kirov, "Rolling of internal threads: Part 1," *J. Mater. Process. Technol.*, vol. 72, no. 2, pp. 214–220, Dec. 1997.

[22]   G. Fromentin, A. Bierla, C. Minfray, and G. Poulachon, "An experimental study on the effects of lubrication in form tapping," *Tribol. Int.*, vol. 43, no. 9, pp. 1726–1734, Sep. 2010.

[23]   P. Stéphan, F. Mathurin, and J. Guillot, "Analytical study of maximal tapping torque during forming screw process," *J. Mater. Process. Technol.*, vol. 211, no. 2, pp. 212–221, Feb. 2011.

[24]   S. Chowdhary, S. G. Kapoor, O. B. Ozdoganlar, and R. E. DeVor, "Modeling and analysis of internal thread forming," *Tech. Pap. Soc. Manuf. Eng.*, vol. 125, no. MR02-172, pp. 1–8, 2002.

[25]   S. Chowdhary, R. E. DeVor, and S. G. Kapoor, "Modeling Forces Including Elastic Recovery for Internal Thread Forming," *J. Manuf. Sci. Eng.*, vol. 125, no. 4, p. 681,

2003.

[26] G. Fromentin, G. Poulachon, and A. Moisan, "Metallurgical aspects in cold forming tapping," *Adv. Manuf. Technol. XVI Proc. eighteenth Natl. Conf. Manuf. Res.*, vol. 18, pp. 373–378, 2002.

[27] A. O. de Carvalho, L. C. Brandão, T. H. Panzera, and C. H. Lauro, "Analysis of form threads using fluteless taps in cast magnesium alloy (AM60)," *J. Mater. Process. Technol.*, vol. 212, no. 8, pp. 1753–1760, Aug. 2012.

[28] A. E. Tekkaya *et al.*, "Metal forming beyond shaping: Predicting and setting product properties," *CIRP Ann.*, vol. 64, no. 2, pp. 629–653, 2015.

[29] H. Sağlam and R. Kuş, "Performance of internal thread rolling head and the mechanical properties of rolled thread," in *6th International Advanced Technologies Symposium (IATS'11)*, pp. 210–217, May 2011.

[30] C. Warrington, S. Kapoor, and R. DeVor, "Finite Element Modeling for Tap Design Improvement in Form Tapping," *J. Manuf. Sci. Eng.*, vol. 128, no. 1, p. 65, 2006.

[31] A. . Riahi, T. Perry, and A. . Alpas, "Scuffing resistances of Al–Si alloys: effects of etching condition, surface roughness and particle morphology," *Mater. Sci. Eng. A*, vol. 343, no. 1–2, pp. 76–81, Feb. 2003.

[32] D. K. Dwivedi, "Adhesive wear behaviour of cast aluminium–silicon alloys: Overview," *Mater. Des.*, vol. 31, no. 5, pp. 2517–2531, May 2010.

[33] R. Antoniou and D. W. Borland, "Mild wear of Al-Si binary alloys during unlubricated sliding," *Mater. Sci. Eng.*, vol. 93, no. C, pp. 57–72, Sep. 1987.

[34] M. A. Moore, "A review of two-body abrasive wear," *Wear*, vol. 27, no. 1, pp. 1–

17, Jan. 1974.

[35] H. Ye, "An Overview of the Development of Al-Si-Alloy Based Material for Engine Applications," *J. Mater. Eng. Perform.*, vol. 12, no. 3, pp. 288–297, Jun. 2003.

[36] H. A. Kishawy, M. Dumitrescu, E.-G. Ng, and M. A. Elbestawi, "Effect of coolant strategy on tool performance, chip morphology and surface quality during high-speed machining of A356 aluminum alloy," *Int. J. Mach. Tools Manuf.*, vol. 45, no. 2, pp. 219–227, Feb. 2005.

[37] J. A. Williams and A. M. Hyncica, "Mechanisms of abrasive wear in lubricated contacts," *Wear*, vol. 152, no. 1, pp. 57–74, Jan. 1992.

[38] S. M. Mahdavian, Y. W. Mai, and B. Cotterel, "Friction, metallic transfer and debris analysis of sliding surfaces," *Wear*, vol. 82, no. 2, pp. 221–232, Nov. 1982.

[39] D. U. Braga, A. E. Diniz, G. W. . Miranda, and N. L. Coppini, "Using a minimum quantity of lubricant (MQL) and a diamond coated tool in the drilling of aluminum–silicon alloys," *J. Mater. Process. Technol.*, vol. 122, no. 1, pp. 127–138, Mar. 2002.

[40] J. M. Dasch *et al.*, "A comparison of five categories of carbon-based tool coatings for dry drilling of aluminum," *Surf. Coatings Technol.*, vol. 200, no. 9, pp. 2970–2977, Feb. 2006.

[41] G. Fox-Rabinovich *et al.*, "Cutting performance of different coatings during minimum quantity lubrication drilling of aluminum silicon B319 cast alloy," *Surf. Coatings Technol.*, vol. 205, no. 16, pp. 4107–4116, May 2011.

[42] E.-G. Ng, D. Szablewski, M. Dumitrescu, M. A. Elbestawi, and J. H. Sokolowski, "High Speed Face Milling of a Aluminium Silicon Alloy Casting," *CIRP Ann.*, vol.

53, no. 1, pp. 69–72, 2004.

[43]   A. K. Srivastava, M. E. Finn, and M. A. Kinney, "Tool/work material/cutting fluid interaction while tapping into AA-319 and AA-A356 T6 lost foam aluminum castings," *Trans. North Am. Manuf. Res. Inst. SME*, vol. 32, pp. 263–270, 2004.

[44]   Y. Zedan, F. H. Samuel, A. M. Samuel, and H. W. Doty, "Effects of Fe intermetallics on the machinability of heat-treated Al–(7–11)% Si alloys," *J. Mater. Process. Technol.*, vol. 210, no. 2, pp. 245–257, Jan. 2010.

[45]   J. H. Tylczak, "Abrasive Wear," in *ASM Handbook, Volume 18, Lubrication and Wear Technology*, ASM International, 1992, pp. 184–190.

[46]   D. M. Turley and E. D. Doyle, "Factors affecting workpiece deformation during grinding," *Mater. Sci. Eng.*, vol. 21, pp. 261–271, Jan. 1975.

[47]   M. C. Shaw and J. O. Cookson, *Metal cutting principles*, vol. 2, no. 8. Oxford university press, New York, 2005.

[48]   J. F. Archard, "Contact and Rubbing of Flat Surfaces," *J. Appl. Phys.*, vol. 24, no. 8, pp. 981–988, Aug. 1953.

[49]   R. I. Trezona, D. N. Allsopp, and I. M. Hutchings, "Transitions between two-body and three-body abrasive wear: Influence of test conditions in the microscale abrasive wear test," *Wear*, vol. 225–229, no. I, pp. 205–214, 1999.

[50]   J. D. Gates, "Two-body and three-body abrasion: A critical discussion," *Wear*, vol. 214, no. 1, pp. 139–146, Jan. 1998.

[51]   R. C. Cozza, D. K. Tanaka, and R. M. Souza, "Friction coefficient and wear mode transition in micro-scale abrasion tests," *Tribol. Int.*, vol. 44, no. 12, pp. 1878–1889,

Nov. 2011.

[52] R. C. Cozza and C. G. Schön, "Evidence of Superposition between Grooving Abrasion and Rolling Abrasion," *Tribol. Trans.*, vol. 58, no. 5, pp. 875–881, 2015.

[53] P. B. Madakson, "The frictional behaviour of materials," *Wear*, vol. 87, no. 2, pp. 191–206, 1983.

[54] F. A. Davis and T. S. Eyre, "The effect of silicon content and morphology on the wear of aluminium-silicon alloys under dry and lubricated sliding conditions," *Tribol. Int.*, vol. 27, no. 3, pp. 171–181, 1994.

[55] B. N. P. Bai and S. K. Biswas, "Characterization of dry sliding wear of Al-Si alloys," *Wear*, vol. 120, no. 1, pp. 61–74, Nov. 1987.

[56] C. Subramanian, "Effects of sliding speed on the unlubricated wear behaviour of Al-12.3wt.%Si alloy," *Wear*, vol. 151, no. 1, pp. 97–110, Nov. 1991.

[57] P. Tallai, S. Csuka, and S. Sipos, "Thread forming tools with optimised coatings," *Acta Polytech. Hungarica*, vol. 12, no. 1, pp. 55–66, 2015.

[58] G. Fromentin, "Étude mécanique et technologique du taraudage par déformation: application aux aciers prétraités," Paris, ENSAM, 2004.

[59] F. Klocke and T. Krieg, "Coated Tools for Metal Cutting – Features and Applications," *CIRP Ann.*, vol. 48, no. 2, pp. 515–525, 1999.

[60] K.-D. Bouzakis, N. Michailidis, G. Skordaris, E. Bouzakis, D. Biermann, and R. M'Saoubi, "Cutting with coated tools: Coating technologies, characterization methods and performance optimization," *CIRP Ann.*, vol. 61, no. 2, pp. 703–723, 2012.

[61] P. Karlsson, "Tribological characterization of selected hard coatings," 2009.

[62] K. Holmberg, H. Ronkainen, and A. Matthews, "Tribology of thin coatings," *Ceram. Int.*, vol. 26, no. 7, pp. 787–795, Aug. 2000.

[63] M. Chowdhury, "Wear behaviour of coated carbide tools during machining of Ti6Al4V aerospace alloy," 2016.

[64] M. Piska and P. Sliwkova, "Surface Parameters, Tribological Tests and Cutting Performance of Coated HSS Taps," *Procedia Eng.*, vol. 100, no. C, pp. 125–134, 2015.

[65] A. Steininger, A. Siller, and F. Bleicher, "Investigations Regarding Process Stability Aspects in Thread Tapping Al-Si Alloys," *Procedia Eng.*, vol. 100, no. January, pp. 1124–1132, 2015.

[66] P. H. Mayrhofer, C. Mitterer, L. Hultman, and H. Clemens, "Microstructural design of hard coatings," *Prog. Mater. Sci.*, vol. 51, no. 8, pp. 1032–1114, Nov. 2006.

[67] C. A. S. Bork, J. F. S. Gonçalves, and J. O. Gomes, "The Jatropha curcas vegetable base soluble cutting oil as a renewable source in the machining of aluminum alloy 7050-T7451," *Ind. Lubr. Tribol.*, vol. 67, no. 2, pp. 181–195, Mar. 2015.

[68] E. Brinksmeier, D. Meyer, A. G. Huesmann-Cordes, and C. Herrmann, "Metalworking fluids—Mechanisms and performance," *CIRP Ann.*, vol. 64, no. 2, pp. 605–628, 2015.

[69] J. P. Davim, P. S. Sreejith, R. Gomes, and C. Peixoto, "Experimental studies on drilling of aluminium (AA1050) under dry, minimum quantity of lubricant, and flood-lubricated conditions," *Proc. Inst. Mech. Eng. Part B J. Eng. Manuf.*, vol. 220,

no. 10, pp. 1605–1611, Oct. 2006.

[70] A. Bierla *et al.*, "Tribological aspect of lubrication in form tapping of high-strength steel," *Lubr. Sci.*, vol. 20, pp. 269–281, Feb. 2008.

[71] Y. Shokoohi, J. M. Paiva, G. Fox-Rabinovich, C. A. S. Bork, and S. C. Veldhuis, "Evaluation of the superabsorbent coolant as a new approach to semi-dry machining," *Int. J. Adv. Manuf. Technol.*, Nov. 2018.

[72] L. De Chiffre and W. Belluco, "Comparison of Methods for Cutting Fluid Performance Testing," *CIRP Ann.*, vol. 49, no. 1, pp. 57–60, 2000.

[73] W. Belluco and L. De Chiffre, "Testing of vegetable-based cutting fluid by hole making operations," *Lubr. Eng.*, vol. 57, no. 1, pp. 12–16, 2001.

[74] W. Belluco and L. De Chiffre, "Surface integrity and part accuracy in reaming and tapping stainless steel with new vegetable based cutting oils," *Tribol. Int.*, vol. 35, no. 12, pp. 865–870, 2002.

[75] N. J. Fox and G. W. Stachowiak, "Vegetable oil-based lubricants-A review of oxidation," *Tribol. Int.*, vol. 40, no. 7, pp. 1035–1046, 2007.

[76] S. Asadauskas, J. M. Perez, and J. L. Duda, "Oxidative stability and antiwear properties of high oleic vegetable oils," *Lubr. Eng.*, vol. 52, no. 12, pp. 877–882, 1996.

[77] "Alloy data," in *NADCA Product Specification Standarts for Die Casting*, 9th ed., North American Die Casting Association, 2015, pp. 3–6.

[78] ISO 68-1:1998, "ISO general purpose screw threads — Basic profile — Part 1 : Metric screw threads." 1998.

[79]   ISO 965-1:1998, "ISO general purpose metric screw threads — Tolerances — Part 1 : Principles and basic data." 1998.

[80]   ISO 1502:1996, "ISO general purpose metric screw threads — General plan." 1996.

[81]   A. A. Voevodin, S. D. Walck, and J. S. Zabinski, "Architecture of multilayer nanocomposite coatings with super-hard diamond-like carbon layers for wear protection at high contact loads," *Wear*, vol. 203–204, no. 1, pp. 516–527, 1997.

[82]   J. Dundurs and M. S. Lee, "Stress concentration at a sharp edge in contact problems," *J. Elast.*, vol. 2, no. 2, pp. 109–112, Jun. 1972.

[83]   K. Holmberg, A. Laukkanen, H. Ronkainen, K. Wallin, and S. Varjus, "A model for stresses, crack generation and fracture toughness calculation in scratched TiN-coated steel surfaces," *Wear*, vol. 254, no. 3–4, pp. 278–291, 2003.

[84]   S. J. Bull, "Failure mode maps in the thin film scratch adhesion test," *Tribol. Int.*, vol. 30, no. 7, pp. 491–498, Jul. 1997.

[85]   J. Chen and S. J. Bull, "Approaches to investigate delamination and interfacial toughness in coated systems: an overview," *J. Phys. D. Appl. Phys.*, vol. 44, no. 3, p. 034001, Jan. 2011.

[86]   B. D. Beake, G. A. Bell, S. R. Goodes, N. J. Pickford, and J. F. Smith, "Improved nanomechanical test techniques for surface engineered materials," *Surf. Eng.*, vol. 26, no. 1–2, pp. 37–49, Feb. 2010.

[87]   A. Leyland and A. Matthews, "On the significance of the H/E ratio in wear control: a nanocomposite coating approach to optimised tribological behaviour," *Wear*, vol. 246, no. 1–2, pp. 1–11, Nov. 2000.

[88] G. S. Fox-Rabinovich *et al.*, "Effect of mechanical properties measured at room and elevated temperatures on the wear resistance of cutting tools with TiAlN and AlCrN coatings," *Surf. Coatings Technol.*, vol. 200, no. 20–21, pp. 5738–5742, May 2006.

[89] K. Yamamoto *et al.*, "Cutting Performance of Low Stress Thick TiAlN PVD Coatings during Machining of Compacted Graphite Cast Iron (CGI)," *Coatings*, vol. 8, no. 1, p. 38, Jan. 2018.

[90] X. Huang, I. Etsion, and T. Shao, "Effects of elastic modulus mismatch between coating and substrate on the friction and wear properties of TiN and TiAlN coating systems," *Wear*, vol. 338–339, pp. 54–61, Sep. 2015.

[91] J. B. Zimmerman, A. F. Clarens, K. F. Hayes, and S. J. Skerlos, "Design of Hard Water Stable Emulsifier Systems for Petroleum- and Bio-based Semi-synthetic Metalworking Fluids," *Environ. Sci. Technol.*, vol. 37, no. 23, pp. 5278–5288, 2003.

[92] S. Bhowmick, "Minimum quantity lubrication machining of aluminum and magnesium alloys," 2011.

[93] S. A. Lawal, I. A. Choudhury, and Y. Nukman, "Developments in the formulation and application of vegetable oil-based metalworking fluids in turning process," *Int. J. Adv. Manuf. Technol.*, vol. 67, no. 5–8, pp. 1765–1776, Jul. 2013.

[94] W. A. Knight and G. Boothroyd, *Fundamentals of metal machining and machine tools*, vol. 198. CRC Press, 2005.

Appendix A: Inspection of drilled and tapped hole

The diameter of the drilled hole was measured a depth of 15 mm from the top of the surface. Table 12 shows the diameter of drilled holes in this research. CMM was used for measuring the diameter of holes at various stages before tapping.

Table 12—Diameter of drilled holes

Hole number						

Hole number	1	360	1080	2160	3240	4320
Uncoated	7.354±0.001	7.353±0.004	7.354±0.003	7.350±0.005	7.358±0.003	7.362±0.003
ZrN	7.353±0.003	7.353±0.003	7.352±0.005	7.354±0.003	7.356±0.003	7.361±0.003
TiAlN	7.354±0.003	7.352±0.005	7.354±0.004	7.358±0.004	7.362±0.006	7.365±0.005
TiCN	7.352±0.003	7.353±0.006	7.356±0.003	7.355±0.007		
TiAlN-2	7.353±0.002	7.354±0.003				

The tapped holes were checked by an ISO M8x1.25 screw plug gauge. The GO end of the gauge checked the minimum condition of pitch diameter and major diameter, and the flank straightness. The NO-GO end of the gauge checks the maximum condition of pitch diameter. The thread gauging results of the tapped holes at various stages of the experiments are shown below in Table 13.

Table 13—Thread gauging results of tapped holes

Condition of thread (Go and No-Go)

Hole number	1	360	1080	2160	3240	4320
Uncoated	Ok	Ok	Ok	Ok	Ok	Ok
ZrN	Ok	Ok	Ok	Ok	Ok	Ok
TiAlN	Ok	Ok	Ok	Ok	Ok	Ok
TiCN	Ok	Ok	Ok	Ok		
TiAlN-2	Ok	Ok				
Tool 1	Ok					
Tool 2	Ok					
Tool 3	Ok					

Appendix B: Effect of metalworking fluids

The objective of this study was to evaluate the effect of different metal working fluids (MWFs) in the drilling and tapping process of the Al-12Si alloy. A critical review of past research on MWFs (see Section 2.9) showed that subsequent processes such as drilling, and tapping are dependent on MWFs. The tapping process depends highly on the drilled hole condition. As such, the influence of MWFs of these processes was studied here. Based on literature review and industry demand, three MWFs were tested in this experiment- a commercial, mineral oil-water emulsion, a sunflower oil-water emulsion without additives, and a novel gel based superabsorbent coolant (SAC). The detailed description of SAC is provided in the Section 2.9. The goal of this experiment was to find a sustainable, safe and environment friendly MWF as an alternative to the existing commercial mineral oil.
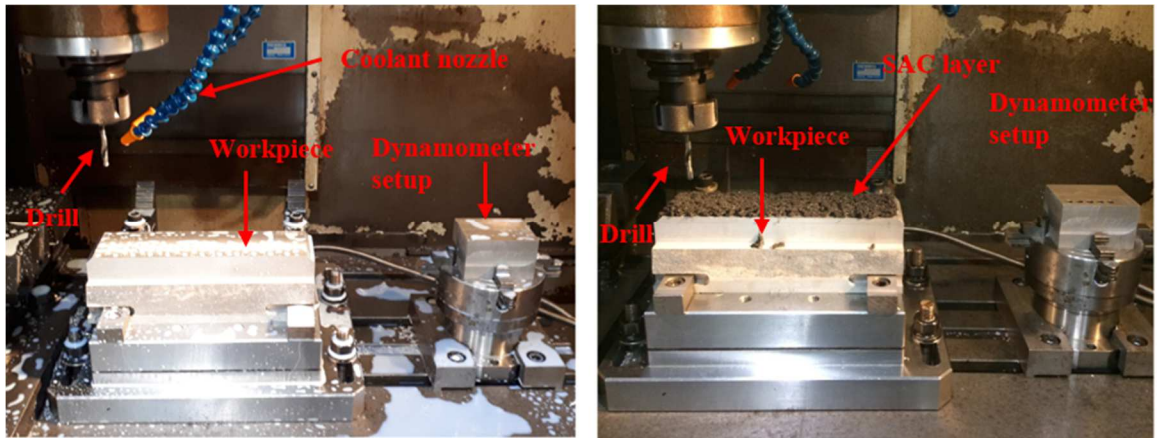
B.1 Experimental methodology

Fig.68: Experimental setup for drilling and tapping tests with three MWFs

The experimental setup on an Okuma Cadet 4020 vertical-CNC milling machine is been shown in Fig.68. The vertical setup was selected to examine the effectiveness of MWFs in removing chips during drilling. Here, the workpiece was the same as in the previous experiments. In order to eliminate any effect of PVD coatings in lubrication conditions, uncoated twists drills and form taps were used with specifications as provided in Table 14. The process parameters for this experiment were adopted based on industry practice (see Table 15).

As shown in Fig.68, a rectangular work piece was mounted to drill 95 holes and another five holes were drilled in the block of the dynamometer setup. The same dynamometer setup was used for this experiment as shown in the Fig.16. Since the drill depth was thrice larger than the diameter of the hole, a pecking cycle ensured proper removal of chips from the deep hole in a vertical setup.

The surface roughness of the drilled holes was measured using a Mitutoyo Surftest SJ-201. The probed length was 4mm, and the cut-off length was 0.8 mm as per ISO 4288 standard. The Keyence VHX 5000 digital microscope was used to record wear on the drill and form tap. The split crest was inspected with the same microscope.

Table 14—Specifications of drills and taps for testing MWFs	
Drill	**Tap**
Type: Metric, twists, no coolant through	Type: Metric, Bottoming Form tap, 3 threads chamfer, 6H
Material: Uncoated Carbide	Material: uncoated High-Speed Steel
Diameter: 7.37 mm	Diameter: 8 mm
Helix Angle: 118 °	Pitch: 1.25 mm
Flutes: 2 (straight)	Grooves: 6, straight
Flute length: 54 mm	Thread height: 74.12%

Table 15—Process parameters

Parameters	Drilling	Form-tapping
Nominal diameter, mm	7.37	8
Hole Depth, mm	25	19
Spindle speed, RPM	2500	1000
Feed rate, mm/min	625	1250

The performance responses consisted of the maximum feed force, maximum torque and surface roughness of the drilled hole. In the case of form tapping, the maximum forward torque, thread profile and split-crest were investigated.

In the first and second set of experiments, a commercial, mineral oil- HOCUT-795H and a vegetable-based mid-oleic Sunflower oil were used in the form of water-based emulsion for the comparative analysis. Tween 20, a non-ionic surfactant, was selected as an emulsifier to create the sunflower oil in water emulsion. This emulsion was prepared by adding 2 % by weight emulsifier to the solution. The chemical identity of Tween 20 is Polyethylene glycol sorbitan-monolaurate, and its hydrophile-lipophile balance (HLB) value is 16.7. A higher HLB is desirable for creating a stable oil-in-water emulsion [91]. No additives were added to the emulsion.

To prepare 1 Kg of SAC, 20g of Sodium Polyacryalite (super absorbent), 1% graphite nano-particle, 10 % semi-synthetic oil, and 89 % water is required [71]. This MWF was prepared by adding graphite nano-particle to soluble oil and mixing with a magnetic stirrer for 20 min. It is followed by the addition of water to the suspension. In order to maintain homogeneity of the nano-particles in the suspension, the mixture was immersed in an ultrasonic bath for two hours. The final step is the addition of superabsorbent polymer to the nano-fluid to create the gel in a period of 10 minutes.

Table 16 shows important characteristics of the selected MWFs in this experiment. The complex viscosity with respect to shear rate for each MWFs was determined by the frequency sweep method (see Fig.69).

Table 16—Characterization of selected MWFs

MWF	Concentration (%)	COF
Hocut 795H	10	0.282
Sunflower oil	10	0.372
SAC	10	0.292
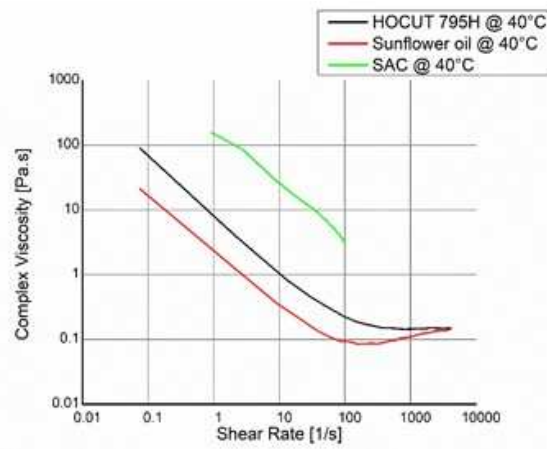
Fig.69: Viscosity vs Shear curve for three MWFs at 40°C

B.2 Results and discussion

In this section, the results of the output variables of the tests will be analyzed to determine the best-cutting fluid in each one.

B.2.1 Cutting force results of the drilling test

Fig.70(a) shows that the maximum feed forces for the drilling process were lowest in the case of mineral oil and highest for sunflower oil. The graph shows that the sunflower oil was not effective in decreasing the thrust force and torque. The reason may be very high aluminum adhesion to the tool resulting in build-up edge (BUE) formation. The average BUE measured after 100 drilling holes at the cutting and chisel

edge was 852 μm and 410 μm as shown in Fig.72. Cutting tool geometry changed with increasing BUE as workpiece material adhered below the nose of the tool causing greater material removal per unit of time [39]. Negligible flank wear was observed after 100 holes.
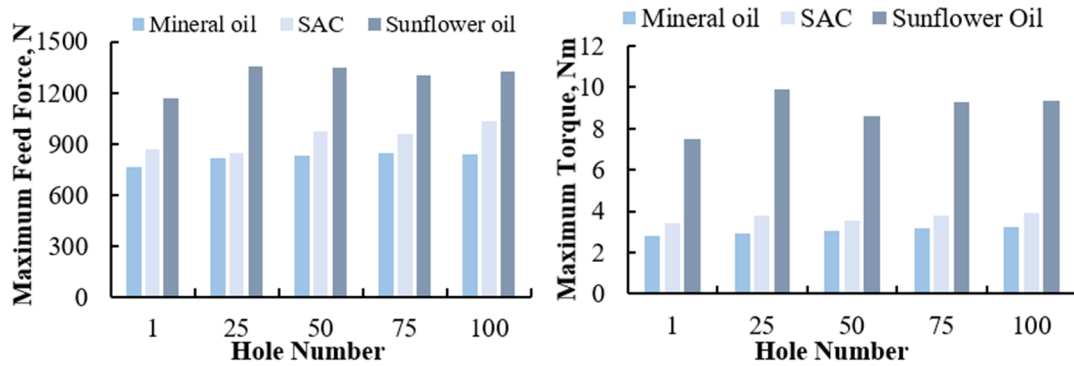

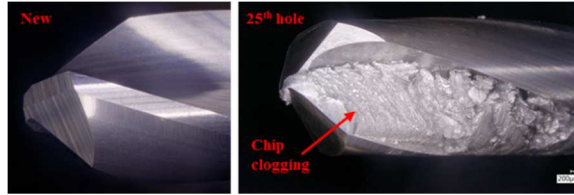**Fig.70: Maximum feed force and torque distribution in drilling**

Fig.71: Chip clogging of drill with sunflower oil

The maximum torque generated during drilling is provided in Fig.70(b). The higher torque values for the sunflower oil were due to the lack of chip removal, which resulted in chip clogging [92]. This was evident at the 25th hole where the entire flute was clogged with chips, which apparently adhered to the surface of the drill flute (see Fig.71). The inferior performance of sunflower oil could be due to low thermal and oxidative stability [93]. Also, Fox and Stachowiack [75] suggested that the narrow range of viscosities limit the application of vegetable oil as industrial lubricant. In this experiment, the sunflower oil did not have any additives to counter such instability of

lubricant. The intention for such a condition was to observe the high lubricity of vegetable oil compared to mineral oil and SAC.
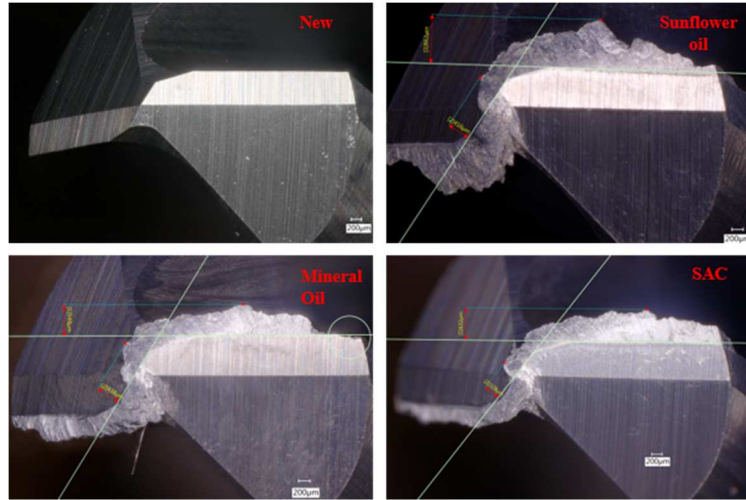

Fig.72: Build-up edge on cutting and chisel edge of the drill producing 100 holes

The feed force and torque results for the mineral oil and gel-based lubricants were comparable, with the mineral oil showing lower forces. The commercial mineral oil with additives reacts with the surface and reduces the surface shear strength [68]. Also, EP additives forms a stable oxide layer preventing metal to metal contact and enhancing lubricity. Therefore, the tool would experience the minimum amount of resistance with mineral oil compared to SAC and sunflower oil. Although SAC was prepared by mixing semi-synthetic oil with water, the amount of EP and other surface reactants was less compared than that of the commercial mineral oil. This could be the cause of the higher cutting forces of the SAC with respect to the mineral oil. The presence of graphite nanoparticles and higher emulsion content of hydrogel particles in the SAC reduced frictional forces and lowered temperature [71].

B.2.2 Surface roughness of drilled holes

Fig.73 illustrates the trend of Ra roughness of drilled holes for the three MWFs. The main purpose of the lubricant is to form a low shear strength film and reduce the intimate metallic contact between the chip and tool. As discussed earlier, the occurrence of BUE at this cutting speed could be the major reason for higher roughness of the drilled holes. BUE on the rake face continuously forms and breaks down. The fractured debris might be carried away on the underside of the chip and above the machined surface. Higher feed forces for sunflower oil indicated a larger BUE which resulted in a rougher surface [94]. Fig.73 shows surface roughness increasing in the order (from least to greater): mineral oil, SAC and sunflower oil. Moreover, the ploughing effect of the BUE could be observed on the drilled hole surface by the groove marks and saw-toothed finish [47],[76].
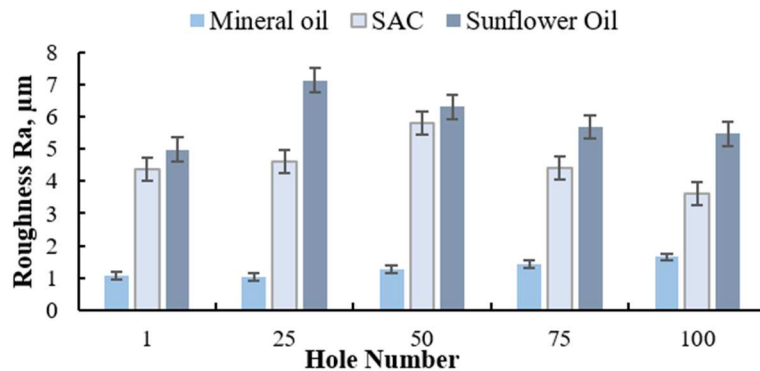

Fig.73:Average roughness of drilled holes, Ra (μm)

B.2.3 Evaluation of torque in the tapping test

Fig.74 shows the behaviour of torque in the tapping process using the selected MWFs in the test. Maximum torque was recorded during the forward movement of the tap in the drilled hole. Form tapping is very sensitive to the MWF due to the larger contact surface between the threaded hole and tap. The torque in form tapping is due to both formation and friction torque. Friction torque was generated by the spring-back effect of material previously deformed in the threaded hole [22]. The formation torque is directly related to the diameter of the pre-tapped hole [22]. The torque was initially higher for all three MWFs and gradually stabilized upon further machining. This could be attributed to tighter drilled holes initially. Upon further machining, the drilled hole diameter became larger than the initial hole diameter as shown in Table 15. The torque stabilized as the drilled hole diameter varied less after producing 50 holes. This could be attributed to a continuous generation of BUE on the drill, which led to an oversized hole and subsequently lower torque [73].
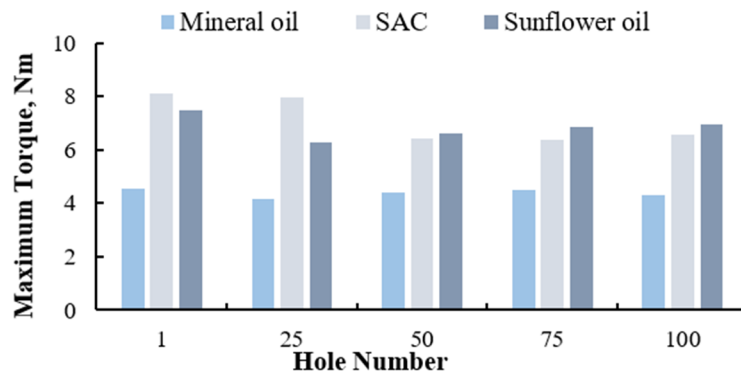

Fig.74: Maximum torque distribution for tapping test

Table 17—Diameter of drilled holes for the three MWFs

	Hole diameter (mm)		
	Mineral Oil	SAC	Sunflower Oil
Hole-1	7.375±0.003	7.374±0.002	7.375±0.003
Hole-100	7.379±0.004	7.381±0.006	7.384±0.005

In order to understand the effect of lubrication on friction, the effect of pre- tapped diameter variation must be removed. A general torque trend for all the three MWFs could be observed from the 50th to 100th hole. The performance of three MWFs in reducing friction was analysed beyond the machining of 50 holes. The mineral oil generated the lowest torque followed by SAC. The greatest torque occurred in tapping with the application of sunflower oil. A high torque value was an indication of greater frictional forces in the forming process. The friction coefficient played an influential role in generating high frictional forces. The sunflower oil had a comparatively higher friction coefficient than the other MWFs. The most effective MWF should decrease frictional forces on the chamfered threads since formation torque has the greatest contribution on the overall torque value in form tapping [22].

B.2.4   Thread profile formation

Generally, the thread produced by roll form taps has a split crest unlike threads machined by cut tapping. The split crest tends to weaken the overall strength of the thread due to higher chances of the tips of the ridge to fracturing during assembly or operation [7]. The split crest is directly dependent on the drilled hole diameter [8]. In Fig.75(c), the thread produced with sunflower oil appeared to be worst and the split crest was higher than that of the other two thread profiles. The threads produced by mineral oil and SAC had a relatively smaller split crest and sharper flanks compared to

the sunflower oil. This could be attributed to the higher friction between the tap and the workpiece during machining with vegetable oil. The lack of sufficient lubrication could have increased the frictional forces in case of sunflower oil. Fold-over of the ridges of the split crest in SAC and sunflower oil indicated higher frictional forces [7]. Another reason for the poor thread profiles could be due to the greater adhesion of aluminum on the crest of taps. This was evident from Fig.76(c). The flanks of the formed thread in the Fig.76(c) did not have sharp edges. The adhered material on the tap's surface had a detrimental effect on the formed threads with sunflower oil. The tendency for adhesion to the uncoated tap was lower in SAC and mineral oil. During tapping with SAC, graphite nanoparticles might have reduced the friction between the tool and workpiece [71]. This resulted in less heat generation and subsequently less adhesion of aluminum to the tap [4].
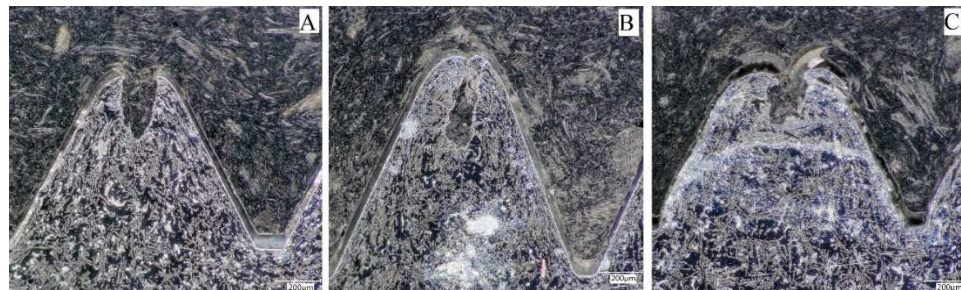

Fig.75: Split crest formation during tapping with (A) mineral oil, (B) SAC, (C)sunflower oil
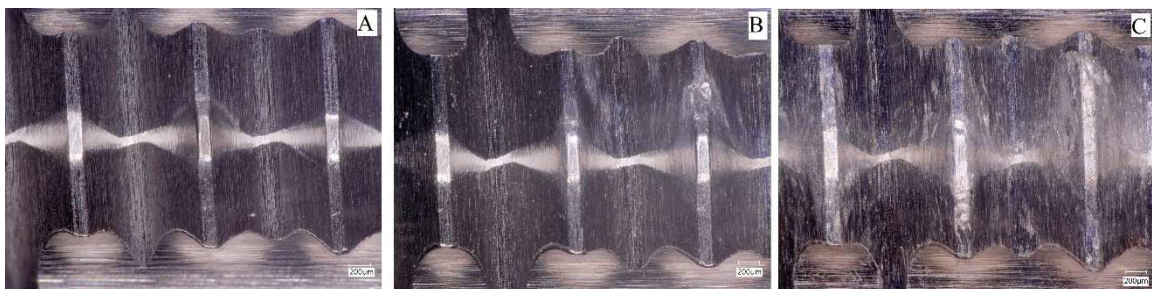

Fig.76: Chamfered threads of form taps machined with (A) mineral oil, (B) SAC, (C) sunflower oil

B.3 Conclusion

Build- up edge on the drill was observed in case of all the three MWFs due to lower cutting speed, and intense aluminum adhesion to the rake face of the tool. Higher feed forces were attributed to the BUE on the cutting edge. Greater torque in drilling was caused by chip clogging in the flutes. In case of drilling, the three MWFs are listed in increasing order of their performance : sunflower oil, SAC and mineral oil.

The maximum torque recorded in form tapping was lowest for mineral oil, followed by SAC. The highest torque was observed in the sunflower oil application. Higher torque could be an indication of a poor split crest. An efficient MWF should reduce the tendency of aluminum adhesion to the form tap's crest and flank, which is detrimental to the flank straightness of formed threads. Investigation of the thread profiles indicated that the mineral oil and SAC performed better than the sunflower oil.